



T O M A S K U N C I U S

**RESEARCH AND
DEVELOPMENT
OF 3D PRINTED
CONTINUOUS CARBON
FIBER REINFORCED
POLYMER COMPOSITE
STRUCTURES**

D O C T O R A L D I S S E R T A T I O N

K a u n a s
2 0 2 2

KAUNAS UNIVERSITY OF TECHNOLOGY

TOMAS KUNCIUS

RESEARCH AND DEVELOPMENT OF 3D
PRINTED CONTINUOUS CARBON FIBER
REINFORCED POLYMER COMPOSITE
STRUCTURES

Doctoral dissertation
Technological Sciences, Mechanical Engineering (T 009)

Kaunas, 2022

This doctoral dissertation was prepared at Kaunas University of Technology, Faculty of Mechanical Engineering and Design, Department of Production Engineering during the period of 2017–2022.

The doctoral right has been granted to Kaunas University of Technology together with Vytautas Magnus University.

Scientific Supervisor

Assoc. Prof. Dr. Marius RIMAŠAUSKAS (Kaunas University of Technology, Technological Sciences, Mechanical Engineering T 009).

Edited by: English language editor Armandas Rumšas (Publishing House *Technologija*), Lithuanian language editor Violeta Meiliūnaitė (Publishing House *Technologija*)

Dissertation Defence Board of Mechanical Engineering Science Field

Dr. Rolanas DAUKŠEVIČIUS (Kaunas University of Technology, Technology Sciences, Mechanical Engineering, T 009) – **chairperson**;

Assoc. Prof. Dr. Regita BENDIKIENĖ (Kaunas University of Technology, Technology Sciences, Mechanical Engineering, T 009);

Prof. Dr. Mangirdas MALINAUSKAS (Vilnius University, Nature Sciences, Physics, N 002);

Prof. Dr. Wiesław OSTACHOWICZ (The Szwalski Institute of Fluid-Flow Machinery, Poland, Technology Sciences, Mechanical Engineering, T 009).

The official defence of the dissertation will be held at 9:00 a.m. on the 27th of May, 2022 at the public meeting of Dissertation Defence Board of Mechanical Engineering Science Field in the Dissertation Defence Hall at Kaunas University of Technology.

Address: Donelaičio 73-403, Kaunas LT-44249, Lithuania.

Phone (+370) 37 300 042; fax. (+370) 37 324 144; email doktorantura@ktu.lt

The doctoral dissertation was sent out on the 27th of April 2022.

The doctoral dissertation is available on the internet at <http://ktu.edu> and at the library of Kaunas University of Technology (K. Donelaičio 20, Kaunas LT-44239, Lithuania), Vytautas Magnus University (K. Donelaičio 52, Kaunas LT-44244).

KAUNO TECHNOLOGIJOS UNIVERSITETAS

TOMAS KUNCIUS

IŠTISINIU ANGLIES PLUOŠTU ARMUOTŲ 3D
SPAUSDINTŲ POLIMERINIŲ KOMPOZICINIŲ
KONSTRUKCIJŲ KŪRIMAS IR TYRIMAS

Daktaro disertacija
Technologijos mokslai, mechanikos inžinerija (T 009)

Kaunas, 2022

Disertacija rengta 2017–2022 metais Kauno technologijos universiteto Mechanikos inžinerijos ir dizaino fakultete, Gamybės inžinerijos katedroje.

Doktorantūros teisė Kauno technologijos universitetui suteikta kartu su Vytauto didžiojo universitetu.

Mokslinis vadovas

Doc. dr. Marius RIMAŠAUSKAS (Kauno technologijos universitetas, technologijos mokslai, mechanikos inžinerija T 009).

Disertaciją redagavo: anglų kalbos redaktorius Armandas Rumšas (leidykla „Technologija“), lietuvių kalbos Violeta Meiliūnaitė (leidykla „Technologija“)

Mechanikos inžinerijos mokslo krypties disertacijos gynimo taryba:

Dr. Rolanas DAUKŠEVIČIUS (Kauno technologijos universitetas, technologijos mokslai, mechanikos inžinerija, T 009) – pirmininkas;

Doc. dr. Regita BENDIKIENĖ (Kauno technologijos universitetas, technologijos mokslai, mechanikos inžinerija, T 009);

Prof. dr. Mangirdas MALINAUSKAS (Vilniaus universitetas, gamtos mokslai, fizika, N 002);

Prof. dr. Wiesław OSTACHOWICZ (Šeivalskio skysčių srautų valdymo institutas, Lenkija, technologijos mokslai, mechanikos inžinerija, T 009).

Disertacija bus ginama viešame mechanikos inžinerijos mokslo krypties disertacijos gynimo tarybos posėdyje 2022 m. gegužės 27 d. 9:00 val. Kauno technologijos universiteto Disertacijų gynimo salėje.

Adresas: K. Donelaičio g. 73-403, Kaunas LT-44249, Lietuva.

Tel. (+370) 37 300 042; faks. (+370) 37 324 144; el. paštas doktorantura@ktu.lt

Disertacija išsiųsta 2022 m. balandžio 27 d.

Su disertacija galima susipažinti interneto svetainėje <http://ktu.edu> ir Kauno technologijos universiteto bibliotekoje (K. Donelaičio g. 20, Kaunas LT-44239), Vytauto Didžiojo universiteto bibliotekoje (K. Donelaičio g. 52, Kaunas LT-44244).

CONTENTS

LIST OF FIGURES	8
LIST OF TABLES	11
LIST OF ABBREVIATIONS	12
INTRODUCTION	13
1. LITERATURE OVERVIEW	17
1.1. The Principle of Fused Deposition Modelling Technology	18
1.2. Overview of the Materials Used in FDM Technology.....	19
1.3. Printing Carbon Fiber Reinforced Composite Structures by FDM Technology	23
1.3.1. Short Carbon Fiber	23
1.3.2. Continuous Carbon Fiber.....	25
1.4. Preparation of Carbon Fiber before Printing.....	28
1.5. Mechanical Properties of 3D-printed Continuous Carbon Fiber Reinforced Composites	30
1.6. Chapter Conclusions	32
2. TECHNOLOGICAL AND EXPERIMENTAL METHODOLOGY	34
2.1. Materials	35
2.1.1. Reinforcing Material.....	35
2.1.2. Matrix Material.....	36
2.2. Development of Impregnation Process	36
2.2.1. Solution Preparation	37
2.2.2. Carbon Fiber Impregnation.....	38
2.3. Development of FDM Process	39
2.3.1. 3D Printer Type	42
2.3.2. FDM Process Parameters.....	43
2.3.3. Main Parameters	43
2.3.4. Auxiliary Parameters	44
2.3.5. The Printing Process	46
2.3.6. Evolution of the Printing Process	47
2.4. Pre-processing of Continuous Carbon Fibers	49
2.4.1. Carbon Fiber Impregnation.....	49
2.4.2. Additive Manufacturing of Composite Samples.....	50
2.4.3. Mechanical Tests.....	50
2.5. Evaluation of Impregnated Carbon Fiber Tow Quality	51
2.6. Investigation of Influence of Printing Parameters	53
2.6.1. X-ray Defectoscopy of Printed Structures	55
2.6.2. Air Voids Investigation Using <i>ASTM D 3171</i> Standard	55

2.7. Determination of Delamination Force and Shear Strength	57
2.7.1. Shear strength test	61
2.8. Improvement of Mechanical Properties by Secondary Impregnation.....	61
2.8.1. Printing Process	63
2.8.2. Secondary Impregnation Process	63
2.8.3. Flexural and Tensile Testing.....	65
2.9. Chapter Conclusions	67
3. CHARACTERIZATION RESULTS	69
3.1. Carbon Fiber Tow Impregnation.....	69
3.1.1. Mechanical Properties of 3D Printed Composite Structures	73
3.2. Quality of Carbon Fiber Tow	74
3.2.1. Adhesion between CCF and Polymer Matrix	76
3.3. Quality of 3D Printed Composite Structures	77
3.4. Delamination Force and Shear Strength in Printed Composite Structures	82
3.4.1. Microscopic Inspection of Test Samples	85
3.5. Improvement of Mechanical Properties by Secondary Impregnation.....	87
3.5.1. Tensile Testing.....	91
3.5.2. Flexural Testing	95
3.6. Chapter Conclusions	98
CONCLUSIONS	101
SANTRAUKA	103
IVADAS	103
1. LITERATŪROS APŽVALGA	106
1.1. Ištinio anglies pluošto spausdinimas LMF Technologija	106
1.2. Literatūros apžvalgos apibendrinimas.....	107
2. METODOLOGIJA	107
2.1. Medžiagos	108
2.2. Impregnavimo procesas	109
2.3. Spausdinimo galvutė	110
3 REZULTATAI	112
3.1. Anglies pluošto impregnavimo proceso analizė	112
3.2. Spausdintų kompozitinių konstrukcijų kokybės vertinimas.....	113
3.3. Spausdintų kompozitinių konstrukcijų atsluoksniavimo jėgos ir šlyties stiprio nustatymas	116
3.4. Mechaninių savybių gerinimas antriniu impregnavimu.....	117

IŠVADOS	120
REFERENCES	122
CIRRCULUM VITAE	129
APPROBATION OF THE RSEARCH RESULTS.....	130
ACKNOWLEDGEMENTS	133

LIST OF FIGURES

Fig. 1.1 Principal scheme of FDM printing process [13]	18
Fig. 1.2 Technologies of carbon fiber reinforced printed composites manufactured with FDM technology [45]	23
Fig. 1.3 Methods to print continuous carbon fiber reinforced composite structures by using FDM technology [67]	26
Fig. 1.4 CCF preparation by melted matrix material [53]	29
Fig. 1.5 CCF impregnation by thermoplastic solution [84]	29
Fig. 1.6 Number of publications of continuous carbon fiber reinforced 3D printed composite structures investigations over 6 years (2016-2022) [45]	30
Fig. 1.7 Tensile strength results for years 2016–2020 as referred in scientific publications.....	31
Fig. 1.8 Flexural strength results for years 2016–2020 in scientific publications	32
Fig. 2.1 Research experimental setup.....	34
Fig. 2.2 Solution preparation and accumulation of buildup: 1 – individual granules; 2 – accumulation of granules.....	37
Fig. 2.3 Scheme for carbon fiber impregnation: 1 – spool; 2 – impregnated CCF; 3 – nozzle; 4 – heating section; 5 – 0.8 mm nozzle (1K); 6 – 1 mm nozzle (1K); 7 – solution; 8 – impregnation section; 9 – CCF spool	38
Fig. 2.4 Standard printing head: 1 – stepper motor; 2 – filament feeding unit; 3 – cooling unit; 4 – heating element; 5 – thermocouple; 6 – guide tube; 7 – nozzle	40
Fig. 2.5 Prototypes of printing heads: a – early prototype; b – improved prototype; 1 and 3 – CCF inlet; 2 – matrix inlet	40
Fig. 2.6 Improved prototype and its cross-sectional view: 1 – PTFE guides for CCF and matrix; 2 – screws for mixing chamber sealing	41
Fig. 2.7 Final design of custom printing module.....	42
Fig. 2.8 Modified <i>MeCreator 2</i> printer: 1 – printhead; 2 – Y-axis motor; 3 – X-axis motor; 4 – printing platform; 5 – Z-axis motor	42
Fig. 2.9 Isometric view of the sample: K – layer height; A – print line spacing.....	44
Fig. 2.10 Scheme of the printing process: 1 – impregnated CCF; 2 – CCF feeding channel; 3 – heating element; 4 – printing platform; 5 – thermoplastic feeding channel; 6 – thermoplastic; 7 – printing nozzle; 8 – homogenous composite filament; 9 – thermocouple; 10 – heater; 11 – borosilicate glass.....	46
Fig. 2.11 Experimental printing with the early printing module prototype	48
Fig. 2.12 Experimental printing with improved printing module prototype	48
Fig. 2.13 Scheme of the designed printing head and printing process: a – 3D printing path; b – Printing process; c – Printed samples	50
Fig. 2.14 Procedure of visual analysis: a – photo of cross-section; b – total area; c – impregnated area	52
Fig. 2.15 Adhesion testing procedure: a – sample preparation; b – testing scheme; c – prepared samples	52
Fig. 2.16 Research workflow for void volume determination by using XCT	53
Fig. 2.17 CT analysis: a – analyzed volume; b – binary threshold; c – mask from the closing procedure; d – detected air voids	55

Fig. 2.18 Research workflow for void determination using matrix dissolving procedure	56
Fig. 2.19 Experiment workflow for delamination force and shear strength	57
Fig. 2.20 Printing process: a – scheme of the printing process; b – pulling effect; 1 – improved heating element; 2 – thermoplastic; 3 – impregnated CCF; 4 – guiding tubes; 5 – nozzle; 6 – borosilicate glass plate; 7 – metal printing platform; 8 – heater; 9 – thermocouple; 10 – overlap area; 11 – steel plate; 12 – Kapton tape	58
Fig. 2.21 Printed sample: a – schematic view of the sample; b – shear area after print; A – length change after pulling	59
Fig. 2.22 Research workflow for the improvement of mechanical properties of 3D printed CCF composite structures by secondary impregnation	62
Fig. 2.23 Cross-section image of sample before and after impregnation	64
Fig. 2.24 Samples ready for the test; the principal flexural test scheme	66
Fig. 2.25 Prepared tensile sample; scheme of the tensile test	67
Fig. 3.1 Mass of carbon fiber after impregnation at different concentrations: a – 3 K carbon fiber; b – 1 K carbon fiber	69
Fig. 3.2 Optical micrographs of the cross-section of impregnated carbon fiber tow: a – 2%; b – 4%; c – 6%; d – 8%; e – 10%	70
Fig. 3.3 Tensile properties of PLA impregnated carbon fiber: a – 1K carbon fiber; b – 3K carbon fiber	71
Fig. 3.4 Tensile properties of PC impregnated carbon fiber: a – 1K carbon fiber; b – 3K carbon fiber	72
Fig. 3.5 Tensile properties of ABS impregnated carbon fiber: a – 1K carbon fiber; b – 3K carbon fiber	72
Fig. 3.6 Values of the tensile strength of samples produced by using 3D printed unidirectional composite materials: a – 1K carbon fiber; b – 3K carbon fiber	74
Fig. 3.7 Adhesion test results and samples after test: a – pullout test results; b – samples after test	76
Fig. 3.8 Content of air voids in samples: a – Group 1; b – Group 2; c – Group 3; d – Group 4	78
Fig. 3.9 Results after matrix dissolving: a – carbon fiber content in processed composite; b – volume of air voids in the structure	79
Fig. 3.10 Results of mechanical testing: a – tensile strength, b – Young's modulus	80
Fig. 3.11 Failure modes: a – the most common failure modes; b – delamination of layers; c – breaking of carbon fiber	81
Fig. 3.12 Stress-strain curves of 3D printed samples	82
Fig. 3.13 Shear force of samples in the groups with different print line spacing and layer height: a – Group 4; b – Group 2; c – Group 3; d – Group 1	83
Fig. 3.14 Shear strength of samples in the groups with different print line spacing and layer height: a – Group 4; b – Group 2; c – Group 3; d – Group 1	85
Fig. 3.15 11 printing lines of G3 group sample after the shear test	86
Fig. 3.16 11 printing lines of G4 group sample after the shear test	86
Fig. 3.17 Observed failure modes after the shear test	87
Fig. 3.18 Examples of sample fracture patterns	87

Fig. 3.19 Tensile stress-strain curves: a – Group 1 impregnated; b – Group 1 unimpregnated; c – Group 3 impregnated; d – Group 3 unimpregnated sample.....	92
Fig. 3.20 Mechanical properties: a – Tensile strength; b – Poisson’s ratio; c – Young’s modulus.....	94
Fig. 3.21 Flexural strength dependency from strain: a – Group 1 impregnated; b – Group 1 unimpregnated; c – Group 3 impregnated; d – Group 3 unimpregnated sample.....	96
Fig. 3.22 Mechanical properties: a – Flexural strength; b – Flexural modulus	97

LIST OF TABLES

Table 1.1 Most commonly used printing parameters for PLA [13, 14, 15].....	19
Table 1.2 Thermoplastics used in FDM printing [23]	20
Table 1.3 Tensile strength of 3D printed carbon fiber reinforced composite structures [57]	25
Table 1.4 Commercial FDM printers capable of continuous fiber printing [74].....	28
Table 2.1 Main characteristics of continuous carbon fiber [98]	35
Table 2.2 Main PLA characteristics [99].....	36
Table 2.3 Main specifications of <i>MeCreator 2</i> printer.....	43
Table 2.4 Recommended printing parameters	46
Table 2.5 Main parameters of printed sample groups	47
Table 2.6 Printing parameters.....	50
Table 2.7 Printing parameters.....	54
Table 2.8 Printing parameters.....	59
Table 2.9 Printed samples with 9 printing lines	60
Table 2.10 Printed samples with 11 printing lines	60
Table 2.11 Shear area overlap length difference	61
Table 2.12 Printing parameters.....	63
Table 3.1 Dissolution time of materials.....	69
Table 3.2 Dimensions of 3D printed samples.....	73
Table 3.3 Cross-sections of impregnated CCF tow and large accumulations of air voids	75
Table 3.4 Quantitative results of visual inspection.....	76
Table 3.5 Flexural sample dimensions before impregnation.....	88
Table 3.6 Tensile sample dimension before impregnation.....	89
Table 3.7 Flexural sample dimensions after impregnation.....	90
Table 3.8 Tensile sample dimension after impregnation.....	91

LIST OF ABBREVIATIONS

AM – Additive Manufacturing
CCF – Continuous Carbon Fiber
FDM – Fused Deposition Modeling
PLA – Polylactic Acid
ABS – Acrylonitrile Butadiene Styrene
PC – Polycarbonate
CF – Carbon Fiber
XCT – X-ray Computed Tomography
PCCF – Prepared Continuous Carbon Fiber
1K – 1000 yarn carbon fiber tow
3K – 3000 yarn carbon fiber tow
PETG – Polyethylene Terephthalate
HPP – High Performance Plastic
PEEK – Polyether Ether Ketone
PEI – Polyetherimide
PSU – Polysulfone
PS/ HIPS – High Impact Polystyrene
PBT – Polybutylene Terephthalate
PBS – Polybutylene Succinate
PMMA – Poly(Methyl Methacrylate)
HDPE – High-Density Polyethylene
PP – Polypropylene
PVC – Polyvinyl Chloride
TPU – Thermoplastic Polyurethane
PPSF – Polyphenylsulfone
PEKK – Polyetherketoneketone
PVDF – Polyvinylidene Fluoride
PA – Polyamide
PVA – Polyvinyl Alcohol

INTRODUCTION

Relevance of the Thesis

Nowadays, industry is moving towards *Industry 4.0* where Additive Manufacturing (AM) technologies are playing a very important role in the manufacturing of products in small and medium quantities. These AM technologies can be easily integrated in production systems and used for the fabrication of free-form products with only minor limitations and a lower amount of waste. These benefits make AM technologies more and more popular, therefore, producers and scientists are looking for novel sustainable and innovative materials denoted by high-level mechanical performance. As little as 10 years ago, the main materials in AM were standard thermoplastics and photopolymers; however, the high demand for composites and multipurpose materials can be observed in the industry and science nowadays. Composite materials offer light weight and outstanding mechanical properties of load-bearing components in comparison with the metal counterparts. Special attention is being paid to composites reinforced with continuous fibers which could be used in the automotive and aerospace industries. The Fused Deposition Modeling technology (FDM) is currently one of the most widely used and fastest advancing AM technologies. The flexibility of this technology for modifications, versatility, the rapidly expanding range of printable thermoplastic materials (which can be used as a matrix material), the advancing equipment and software as well as accessibility make it perfect selection for continuous carbon fiber (CCF) reinforced composite structure fabrication.

AM of composites reinforced with CCF is very complicated because FDM equipment is not directly applicable, hence it must be adapted with a custom or specialized printing head. Moreover, the identification of the process parameters and their influence on the FDM process must be analysed and determined. It is worth mentioning that the effectiveness of the carbon fiber tow impregnation process should be investigated in order to ensure the repeatability of the mechanical properties of the produced composite structures. The impregnation process plays a highly important role to the inter-layer adhesion, the fusion between the thermoplastic matrix and CCF reinforcement, the air void content, and the composite flowability. All these factors have an impact on the mechanical properties of printed composite structures.

The relevance of the study can be emphasized by significantly increasing the interest in additive manufacturing technologies as well as by the high demand of continuous carbon fiber reinforced structures in the industry, closure of the existing technologies and the lack of the know-how about AM manufactured composite structures.

Research Aim and Objectives

The main aim of the scientific research is to develop and validate an FDM technology for the rapid fabrication of geometry complex continuous carbon fiber reinforced composite structures. To achieve this aim, the following objectives were set:

1. To develop a carbon fiber tow impregnation technology and to investigate the influence of the impregnation solution concentration and the dissolving material on the printed CCF and thermoplastic matrix composite structures.
2. To develop a technology based on FDM for printing composite structures reinforced with CCF.
3. To investigate the quality of printed composite structures by measuring the percentage of air voids and the carbon fiber content.
4. To determine the main mechanical properties of 3D printed composite structures including tensile, flexural and shear strength, the tensile and flexural module, as well as the Poisson's ratio.
5. To investigate the influence of secondary impregnation with epoxy resin on the mechanical properties of 3D printed continuous CCF composite structures.

Research Methods

This research involved the following methods: theoretical, technological-practical, analytical, and experimental studies to develop impregnation and printing processes. By using computer-aided design, software printing equipment was designed. The following software tools were used in this study: *MATLAB*, *Simplify3D*, *PrusaSlicer*, *SolidWorks*, *Avizo*, *ImageJ2x* and *NIS Elements D*. The research work was carried out at the Faculty of Mechanical Engineering and Design of Kaunas University of Technology, the Department of Production Engineering, the Institute of Mechatronics and the Institute of Ultrasound. The developed technology has been experimentally tested by determining the mechanical properties using universal machine *Tinius Olsen H25KT*, the air void content was determined by two methods: by using the *ImageJ2x* image processing software package and an automated *Nikon Eclipse LV100ND* microscope with a high-resolution camera *DS-Ri2*, whereas the defectoscopy tests were conducted by means of the X-ray computed tomography system *RayScan 250E*.

Scientific Novelty

1. A novel method for improving the technological process of CCF impregnation has been developed.
2. An innovative custom extrusion module has been developed which is capable to produce CCF reinforced composite structures.
3. The process for improving the tensile and flexural properties of printed structures, the secondary impregnation at vacuum chamber in epoxy resin has been developed and tested.

Practical Value

The manufacturing methodologies and equipment developed in the course of this research can be used for the production of continuous carbon fiber reinforced composite functional parts of a complex structural design. The results of technological development, such as various impregnation techniques, printing modules and the identification of the most suitable FDM process conditions as well

as parameters can be used for rapid fabrication of customized lightweight functional components employed in the automotive and aviation industries or medical sectors and any other newly emerging scope of applications including but not limited to autonomous robotics, human assistive devices, vehicle or aircraft parts where the mass-to-stiffness ratio is of top importance. The developed technologies and equipment are dedicated to use with a wide range of CCF tows with minimal adjustment. The mechanical properties and print quality characterizations of printed composite structures provide valuable information and knowledge for the further technological development of the process.

Statements to be Defended

1. The developed continuous carbon fiber impregnation technological process is capable of decreasing the air void content while increasing the interlayer and matrix-reinforcement adhesion and printability.
2. The developed technological process and the original custom-made extrusion module based on the FDM technology is capable to ensure the manufacturing of continuous carbon fiber reinforced composite structures.
3. The mechanical properties of printed composite structures may be improved by the developed process of secondary impregnation.

Research Approbation

The results of this dissertation were published in 4 scientific papers: 3 in international journals with the impact factor indexed in the *Web of Science* database, and 1 without it.

The research results were also presented at 7 international scientific conferences: Mechanika 2018 (Kaunas, Lithuania), iCAT 2018 (Maribor, Slovenia) 3D printing technology and innovations 2019 (Rome, Italy), Advanced materials and technologies 2019 (Palanga, Lithuania), POLCOM 2020 (Bucharest, Romania), Conference on composite structures 2021 (Porto, Portugal), MECHCOMP7 2021, (Porto, Portugal).

Part of the research activities was funded by projects *Additive Manufacturing of Continuous Fibers Reinforced Polymer Composite Materials for High Performance Structural Applications* and *Investigation of 3D Printing Technologies Possibilities of Polymeric Matrix Composite Structures Reinforced with Continuous Carbon Fibers*.

Structure of the Dissertation

The dissertation consists of an introduction, three chapters, conclusions, references, and the list of the author's publications. The total volume of the dissertation is 134 pages, 55 figures and 24 tables. The list of references contains 102 sources. In the Literature overview, the main principles of Fused Deposition Modeling are analyzed together with the main materials used in this technology, along with the currently existing composite materials and printing methods which were examined in detail. The Methodology part describes how all the planned studies were performed, thereby explaining the development of an innovative

additive manufacturing technology and the FDM printing module. The Results chapter presents the main experimental achievements: the void content results, the mechanical properties of the composite material, the effectiveness of the secondary impregnation method and its impact on the strength of printed structures.

1. LITERATURE OVERVIEW

Additive manufacturing (AM) or 3D printing is one of the most rapidly developing and increasingly more sophisticated non-traditional manufacturing methods. This innovative manufacturing technology with a virtually unlimited potential originated in the 1980s. As the name of this technology suggests, its principle is the creation of a three-dimensional object (product) by using the layer-by-layer manufacturing method. Subject to the additive manufacturing technology, it allows almost full elimination of any production waste because the product is created from zero rather than cut out of a standard workpiece: the only waste is the structural supports. When comparing the additive manufacturing technologies with the traditional manufacturing methods (such as grinding, milling, casting, etc.), AM technologies are characterized not only by higher productivity (especially in the case of prototyping), applicability, universality and individuality, but they also provide the developer with virtually unlimited freedom of design, geometry or shapes. It usually offers a great advantage if compared with the traditional manufacturing methods [1]. Additive manufacturing is becoming increasingly more widespread in industrial applications. This innovative and extremely flexible manufacturing technology goes hand in hand with the traditional manufacturing methods and, quite often, even fully replaces them. It is fairly popular in the automotive, aviation, medicine as well as a few other industries [2, 3]. One of the main problems which seriously restrict a wider application of the additive manufacturing technologies was the limited choice of printing materials. Printing materials are usually limited to various polymers: polylactic acid (PLA), polycarbonate (PC), acrylonitrile butadiene styrene (ABS), etc.; however, these technologies can now offer various materials ranging from thermoplastics and metals [4, 5] to ceramics [5, 6, 7], or composites [8, 9] to biocompatible materials [10]. Although additive manufacturing covers many different technologies, they are usually classified into seven main categories described under the scope of ASTM F 42 Standard:

1. VAT Photopolymerization: this technology uses a liquid photopolymer resin. The product is made layer by layer by hardening a liquid light-sensitive material with a laser or any other source of light.
2. Material Jetting: in this case, the product is created by ejecting the material layer by layer in drops or by any other method and by hardening it afterwards. The principle of this technology reminds of the principle of the ink-jet printer.
3. Binder Jetting: this technology uses two different materials: the model and the binder. The binding material is usually in the liquid state, whereas the main material is a powder.
4. Material Extrusion: it is one of the most popular technologies due to its simplicity and easy modification. In this case, the printing material is melted in the printing head and extruded layer by layer through the printing nozzle on the printing platform.
5. Powder Bed Fusion: a group of the most common types covering such technologies as Direct Metal Laser Sintering (DMLS), Selective Laser

Sintering (SLS), Electron Beam Melting (EBM), etc. In this case, the powder-form material is usually melted by using a CO₂ laser or an electron beam.

6. Sheet Lamination: this group covers such technologies as Ultrasonic Additive Manufacturing and Laminated Object Manufacturing. In the case of manufacturing based on the ultrasonic technology, the product is created by connecting sheets of metal by using ultrasound.
7. Direct Energy Deposition: it is one of the most complicated groups of additive manufacturing technologies which covers several different methods, such as Laser Engineered Net Shaping, Direct Metal Deposition, Direct Light Fabrication or 3D Laser Cladding. This printing group is usually used in order to repair or add additional material onto already existing elements or components.

This research work focuses on material extrusion based on the Fused Deposition Modelling (FDM) technology and its applicability to print CCF reinforced composite structures.

1.1. The Principle of Fused Deposition Modelling Technology

Fused Deposition Modelling is one of the earliest and one of the most widely used additive manufacturing technologies [11] characterized by the simplicity of the process, and, if necessary, the possibility of easy variation between the process parameters or the modification of equipment, wherever necessary [12]. According to ISO/ASTM 52900:2017 Standard, the FDM technology is assigned to additive manufacturing processes based on material extrusion. The principal scheme of this technology is illustrated in Fig. 1.1.

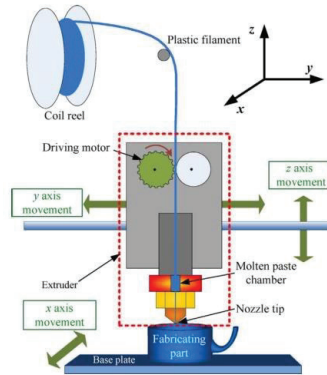


Fig. 1.1 Principal scheme of FDM printing process [13]

As shown in Fig. 1.1, the thermoplastic filament that is pulled from the coil reel by the driving motor passes into the heating element of the printing head (extruder). The heating element is heated up to the melting temperature of the thermoplastic material which is being used. The melted thermoplastic is extruded onto the printing platform through the printing nozzle. Subject to the thermoplastic used in the printing process, the printing platform is also heated up to the respective temperature to achieve better adhesion between the printed model and the platform.

Depending on the printer design, the printing platform can move in the x , y or z directions, i.e., if the printing head moves in the x and y directions, then the printing platform will move only in the z direction, and, vice versa, if the printing head moves in the z direction, the platform will move in the x and y directions. Other combinations of movement trajectories of elements are also possible. Table 1.1 below presents the most common printing parameters for printing PLA thermoplastic.

Table 1.1 Most commonly used printing parameters for PLA [13, 14, 15]

Nozzle diameter, mm	0.25/0.4/0.8
Printing speed, mm/s	30–80
Print line spacing, mm	0.45
Extrusion multiplier, %	100
Layer height, mm	0.06–0.3
Printing head temperature, °C	180–220
Platform temperature, °C	60
Cooling, %	60–100

The quality of the printed structure is mostly affected by the printing nozzle, the speed of printing and the height of the layer. When the diameter of the printing nozzle, the height of the layer or the printing speed increases, the quality of the printed product inherently decreases, but the printing time of the model is significantly reduced. In order to print the model of the maximum accuracy, the above mentioned parameters have to be as low as possible. It is particularly important to pay attention to the proper selection of the height of the layer as it bears the greatest impact on the roughness of the surface of the printed model [13]. Another important printing parameter that is related to the mechanical properties of the structure to be printed is the printing direction and the raster angle [16]. The proper selection of the printing parameters not only exerts influence on the quality of the structure of the model to be printed, the roughness of the surface, and on the number of voids in the structure, but also on its mechanical properties. Therefore, it is fundamentally important to choose the optimum printing parameters when using this technology [17, 18]. FDM technology printers, subject to the construction properties and the manufacturer, can use a Ø1.75 mm (*Prusa*, *Raise3D*, etc.) or a Ø2.85 mm (mainly *Ultimaker*) thermoplastic filament.

1.2. Overview of the Materials Used in FDM Technology

Traditionally, the FDM technology uses various thermoplastics that are different from one another not only by the melting temperatures, but also by the chemical, mechanical and physical properties [19]. The most common thermoplastics used in this technology include PLA, Nylon, ABS, PC, and polyethylene terephthalate (PETG) [20]. These thermoplastics are used due to the rather low printing temperatures, good mechanical characteristics and excellent compatibility with the FDM technology itself. Yet, at the moment, high-performance plastics (HPP), engineering thermoplastics, such as polyether ether ketone (PEEK), polyetherimide (PEI), polysulfone (PSU), etc., are becoming

increasingly more popular and available for wider application in the FDM technology [21]. These thermoplastics are characterized by high resistance to environmental factors, such as a high operating temperature, a high pressure, or high resistance to friction or chemically aggressive environments. According to Hergenrother *et al.* [22], high-performance polymers should meet the following requirements:

1. Have a high glass transition temperature and high mechanical characteristics;
2. Change in the mass should not exceed 5% when working at a temperature of 450 °C;
3. Loss of mass under higher operating temperatures should be minimal;
4. The polymer shall maintain high mechanical, chemical, physical properties under temperatures up to 177 °C;
5. The temperature that causes 10% deformation under 1.52 MPa load should not be lower than 177 °C.

Table 1.2 provides summarized information about the most commonly used thermoplastics in the FDM technology, their applications in 3D printing, mechanical characteristics and printing temperatures. Where the properties of a material are illustrated with the plus and the minus sign, the more pluses or minuses, the better or worse are the characteristics, and +/- means that it is difficult to evaluate the characteristics.

Table 1.2 Thermoplastics used in FDM printing [23]

Polymer	Extrudability	Printability	Mechanical Properties	Printing Temperature, °C	Ultimate Tensile Strength, MPa
PLA	+/-	++	—	180–210	37–46
ABS	++	++	+	210–250	22–37
Nylon	+	+/-	+	235–260	34–68
PS/HIPS	++	+	+/-	240	20–42
PETG	+	++	+/-	230–250	41–53
PBT	+	+	+	220–250	39–60
PBS	+	+/-	+	120–140	19–34
PC	++	+/-	++	275–285	57–72
PMMA	+	—	+	180–250	52–70
HDPE	+	+/-	+	120–150	11–45
PP	+	+/-	+	130–170	9–80
PVC	+/-	+/-	++	200–300	1–59
TPU	+/-	+	+	210–225	6–33
PEI	++	+	++	350–390	69–81
PEEK	++	+	++	360–450	48–265
PPSF	++	+	+/-	350	55
PEKK	++	+	++	350	90–110

Innovative materials, such as a polymer characterized by piezoelectric properties – polyvinylidene difluoride (PVDF) – are becoming increasingly more popular. This substance is attractive due to the possibility to print complex piezoelectric sensors and equipment [24].

Composites are materials made of two or several different constituent materials. One of them is a binding material – the so-called matrix – whereas the other one is the material that improves the physical, chemical or mechanical properties of the binding material, the so-called reinforcement. Composite materials that are currently being used in the FDM technology can be classified into three groups [25]:

1. Advance thermoplastic composites;
2. Nanomaterial reinforced composites;
3. Fiber reinforced composites.

Advanced thermoplastic composites cover composite materials with a thermoplastic binding material and the reinforcement composed of various metal particles and their compounds. Subject to the reinforcement material in use and its quantity, such composite materials can significantly improve the mechanical properties of the printed structure, such as the tensile or flexural strength, the Young's modulus, and the elongation coefficient. However, the insertion of these substances into a thermoplastic also leads to considerable adjustment of the fluidity of the matrix material, the mixing characteristics, the printing quality, the layer adhesion and some other parameters. In the scientific literature, the most common are Fe-Nylon [26], Fe-ABS [27], copper-ABS composites [28], strontium titanate (SrTiO_3)/ABS [29] or alumina (Al_2O_3)/ABS [29], tricalcium phosphate/polypropylene [30], hydroxyapatite/polylactic acid (PLA) [31], Graphite/PA6/PS/POE-g-MAH [32] and other composites. Metal additives are used to the filament in order to obtain the metal gloss and the metal appearance of the printed products. The change in the mechanical characteristics highly depends on the type of reinforcement, the size and the quantity of particles. These parameters have impact on the adhesion of the printed composite structure. However, the tricalcium phosphate/polypropylene composite can be used in medical applications due to its higher biological compatibility and applicability [30], whereas hydroxyapatite/polylactic acid (PLA) is a material characterized by melting of fine cracks when heated, or else it is characterized by the shape memory effect [31].

Nanomaterial reinforced composites are composites made of a polymeric matrix and a reinforcing material with the particle size less than 100 nm. Nano particles can provide composites with better mechanical, electromechanical, thermal, optical and other physical properties [25]. The properties provided to the composite by the reinforcement material depend on the size of the particle [33]:

1. <5 nm – increases the activity of the material as a catalyst;
2. <20 nm – provides softness to a hard material;
3. <50 nm – changes the reflective index of the material;
4. <100 nm – improves the mechanical, magnetic or electrical properties of material.

The most common reinforcement materials used in the FDM technology include graphene oxide [34], titanium oxide [35], zinc oxide [36], cloisite 30B [25], carbon nanotubes [37]. Added to the PLA matrix titanium oxide does not change the mechanical properties of the material; however, the structure of the polymer becomes more stable due to the stronger covalent chemical bonds. In addition, this printed composite structure is biocompatible, and, due to its high potential, it can be used in medical applications, for example, in the replacement of a bone after a fracture. The insertion of ZnO provides the composite with shape memory properties. According to Singh *et al.* [36], the tensile strength of printed composite structures reached 14.32 MPa, whereas the Young's modulus was 234 MPa. When using graphene oxide as the reinforcement nanomaterial, the tensile and compression modules of printed composites increased by 75.5% and 167%, respectively if compared with the mechanical characteristics of the thermoplastic matrix; moreover, the thermal stability of materials also increases. According to Chen *et al.* [38], such composites are denoted by huge potential in the field of medicine due to their biocompatibility with NIH_3T_3 cells. However, when adding nanoparticles to a polymeric matrix, the decrease in the layer adhesion of printed composite structures was noticed in almost all cases.

Fiber reinforced composites are one of the most popular groups of composites used in the FDM technology. Fused deposition modelling is one of several additive manufacturing technologies capable of printing both short and continuous fiber reinforced composite structures [39]. Two main subgroups are distinguished: composites reinforced with natural fibers and synthetic fibers. Jute is the most commonly used natural fiber. However, the natural fiber is rarely used for composites printed with the FDM technology. As noted by Torrado *et al.* [29], when experimenting with printed composites of this reinforcing type, at higher temperatures, the jute fiber loses mechanical properties, and air voids start appearing in the structure due to thermal degradation. As a result, adhesion between the layers of printed composite structures decreases, and the tensile strength of the material decreases more than twice in comparison with the pure ABS – from 17.7 MPa down to 8.6 MPa, respectively. Other experiments with this fiber revealed similar tendencies: air voids appear because of the irregular and chaotic orientation of fiber in the structure, and low adhesion between the fiber and the matrix [12, 40] may develop. Synthetic fibers, such as glass, Kevlar and carbon fiber, are more common. As mentioned above, all these fibers could be used as short or continuous. In the scientific literature related to composites printed with the FDM technology, glass or Kevlar fiber are less common than carbon fiber. In one of the experiments, Carneiro *et al.* [41] tested the use of short glass fiber as a reinforcement material in the polypropylene thermoplastic matrix, and determined that, after adding 30% of glass fiber, the tensile module and the tensile strength of composite structures increased approximately by 30% and 40%, respectively. Another study focused on the possibilities of application of glass fiber together with ABS. Considerable improvement in the mechanical strength characteristics of the material was noted; however, it reduced the flexibility of the printed structures [42]. Gholamhossein *et al.* [43] carried out detailed studies related to the use of short glass fiber when

printing composite structures with the PP matrix: 30% of short glass fiber was mixed with the filament during the test. Mechanical, rheological and morphological characteristics of printed composite structures were analysed during these studies. Such printed composite structures have been observed to possess the tendency of shrinkage and deformation. Furthermore, although the tensile strength increased from 20 MPa (pure PP) up to 34 MPa, accordingly, after entering short glass fiber as the reinforcement material, it had a negative effect on the plasticity of the structure thus causing it to deteriorate, while the elongation of samples up to the fracture point decreased almost twice.

1.3. Printing Carbon Fiber Reinforced Composite Structures by FDM Technology

Carbon fiber is the most widely used reinforcement material in the FDM technology. It comes in the form of both continuous fiber and short fiber. The use of and the demand for carbon fiber has been increasing recently. In the early 2010s, the carbon fiber market amounted to 1.75 billion EUR, and it is now forecasted to grow by 10–12% in the next year [44]. With the increasing global demand, the interest in the application of this fiber for the reinforcement of structures printed with the FDM technology also increases. The summarized possibilities and technologies of carbon fiber reinforced printed composites manufactured with the FDM technology are provided in Fig. 1.2.

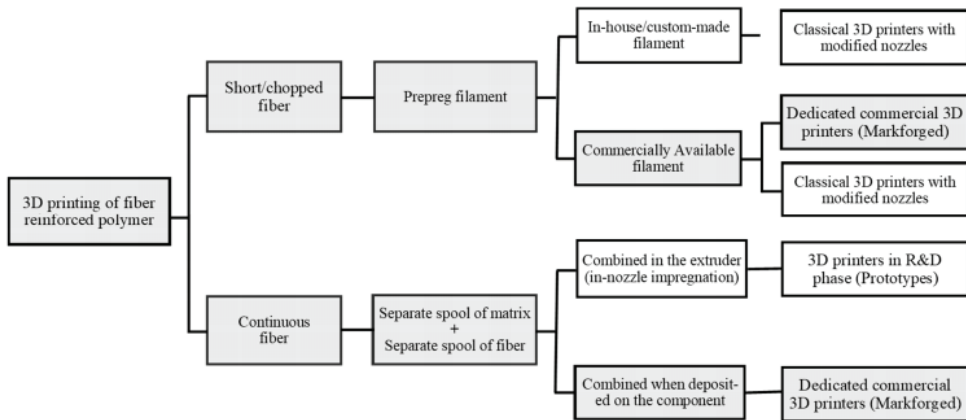


Fig. 1.2 Technologies of carbon fiber reinforced printed composites manufactured with FDM technology [45]

1.3.1. Short Carbon Fiber

Prior to 2016, short carbon fiber was the most widely used state when printing carbon fiber reinforced structures with the FDM technology. The first article by Matsuzaki *et al.* [12] on continuous carbon fiber reinforced structures printed with the FDM technology which was published in 2016 triggered a huge breakthrough and gave rise to a considerable interest among scientists, thereby reducing short carbon fiber reinforced structures to the second choice in terms of popularity.

However, the use of this technology and the choice of the short carbon fiber as the reinforcement material offers several advantages if compared with the continuous carbon fiber. First of all, a reinforcing material is inserted into the matrix, i.e., a thermoplastic filament, during the filament preparation stage. It allows avoiding replacement and modification of the printing equipment; in other words, composite structures can be printed by using the same FDM printer just like non-composite structures. Another advantage is the reliability and stability of the printing process. As the reinforcement material is inserted in the standard thermoplastic filament (PLA, ABS, Nylon, etc.), the printing parameters, such as the temperature, the speed of printing, the height of the layer, do not change much if compared with the pure matrix material used for printing. Another important aspect that makes the printing process reliable is the simplicity of equipment compared with the continuous carbon fiber printing equipment. It should be noted that, when printing composites with FDM printers, it is recommended to choose the printing nozzle of hardened steel or ruby. Due to the higher abrasion impact of the printing material on the printing nozzle, the soft printing nozzle (made of bronze) tends to wear fast, thus losing the initial size of the output diameter. It has negative influence on the quality and precision of the surface of printed structures.

Short carbon fiber reinforced structures are characterized by improved mechanical properties if compared with the structures printed with pure matrix material [46]. Ning *et al.* [47] and his team examined materials of various fiber percentage fillings – 3, 5, 7.5, 10 and 15% ABS and short carbon fiber materials. According to the results of these experiments, after inserting 15 wt% of short carbon fiber into the ABS matrix, the tensile strength of the composite structure reached 42 MPa, and a Young's modulus value of 2.5 GPa was achieved.

Although composite structures can be printed with short carbon fiber by using the standard printing parameters recommended for the thermoplastic matrix, however, their quality and mechanical properties heavily depend on such printing parameters as the height of the layer, the speed of printing, the raster angle and width [48]. It is recommended to choose a slightly higher printing temperature and a lower printing speed if compared with a single polymeric material. It is worth noting that, although the insertion of carbon fiber into the matrix material increases the mechanical properties of the printed structures, it also reduces the adhesion between the layers. Lee *et al.* [49] carried out tests with two different sample printing orientations: the first group was printed along the x axis, whereas the second one was printed along the z axis. The obtained results revealed that, when printing samples in the x axis direction, they became stiffer and stronger, however, the strength of the samples printed along the z axis decreased due to low adhesion between the printed layers. Another important factor that has an effect on the mechanical characteristics of composite structures is the orientation of short fiber in the printed structure. If fiber is oriented along the tension force vector, its numerical value will be higher [50]. Due to these characteristics, printing with the FDM technology always results in air voids between the printing lines or layers [51]. However, the insertion of short carbon fiber into the filament dramatically increases the number of air voids. Due to poor adhesion between the fiber and the matrix, air

voids appear not only between the printing lines and layers, but also between the matrix and the reinforcement material [46]. The number of air voids which appear due to the technology itself can be controlled by the optimization of the printing parameters and the diameter of the printing nozzle. Unfortunately, it is almost impossible to control how many voids are caused by the reinforcing material [52]. Due to this phenomenon and a slight increase in the mechanical characteristics along with low adhesion compared with the pure matrix material, when searching for alternatives, scientists switched their focus towards continuous carbon fiber and the possibilities of its application in the printing of composites with the FDM technology. A brief list of the tensile strength values of composite structures is provided in Table 1.3.

Table 1.3 Tensile strength of 3D printed carbon fiber reinforced composite structures [57]

Reinforcing material	Matrix material	Tensile strength, MPa
CCF	PLA	74.2–541.7 [53]
CCF	PLA	40–185 [12]
CCF	ABS	30–200 [54]
CCF	PLA	110–335 [20]
CCF	PLA	28–91 [55]
CCF	PLA	34–203 [56]
SCF	ABS	35–65 [46]
SCF	PLA	68.3–100 [57]
SCF	PA6	38–86 [58]
SCF	ABS	3.14–4.9 [59]
SCF	PTFE	33.8–85 [60]
SCF	PP	38.2–43.4 [61]

As it can be observed from the data provided in Table 1.3, after the insertion of continuous carbon fiber, the tensile strength can be three times higher compared with short carbon fiber.

1.3.2. Continuous Carbon Fiber

As the industry is rapidly moving towards the fourth industrial revolution, additive manufacturing becomes one of the key factors to achieve this goal [62, 63, 64]. With the new AM application possibilities emerging, the demand and requirements for printing materials is increasing as well. The use of continuous carbon fiber in the FDM technology was first described by Matsuzaki *et al.* [12] in 2016. Since then, the number of scientific publications and the number of studies has indicated an exponential increase over the last six years, which is witnessed not only by the number of publications related to the mechanical properties, printing process or preparation of fiber increases, but also by the number of overview articles [65].

Five major printing methods for continuous carbon fiber reinforced composites using the FDM technology can be found and distinguished in today's scientific publications:

1. In-situ impregnation: untreated fiber passes to the printing nozzle, whereas the matrix material is fed through one or several entry channels. The fiber is impregnated in the heating element just before the composite yarn passes from the printing nozzle onto the printing platform [66].
2. Co-extrusion with towpreg: instead of untreated fiber, continuous carbon fiber that is processed before printing passes to the printing nozzle at the same time as the matrix material. Usually, the material for carbon fiber impregnation or preparation is the same as the printed composite matrix material [20, 55].
3. Towpreg extrusion: impregnated carbon fiber is extruded without any additional matrix material [53].
4. In-situ consolidation: this is a technology based on automatic fiber layout in the thermoplastic model. In this case, treated or untreated carbon fiber is fed via the printing nozzle to the working area. In the working area, an external thermal source heats the working area or the previously printed layers, and the roller presses the fiber into the matrix [66].
5. Inline impregnation: fiber is impregnated during the printing process, just before the carbon yarn passes to the printing head.

Schemes depicting each technology are provided in Fig. 1.3.

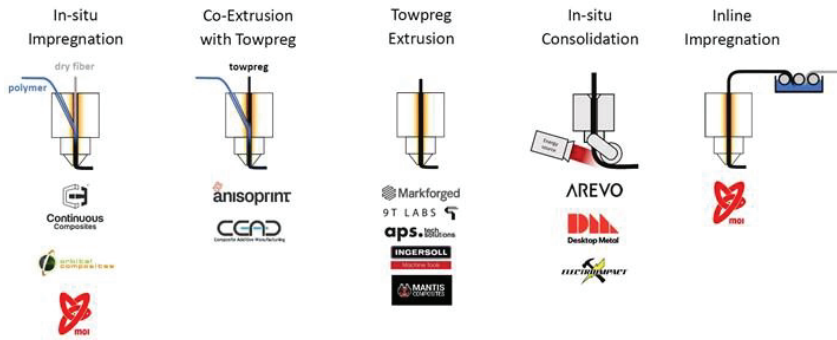


Fig. 1.3 Methods to print continuous carbon fiber reinforced composite structures by using FDM technology [67]

The most common of the five methods referred to above are the co-extrusion with the towpreg and the towpreg extrusion methods. Two entry channels are used in the co-extrusion technology: one for the impregnated carbon fiber and one for the polymer matrix. Secondary fiber impregnation takes place in the printing head. Then, the composite filament is extruded through one printing nozzle onto the printing platform [54]. The towpreg extrusion method is characterized by a slightly different principle. Here, the printing head has two separate printing nozzles. One nozzle prints only the matrix material, while the other one prints only the reinforcing material [68]. This method is denoted by several advantages if compared with the single printing nozzle system. First of all, the two-nozzle system offers more freedom when printing a composite structure, as the carbon fiber can be inserted only where it is required the most. This allows reducing the production costs, and, usually, the duration of printing as well, as the printing of only matrix material

allows benefiting from a higher printing speed. It is worth mentioning that, when applying the towpreg extrusion method, only the polymer matrix or only the reinforcing carbon fiber can be printed at once. In other words, separate printing nozzles never function at the same time [69]. This gives rise to the advantage of the co-extrusion method: the secondary impregnation of printed carbon fiber in the printing head just before the composite yarn passes onto the printing platform. Since the fiber has no possibility for secondary impregnation when printing composites by the towpreg method, it is printed onto the base of the polymer matrix straight away, and, after the completion of the insertion of the reinforcement material, the matrix substance is printed onto the fiber again. It allows creating composites without the secondary impregnation of fiber, and this has impact on the strength, stiffness and adhesion of the printed composite structures. In the case of co-extrusion printing, it is important to ensure a smooth and constant feed of the impregnated carbon fiber and the polymer matrix to the printing area. Any disruptions or deviations exert influence on the mechanical and quality properties of the printed structure [70]. With the improvement of the printing equipment and the increase of robotization, such printing heads and methods of printing composites with the FDM technology can be transferred to robots manipulators (5-axis movement), thus providing much more flexibility and freedom to the technologies for the creation of essentially unlimited geometry and shapes [71].

At the moment, there are about fifteen companies on the market that are offering or investing in the creation and development of continuous carbon fiber reinforced technologies for printing with the FDM technology. These companies are listed in Fig. 1.3. Two companies need to be distinguished among them, notably, *Markforged* and *Anisoprint*. *Markforged* was founded in 2014 as a start-up in the US and is now occupying a major share of the market of printing carbon fiber reinforced composites. *Markforged* printers use the towpreg extrusion method, i.e., they have two separate printing nozzles. The most common matrix material in use is nylon containing short carbon fiber. Reinforcement materials can include continuous fibers, such as carbon fiber, Kevlar, or glass fiber [72]. *Anisoprint* is a Russian company which also started to operate as a start-up in 2014. Unlike *Markforged*, *Anisoprint* printers are based on the co-extrusion with the towpreg method, i.e., they have only one printing nozzle and two input channels for the impregnated fiber and the thermoplastic matrix. This producer offers continuous 1.5K carbon fiber as the reinforcement material, and smooth PA as a matrix material [73]. Summarized information about commercially available printers printing only continuous fiber reinforced structures is provided in Table 1.4.

When summarizing, it is important to focus on the type of software. *Closed source* (Table 1.4) means that only continuous carbon fiber or thermoplastic filament of the same manufacturer can be used, whereas *open source* (Table 1.4) allows the user to choose any printing material. Currently, the majority of scientific studies covering the testing of mechanical or quality properties of structures printed with the continuous carbon fiber reinforced FDM technology are carried out by using *Markforged Mark One* or *Mark Two* printers and materials. However, as this field is becoming increasingly more popular, more and more scientists start

modifying FDM printers by themselves by creating printing heads, by searching for the optimum printing process, its parameters and possibilities for the preparation or impregnation of carbon fiber before printing [75, 76, 77].

Table 1.4 Commercial FDM printers capable of continuous fiber printing [74]

Company	Printer	Software type	Fiber material	Working principle	Available since
Anisoprint	Composer A4/A3	Open source	Carbon, Glass, Aramid	Co-extrusion with towpreg	2014/2016
Markforged	Mark One/Two	Closed source	Carbon fiber	Towpreg extrusion	Early 2020
CEAD	CFAM Prime		Carbon, Glass	Co-extrusion with towpreg	2018
Desktop metal	Fiber series				Early 2020

Scientists are creating alternatives of commercial products with the purpose to examine in detail the impact of the parameters of the printing process, the printing construction, the shape and size of the printing nozzle, the materials and preparation needed for printed composite structures. The companies do not share most information how this technology operates, what the critical printing parameters are, and how the carbon fiber is impregnated, etc. This issue limits not only the further testing of this field and better understanding of the technology, but also its development and improvement.

1.4. Preparation of Carbon Fiber before Printing

One of the main problems when printing fiber reinforced composite structures is the low adhesion between the matrix and the reinforcement material. This problem is relevant both when printing with short carbon fiber and continuous carbon fiber. However, this problem can be reduced by impregnating or treating continuous carbon fiber before printing. Carbon fiber tow consists of several hundred to several thousand smaller fibers that not only cause problems with adhesion but also pose difficulty in terms of feeding to the printing head, thus, making the printing process more difficult and less reliable. Currently, most of the continuous fibers used for printing with the FDM technology are either treated or impregnated. The ultimate goal for this is to improve the adhesion between the reinforcement and the matrix material as well as to bind separate fibers [78, 79]. The impregnating material should be selected considering the compatibility and cohesion with the matrix material. When producing composite structures, the carbon fiber tow is usually impregnated or covered with a thin layer of epoxy resin. However, impregnation with epoxy resin is not recommended for 3D printing due to the high printing temperatures, as it begins to degrade when it reaches 250 °C [80]. It is possible to find several examples in the scientific literature on how the fiber is treated before printing [81, 82]. Essentially, there are two methods:

1. Pouring of the matrix material onto the carbon fiber before printing;
2. Covering the carbon fiber with polymer by evaporating the solvent material.

The more common one is the pouring of matrix material onto the fiber. It is used due to its simplicity and safety, as no additional chemical substances or solvents are required. The process scheme is provided in Fig. 1.4. The carbon fiber from the coil travels to the heating pipe where it is heated, and, from there, it passes to the filling chamber where it is submerged into the melted matrix substance. Then, it travels through the nozzle to the heating chamber filled with water, and then it is dried and twisted on the prepared fiber coil. Examples of this type of preparation of carbon fiber can be found in the studies by Hu *et al.* [53] and Iragi *et al.* [83]. A great advantage of the fiber prepared in this way is the possibility to print without feeding any additional matrix material to the printing head. It depends on the diameter of the prepared fiber, or, in other words, on the quantity of the matrix material on the fiber.

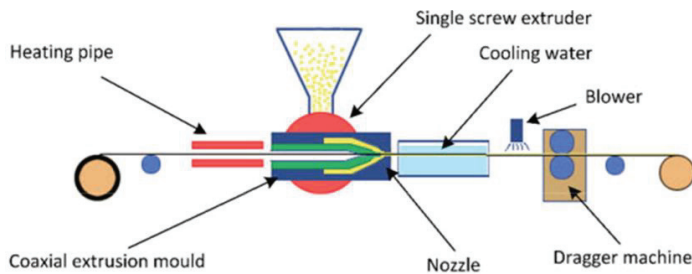


Fig. 1.4 CCF preparation by melted matrix material [53]

Another way to prepare a fiber before printing is to impregnate it in thermoplastic solutions. One of the examples of this impregnation is provided in Fig. 1.5. In this case, a thermoplastic or any other impregnating material is dissolved in the solvent by selecting the necessary concentration. Carbon fiber is passed through the bath of such a solution and dried, and then it can be used for printing. The repeated passing of such impregnated fiber through a nozzle of a small diameter is usually used after such impregnation. This is done in order to remove the cavities appearing inside the impregnated fiber and to remove the excess of impregnated material on the fiber, thus providing it with the necessary geometry and shape.

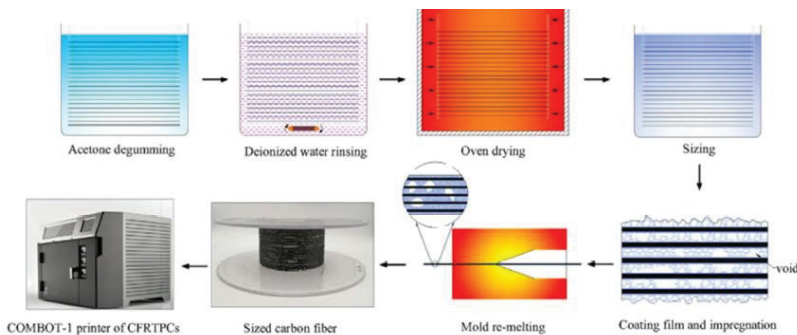


Fig. 1.5 CCF impregnation by thermoplastic solution [84]

The substances used in impregnation, such as PVA [85], PA6 [84, 86] and others, are listed in the scientific literature. CCF impregnation by thermoplastic solution is more advantageous because the impregnation medium is of lower viscosity, and thus it is easier for the impregnated material to penetrate inside the fiber tow and provide better bonding characteristics between the individual fiber yarns compared to the thermoplastic melting method. Furthermore, due to the lower amount of the impregnation material on the fiber, it remains flexible and less brittle.

1.5. Mechanical Properties of 3D-printed Continuous Carbon Fiber Reinforced Composites

One of the main reasons for the insertion of carbon fiber into the polymer matrix is to improve the mechanical properties of printed structures. The majority of scientific research related to the mechanical properties of 3D-printed continuous carbon fiber reinforced structures is currently oriented towards the determination of the tensile strength. Only a third of such tests include experiments related to the resistance to bending or compression. It is reflected in Fig. 1.6.

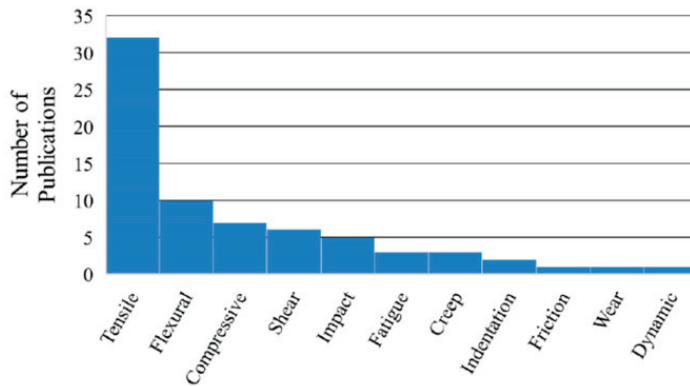


Fig. 1.6 Number of publications of continuous carbon fiber reinforced 3D printed composite structures investigations over 6 years (2016-2022) [45]

The mechanical characteristics of printed composites depend on the printing parameters, the percentage of carbon fiber, and the layout of fiber on the printed structure [87]. Summarized results of tension tests published from 2016 to 2020 are provided in Fig. 1.7. Nanya *et al.* [55] were among the first to test continuous carbon fiber reinforced structures. It was revealed that, after adding impregnated continuous carbon fiber to the PLA matrix, the tensile strength reached 91 MPa. Matsuzaki *et al.* [12] also performed tension tests with the continuous carbon fiber reinforced PLA matrix and achieved 185 MPa tensile strength. According to the authors, the carbon content in the samples amounted to 6.6% and more. In 2017, Bettini *et al.* reached 203 MPa tensile strength after inserting approximately 6% CCF into the printed PLA structure [56]. In the same year, Dickson *et al.* [88] inserted approx. 11% continuous carbon fiber into the Nylon polymer matrix and reached 216 MPa tensile strength. Haider *et al.* [89] also experimented with the tensile strength of Nylon and continuous carbon fiber structures (at a ratio of 60–40%). The tensile

strength of such structures was found to reach 330 MPa. Isobe *et al.* [90] achieved similar results with the PLA (10% short fiber) matrix by inserting approx. 35.7% continuous carbon fiber, and, in this case, the tensile strength of the structure reached 360 MPa. In 2019, when testing continuous carbon fiber reinforced Nylon composites, Cagri *et al.* [91] achieved 250 MPa tensile strength when the carbon fiber content amounted to 14.1% of the volume of the structure. Whereas, Mohammadizadeh *et al.* [72] experimented with continuous carbon fiber reinforced Nylon composites with the carbon fiber content amounting to 58%. When carrying out tension tests, 404 MPa tensile strength was achieved. 109 MPa tensile strength was reached when testing continuous carbon fiber and PLA matrix composite structures without additional impression of printed yarn into the printing platform. Zhang *et al.* [70] tested samples with 10.3% carbon fiber. In the same year, Dou *et al.* [92] also carried out tests with the PLA matrix and continuous carbon fiber reinforcement composites with the fiber content amounting to approx. 24% and achieved 244 MPa tensile strength. It could be summarized that the tensile strength mostly depends on the carbon fiber content in the printed structure: the higher is the percentage, the higher is the tensile strength. However, a tendency of the increase in the tensile strength is obvious when printing with the PLA matrix. From barely 91 MPa in 2016, it reached 244 MPa (24% more) in 2020. This was achieved by improving printing process, optimizing parameters and equipment. With the development of technologies, scientists find ways to insert increasingly more carbon fiber into printed composite structures.

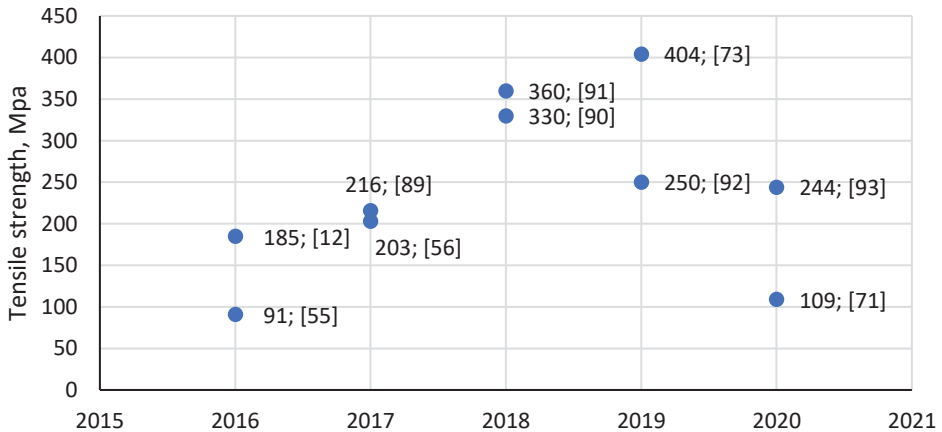


Fig. 1.7 Tensile strength results for years 2016–2020 as referred in scientific publications

The earliest bending tests with printed continuous carbon fiber reinforced composites were carried out in 2016. The summarized 5-year results of flexural strength are provided in Fig. 1.8. As it can be seen from the figure, the strength when bending varied from 133 MPa [12] to 335 MPa in 2016 [20]. In both cases, the composite material was made of the PLA matrix and continuous carbon fiber with the percentage content reaching 18% and 27% in the structures. In 2017, the tensile

strength reached 147 MPa in ABS/CCF in samples with 10% carbon [54] and 263 MPa in PLA and 25% carbon fiber composites [93]. In 2018, Liao *et al.* [94] experimented with 10% carbon fiber and PA12 composites and determined 125 MPa tensile strength, whereas Qingxi *et al.* [53] reached 248 MPa in PLA and 25% CCF composite structures. Heidari-Rarani *et al.* [75] experimented with 20% PVA impregnated carbon fiber and PLA matrix composite structures and achieved 152 MPa strength when bending, whereas Chacón *et al.* [95] tested 15% carbon fiber and Nylon structures and obtained 355 MPa flexural strength. In 2020, when experimenting with 35% carbon fiber and PA12 and 28% CCF and Nylon samples, accordingly, the flexural strength of 451 MPa [96] and 558 MPa [97] were determined, respectively. As observed from the summarized data, the flexural strength when bending depends directly on the carbon fiber content in printed composites and on the polymer material being used. Structures with Nylon or PA12 are stronger than structures with the PLA or ABS matrix material.

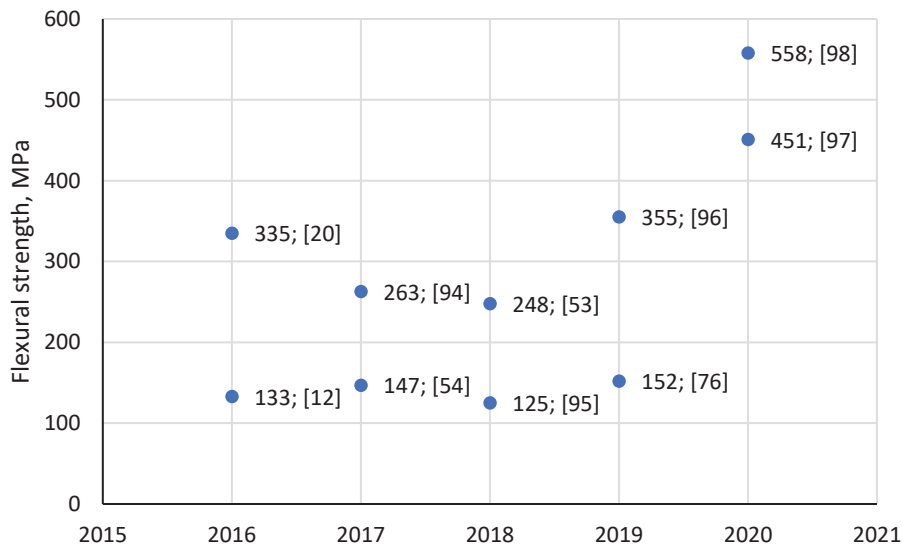


Fig. 1.8 Flexural strength results for years 2016–2020 in scientific publications

1.6. Chapter Conclusions

The demand for 3D printed composites and other advanced structural materials has been demonstrating a rapid increase recently. The AM technologies also start to be treated not only as the prototyping technologies, but also as the method for the rapid fabrication of functional complex components that can actually be used in the fields of automotive, aerospace, medical and electronic industries. These two reasons encourage the researchers to search for possibilities and new innovative solutions to apply AM for industrial needs where the production speed, versatility and flexibility is needed. Carbon fiber reinforced composites are one of the most widely used groups of composites in the aviation and automotive industry. In comparison with glass fiber, carbon fiber structures are lighter, more rigid, and they

are less prone to distortions (warping) and expansion. The FDM technology is currently one of the most widely used AM technologies for printing CCF reinforced structures. Its popularity stems from the flexibility of this technology for modifications, versatility, the rapidly expanding range of printable thermoplastic materials (which can be used as the matrix material), the advancing equipment and software. Considerable benefits for the mechanical properties of CCF reinforced printed structures have also been reported. After inserting continuous carbon fibers into the printed polymer matrix, the tensile strength may be increased from 3 to 7 times compared with the pure thermoplastic print. The earliest tests and scientific publications related to continuous fiber printing with the FDM technology emerged only in 2016. In the same year, two major market leaders, *Markforged* and *Anisoprint*, were established. For a long time, *Markforged* printers, materials and printed structures were the only research objects in this field. Therefore, in the view of more profound understanding of the printing process of CCF composites, the effect of the individual printing parameters, the carbon fiber content, as well as its preparation and impregnation, on the physicochemical and mechanical properties and on the performance characteristics of the prints need to be tested. Researchers started to search for new alternative printing impregnation technologies and equipment as trade secrets made this impossible with the printers which were available on the market, which was hampering the progress and development in this area. Therefore, in this dissertation, the printing and carbon fiber impregnation technology and equipment shall be developed, and the influence of the FDM parameters and impregnation processes on the mechanical and print quality characteristics, such as microstructural properties, physicochemical, and CCF content influence shall be tested.

2. TECHNOLOGICAL AND EXPERIMENTAL METHODOLOGY

The main aim of this thesis is to develop and validate the FDM technology for the rapid fabrication of complex geometry continuous carbon fiber reinforced composite structures. The research work done during the preparation of the dissertation was divided into three main parts that are demonstrated in Fig. 2.1:

1. Preparation. At this stage, the following were created: the CCF impregnation technology and a custom printing head that can print CCF reinforced composite structures.
2. Printing. At this stage, the following were created: the FDM technology-based process that can print CCF reinforced structures. Moreover, by using this process, samples were made for the further investigation of the mechanical properties.
3. Testing. At this stage, all the planned experiments and research activities necessary for the analysis of 3D printed CCF reinforced structures and the determination of the main mechanical properties were made.

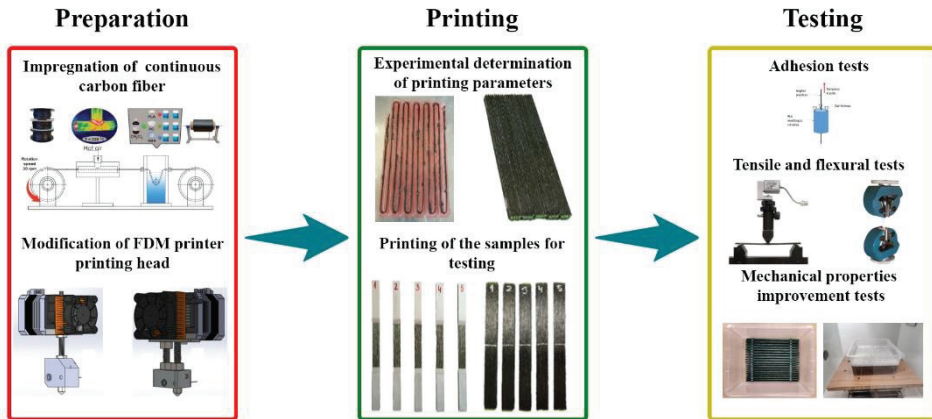


Fig. 2.1 Research experimental setup

As Fig. 2.1 demonstrates, during the research, several studies were conducted with the objective to evaluate the possibilities and applicability of the printing head, the reinforcement material preparation technologies and the printing process. Moreover, the mechanical characteristics of the printed CCF composite structures, the number of air voids in the printed structure, and print quality characteristics were determined. For the analysis of 3D printed CCF reinforced composite structures, the following experiments were performed:

1. Impregnation of carbon fiber in a thermoplastic solution for 3D printed CCF composite structures to analyse the impregnation material's compatibility and improved printability;
2. Research of the impregnated CCF tow mechanical and physical characterization methods for the printing of composite structures;
3. Investigation of the influence of printing parameters on the quality of 3D printed composite structures;

4. Determination of the delamination force and shear strength of printed composite structures;
5. Improvement of the mechanical properties of printed composite structures by secondary impregnation.

2.1. Materials

Composite materials consist of two or more materials with different mechanical properties. The binding material is called the *matrix*, and the material that provides strength is called the *reinforcing material*. The composite structures analysed in this thesis are made of a thermoplastic PLA matrix and a continuous carbon fiber reinforcing material.

2.1.1. Reinforcing Material

While printing 3D composite structures, *Toray Industries* (Japan) high-quality nonwoven continuous carbon fiber tow was used. Depending on the test and the printed structure, 1K (1000 carbon fiber strands) *T300B-1000* or 3K (3000 carbon fiber strands) *T300B-3000* continuous carbon fiber tow was used in the experiment. The carbon fiber tow of this manufacturer is made of polyacrylonitrile. As a reinforcing material, CCF was opted for due to its high resistance to aggressive chemicals, superior mechanical characteristics and a wide range of application for the production of composite structures in the aviation and automotive industries. Carbon fiber is even lighter than glass fiber, and it is 40% lighter than aluminium and 70% lighter than steel. Due to the negative coefficient of thermal expansion, it can be used across a wide temperature range, which is relevant in 3D printing since the printhead may be heated up to 280 °C or more depending on the matrix used for printing. Table 2.1 below provides the main 1K and 3K continuous carbon fiber characteristics.

Table 2.1 Main characteristics of continuous carbon fiber [98]

Carbon Fiber Tow	Number of Fibers	Tensile Strength, MPa	Young Modulus, GPa	Elongation, %	DTEX, g/1000 m	Density, g/cm ³
T300B-1000	1000	3530	230	1.5	66	1.76
T300B-3000	3000				198	

The CCF tow was impregnated before the printing. This is for two reasons: firstly, the carbon fiber filaments are bound together, and, secondly, the technological FDM process is facilitated. On the other hand, impregnation increases adhesion between the matrix and the reinforcing material and significantly improves the mechanical properties of the printed composite structures.

2.1.2. Matrix Material

Various thermoplastics can be used as the matrix material in 3D printing of CCF reinforced composite structures using the FDM technology. Currently, the most popular thermoplastics used in this technology are PLA, ABS, PETG, PC and Nylon. Meanwhile, for these analyses, the samples were printed by using polylactic acid (PLA) thermoplastic. PLA was chosen as the matrix material due to its easy printing, low printing temperature, superior adhesion with the printing platform and the impregnated CCF, universal availability, recyclability, and adequate mechanical properties. It is important to note that polylactic acid is made of renewable sources, such as corn starch. It is denoted by better biodegradability compared with other conventional polymers used in FDM and biocompatible depending on the type of PLA. Due to the low printing temperature, small amounts of harmful particles and vapours are emitted when printing PLA thermoplastics. The recommended printing speed ranges from 30 to 40 mm/s, whereas the temperature of the printing platform is between 20–70 °C, and the temperature of the printhead is 160–220 °C. When choosing the matrix material for the printing of CCFRC structures, it is important to consider two main parameters: the thermoplastic melting point (for this class of printers, the limit cannot exceed 250 °C to 280 °C), and the compatibility with the solvent used during impregnation. For better adhesion and compatibility properties, the matrix material should be the same as the thermoplastics used for impregnation. The main characteristics of the PLA material are provided in Table 2.2.

Table 2.2 Main PLA characteristics [99]

Melting Temperature, °C	Tensile Modulus, GPa	Tensile Strength, MPa	Flexural Strength, MPa	Flexural modulus, MPa	Glass transition temperature, °C
180-220	2.3	45.6	103	3150	~60

2.2. Development of Impregnation Process

One of the main challenges before printing CCF reinforced composite structures is the appropriate preparation of the tow. As mentioned above, two different types of carbon fibers (1K and 3K) were used for the printing of composite structures. This means that, in one case, the fiber tow consists of 1000, whereas, in the other case, of 3000 strands of 7µm diameter. Due to the low stiffness of the CCF tow, it is virtually impossible to feed such unprepared carbon fiber to the printhead. It tangles easily, and individual strands can break and accumulate inside the printhead. These fiber accumulations clog the input and output channels, thereby breaking the filament and stopping the printing process. Another important aspect is the poor adhesion between the matrix and the reinforcing material. PLA or other thermoplastic does not tend to adhere to the pristine CCF because of the low interfacial bonding strength. This causes considerable difficulties in printing since low fusion between these materials causes poor adhesion between the layers, the print lines and the printing platform. This has an impact on the mechanical properties of the printed composite structures and their quality. The impregnation

process consists of two main stages: *solution preparation* and *impregnation*. The decision was made to soak the CCF in the solution of methylene chloride CH_2Cl_2 and thermoplastic. Methylene chloride was chosen for its rapid evaporation and rapid dissolution of various thermoplastics, such as PLA, PETG, PC, etc. The three most commonly used thermoplastics in the FDM technology were tested for impregnation: PLA, ABS, PC. These thermoplastics differ not only in terms of the chemical composition, but also regarding the mechanical and physical properties. The required concentration of the solution was determined by the trial-and-error approach, and the thermoplastic was selected whichever could ensure the highest adhesion between the matrix and the reinforcement, and reduce the air void volume inside the fiber thus making it more homogenous.

2.2.1. Solution Preparation

One of the most important stages in carbon fiber impregnation is the preparation of the appropriate solution. Due to CH_2Cl_2 being used for the dissolution, the preparation process was performed in a fume cupboard. The solution was prepared according to the weight ratio of the solvent to the solute. The experiment showed that the best impregnation result is obtained when the solution concentration is equal to 10%, which means that 100 g of the solution contains 10 g of the PLA material and 90 g of CH_2Cl_2 solvent. First, 90 g of solvent is added to a glass vessel. 10 g of PLA thermoplastic granules is then added to the solution stirred with a magnetic stirrer. The preparation of the solution and the accumulation of buildup is depicted in Fig. 2.2. It is important to add PLA granules slowly; otherwise, individual granules (1, Fig. 2.2) tend to agglomerate and stick to large thermoplastic buildup (2, Fig. 2.2). The accumulation of buildup delays the dissolution time significantly. On average, without heating, the solution on the magnetic stirrer is prepared in 45 minutes. This time can be extended up to 2 hours in the case of buildup. In order to reduce the dissolution time, heating can be used. It is important to choose the right temperature and not to boil the solution. When heating methylene chloride, its evaporation increases greatly, so the concentration of the solution may change.

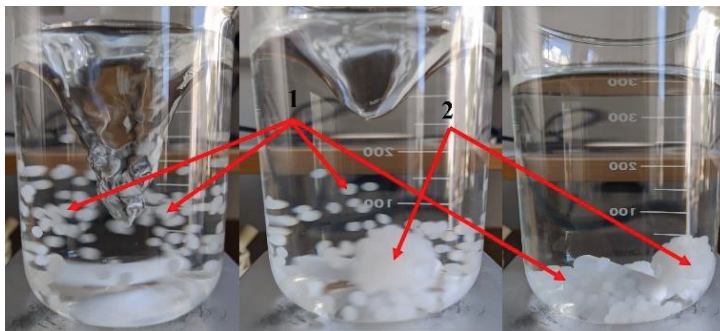


Fig. 2.2 Solution preparation and accumulation of buildup: 1 – individual granules; 2 – accumulation of granules

2.2.2. Carbon Fiber Impregnation¹

During the development of the impregnation technology, an impregnation device was created whose scheme is presented in Fig. 2.3.

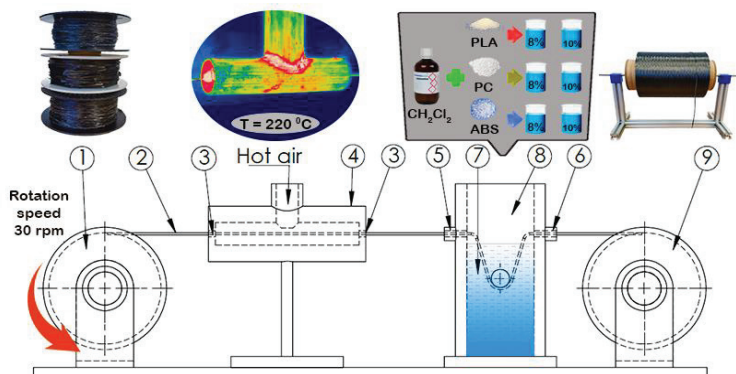


Fig. 2.3 Scheme for carbon fiber impregnation: 1 – spool; 2 – impregnated CCF; 3 – nozzle; 4 – heating section; 5 – 0.8 mm nozzle (1K); 6 – 1 mm nozzle (1K); 7 – solution; 8 – impregnation section; 9 – CCF spool

The device was made of a spool on which the impregnated carbon fiber is wound, carbon fiber, the heating section, the impregnation section and a spool with standard unimpregnated carbon fiber. The inlet and outlet openings (4) of the heating section have nozzles (3) of the identical diameter, while the impregnation section (8) uses nozzles of different diameters (5) and (6). In order to maintain the conditions as constant as possible, the winding speed and the heating conditions are kept constant. The winding speed in the spool (1) was kept constant at 30 rev/min, regardless of the used solution concentration or continuous carbon fiber. The operation of the device is based on pulling the impregnated carbon fiber through a bath filled with the impregnation solution. While turning the impregnated fiber spool (1) counter-clockwise, carbon fiber (2) was unwound from the second spool (9). Firstly, the carbon fiber goes through the nozzle (6) in the impregnation section (8) where it is immersed in the solution (7) up to the fixed roller. Through the nozzle (5) mounted on the other side of the device, the fiber is pulled out, and it enters the heating area. Hot air is constantly supplied to the heating section, and impregnated carbon fiber enters the heating element through the nozzles made of polytetrafluoroethylene (PTFE). The heating temperature is measured by using a *Flir T420* thermal imager. The thermal sensitivity of the thermal camera is 0.04 °C, and the temperature measurement range is from -20 to 650 °C. In order to ensure stable heating conditions, hot air is supplied to the heating section (4) of the impregnating device until the temperature is stabilized. The measured temperature inside the heater is about 220 °C.

The inner diameter of the nozzles (3) of the heating section is 5 mm. The dried impregnated carbon fiber extracted from the heating section is wound on the spool

¹ The material in this section was previously published in [100]

(1) at a constant speed. The diameter of the nozzle used in the impregnating section depends on the type of the carbon fiber. The inlet nozzle (6) is made of PTFE, and its internal diameter is 2 mm. The outlet nozzle is made of bronze, and its internal diameter for 1K carbon fiber is 0.6 mm; meanwhile, for 3K carbon fiber, it is 0.8 mm. The diameter of the nozzle (5) is important because it influences how much solution will remain on the impregnated carbon fiber. Identical nozzles (3) in the heating section allow keeping the carbon fiber in the center and preventing it from sticking to the walls of the device.

Impregnation in a solution of thermoplastic and methylene chloride solves many of the problems associated with printing unimpregnated continuous carbon fiber. Firstly, after impregnation, the carbon fiber filament becomes stiffer and homogenous, i.e., individual fiber filaments of 7 μm are bound into one continuous tow. This allows the fiber to be easily fed to the printhead during the printing process, and such carbon fiber tow is far less prone to deformation, breaking or tangling. Secondly, impregnated carbon fiber allows for a more predictable and reliable 3D printing process. One more important aspect is the greater adhesion between the printing filaments, the structure layers and the printing platform. This was demonstrated experimentally in further studies. When using impregnated carbon fiber, the amount of air voids in the printed structure also decreases. The amount of air voids in the structure depends on the voids that appear during the printing process and the voids that are already present in the carbon fiber. In addition to the qualitative advantages over unimpregnated continuous carbon fiber, considerable improvement in mechanical properties is observed (see Chapter 3.5).

2.3. Development of FDM Process

One of the major challenges in the printing of CCF reinforced components is the unavailability of economically affordable and well-established FDM technology and equipment. However, the simplicity, availability and modification possibilities of the FDM technology allow printing CCF reinforced composite structures. As it was discussed in the literature analysis, there are currently five main methods to insert carbon fiber into the polymeric matrix.

For the printing of composite structures with continuous carbon fiber reinforcement, co-extrusion with the towpreg method was chosen. In this case, modifications of the printhead are unavoidable. The supply of carbon fiber directly to the printhead offers several major advantages. Firstly, the mixing of carbon fiber and plastic is performed in an enclosed high-temperature environment, which allows increasing the adhesion and decreasing the possibility of delamination between the matrix and the reinforcement. Secondly, there is no need for the second printing nozzle, and this allows decreasing the printhead dimensions as well as its weight, and therefore simplifies its construction.

The analysis of the standard printhead is provided further. Its design can be divided into two main zones: *hot* and *cold* (Fig. 2.4).

The cold zone is responsible for the proper plastic supply to the hot zone. It consists of the stepper motor (1), the filament feeding unit (2), and the cold zone cooling unit (3). The hot zone is responsible for the melting of the plastic and

feeding to the printing zone. It consists of the heating element (4), the thermocouple (5), the guide tube (6), and the nozzle (7). Even though this design is perfect for the printing of parts of various plastics (ABS, PLA, PC, etc.), the appropriate location for the insertion of the reinforcing material needs to be found for the printing of continuous carbon fiber composites.

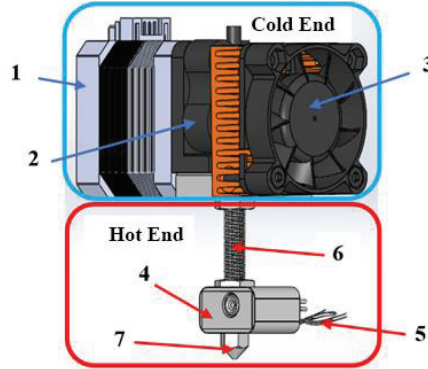


Fig. 2.4 Standard printing head: 1 – stepper motor; 2 – filament feeding unit; 3 – cooling unit; 4 – heating element; 5 – thermocouple; 6 – guide tube; 7 – nozzle

It was decided to produce two different prototypes after the analysis of the printing process; the gathered knowledge was related to the impregnation of CCF and production of composites, and the evaluation of the requirements for plastic and fiber to be mixed in the heating element was performed. Fig. 2.5 indicates the two prototypes which were fabricated based on the standard head.

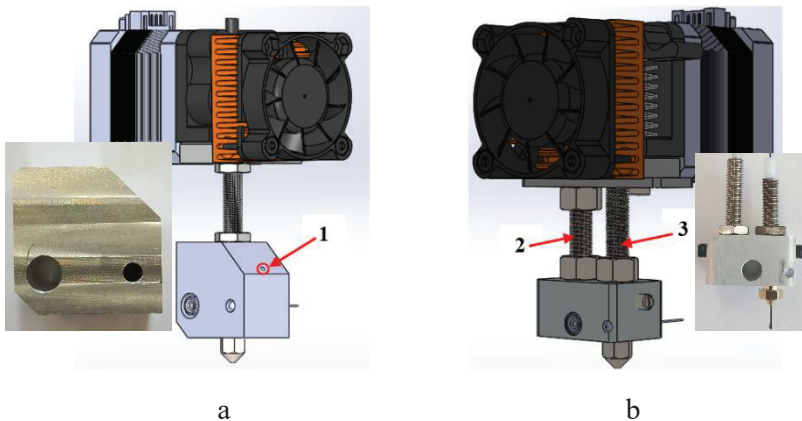


Fig. 2.5 Prototypes of printing heads: a – early prototype; b – improved prototype; 1 and 3 – CCF inlet; 2 – matrix inlet

It can be observed that the cold zone remained stable in both cases. The only difference is that the improved prototype (Fig. 2.5 b) has a channel in the cold zone for fiber entrance to the hot zone. Major changes can be observed in the hot zone. The later prototype features two inlet tubes: one for the matrix material guidance (2),

and the other for the carbon fiber guidance (3). The fiber guidance tube performs several functions and solves the problems which were detected while using the early prototype (Fig. 2.5 a):

1. The tube ensures consistent and safe entry of carbon fiber to the printing area;
2. It helps to maintain the temperature and the appropriate pressure in the heating element;
3. It prevents plastic from rising into the fiber feed zone;
4. It allows the fiber to enter the heating element directly, while avoiding corners or sharp edges.

When printing with the first prototype, carbon fiber entered the heating element at an angle of 45° through the opening (1). It was noticed that, in the case of an opening in the heating element, the plastic tended to flow not to the printing area, but rise to the top of the opening instead. This caused lack of plastic in the composites and complicated fiber feeding. Complicated carbon fiber feeding to the heating element with 45° deflection caused fracture(s) in the reinforcing material. The second improved prototype was developed to eliminate these factors. The cross-section of the new heating element with the prototype is demonstrated in Fig. 2.6.

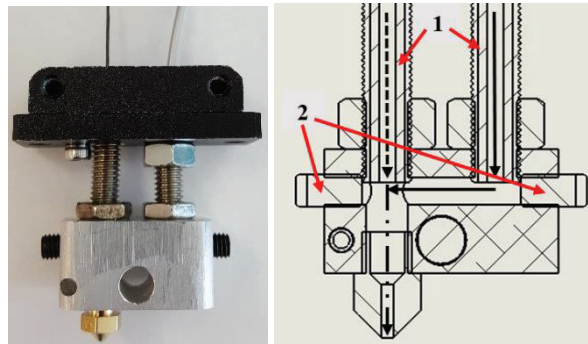


Fig. 2.6 Improved prototype and its cross-sectional view: 1 – PTFE guides for CCF and matrix; 2 – screws for mixing chamber sealing

Fig. 2.6 indicates PTFE inserts (1) designed for improved sliding with the guide tubes. The matrix materials (the solid line), the reinforcing materials (the dotted line), and the trajectories of mixed materials are also visible. The path of the reinforcing material in this element is always straight, which helps to reduce the probability of breakage and tangling. The construction and assembly allow easy cleaning of the heating element, which was not possible in the first version.

The improved prototype of the printhead is demonstrated in Fig. 2.7. The heating elements were made of AW5754 aluminium alloy by using milling, drilling and threading technologies. In order to improve the adhesion of the composite and the platform to the printing device, a cooling device consisting of a fan and an air guide was installed. Unlike in the basic cooling solutions, here, the cool air is fed into the printing contact area with five 360° -angled openings. This ensures the minimum cooling of the heating element itself. These improvements allow

decreasing the heating head's temperature changes and ensure consistent flow of plastic as well as better impregnation during printing.

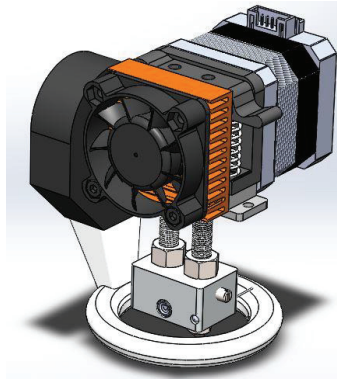


Fig. 2.7 Final design of custom printing module

It is important to highlight that the cooling intensity has to be precisely chosen because excessive airflow cools the heating element and the nozzle below the critical temperature, thus reducing the fluidity of the matrix material and breaking the continuous carbon fiber filament.

2.3.1. 3D Printer Type

For all the tests, composite samples were printed by using the half-open FDM printer *MeCreator 2* developed by *GEEETECH* (China) with a modified printhead (the improved prototype) which can print continuous carbon fiber reinforced structures (Fig. 2.6). This printer is easily modifiable and features a half-open work area which allows monitoring the printing process at a 270° angle. Moreover, an open printer ensures easy access to the printing area. This access allows easy feeding of impregnated CF to the printhead. One more important aspect is that this printer uses open-source software, which allows using not only the specific printing preparation program, but also a user-defined one. All the samples were printed by using *Simplify3D* software for the preparation of the printing process and its control. The modified printer consists of the major parts indicated in Fig. 2.8.

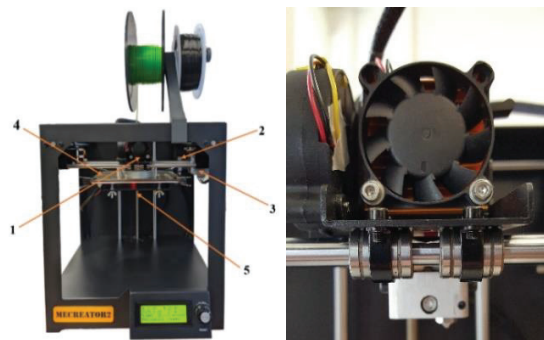


Fig. 2.8 Modified *MeCreator 2* printer: 1 – printhead; 2 – Y-axis motor; 3 – X-axis motor; 4 – printing platform; 5 – Z-axis motor

The main technical specifications of the printer are provided in Table 2.3.

Table 2.3 Main specifications of *MeCreator 2* printer

Printing platform	160×160×160mm
Printer resolution	0.05 mm
Axis accuracy	X/Y – 0.05 mm. Z – 0.02 mm
Printing speed	1–80 mm/s
Filament diameter	1.75 mm
Standard printing nozzle	0.4 mm
Step motor	1.8° step angle with 1/16 step
File type	STL, 3ds, obj, amf, dae, G-code
Filament type	Thermoplastic
Maximum plate temperature	~110 °C
Maximum head temperature	~250 °C
Platform	Aluminum plate + heater
Axis	Stainless steel
Printer size	320×320×360 mm
Printer weight	9 kg

2.3.2. FDM Process Parameters

The printing technology for producing CCF reinforced composite structures was developed experimentally, that is, with a modified FDM printer featuring a custom-designed printing module (the early and the improved prototypes) for printing multi-layer composite samples. The following printing parameters were changed in the real time: the layer height, the printing speed, the extrusion multiplier, the cooling intensity, the print line spacing, the nozzle diameter, the heating element, and the printing platform temperature. The optimal numerical values for these printing settings were determined. Each of these parameters influences the quality of the composite structure printing and the repeatability of the printing process. All the above listed printing parameters can be divided into two groups:

- The main parameters strongly depended on the CCF tow being used (1K or 3K) and had influence on the amount of carbon fiber and the mechanical and print quality characteristics of the composite structure;
- The auxiliary parameters did not change depending on the carbon fiber in use and did not have major influence on the quality of the printed composite structure or mechanical characteristics.

2.3.3. Main Parameters

The layer height (see Fig. 2.9) is one of the printing parameters used for the printing of CCF reinforced composite structures. If the selected layer height is too high, the composite filament may not adhere to the previous layer. The low layer height affects the flow of plastic from the printing nozzle to the work area and carbon fiber cutting. Broken carbon fiber cannot escape the heating element through the print nozzle and accumulates inside thus forming a clog, and, eventually, the carbon fiber tow breaks down. This parameter is directly related to the content of CCF in the printed composite structure; while the height of the layer decreases, the

content of carbon in the structure increases. During the experiment, the layer height was changed from 2 mm to 0.1 mm, depending on the carbon fiber being used. The recommended layer height range for the high-quality printed composite structure and continuous printing process was determined: 1K – 0.3/0.4 mm and 3K – 0.5/0.7 mm.

The print line spacing (Fig. 2.9) is the distance between two horizontal parallel composite print lines. As in the layer height, the appropriate distance is also important because it directly affects the content of carbon fiber in the printed composite structure. The lower print line spacing means the larger content of CCF in the composite structure. If the distance is too large, the lines may not connect and bond together. Reducing this distance too much will cause the lines to overlap and clog the print nozzle, and thus break the carbon filament. During the experiment, the print line spacing was changed from 2 mm to 0.8 mm. The recommended print line spacing for the high-quality printed composite structure and continuous printing process was determined: 1K – 1 mm/1.2 mm and 3K – 1.4/1.6 mm.

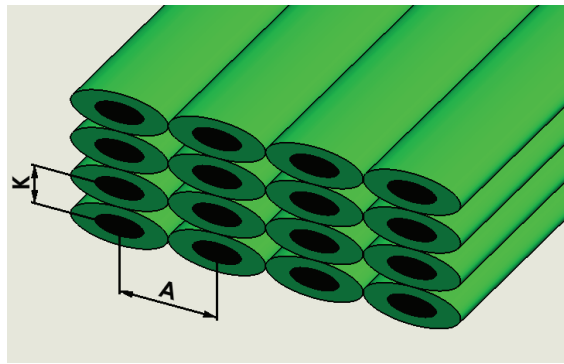


Fig. 2.9 Isometric view of the sample: K – layer height; A – print line spacing

The extrusion multiplier: when printing thermoplastic parts with FDM technology printers, this parameter reaches 100%. When printing composite structures, the plastic and carbon fiber are extruded at the same time through the printing nozzle. Therefore, the percentage of the fed plastic must be lower as, otherwise, the plastic will be fed to the heating element faster than it can escape through the nozzle and the printhead, and it will consequently accumulate in the heating element. Due to being unable to escape, the plastic begins to rise in the carbon fiber feeding channel, and it reaches the cold printhead zone. In the cold zone, the temperature of the thermoplastic decreases significantly, and, at the same time, the plastic turns from liquid to solid. The hardened plastic prevents the carbon fiber filament from moving, and it breaks. In determining the appropriate plastic feed percentage, it varied from 40% to 100%. The recommended extrusion multiplier range was determined experimentally: 1K – 60/80% and 3K – 40/60%.

2.3.4. Auxiliary Parameters

The diameter of the printing nozzle is the parameter for high-quality and reliable composite structure printing. It is important to select the appropriate

diameter of the nozzle so that the plastic and CCF are easily extruded from the heating element to the printing platform. If a bigger nozzle diameter is selected, the plastic and fiber will escape the heating element too quickly, and there will be no precise print line spacing. If the diameter of the nozzle is too small, the composite matrix and the reinforcing material filament will not be able to escape the heating element thus causing the blockage of the printing nozzle and the breakage of the carbon fiber. The market-available diameter printing nozzles were tested experimentally: 0.8, 1, 1.2, 1.5, 2 mm. It was noted that the stable printing process is achieved by using a 1.5 diameter nozzle; however, when printing with 3K carbon fiber, the nozzle tended to get blocked. Therefore, the diameter of the nozzle was increased to 1.6 mm, which solved the issue. During the experiments, it was also noted that the diameter of the nozzle does not depend on the carbon fiber in use. The recommended printing nozzle diameter for 1K and 3K carbon fiber is 1.6 mm.

The printing speed: the average printing speed when printing thermoplastic items is 40–60 mm/s; however, when printing composite continuous carbon reinforced structures, the speed must be significantly lower. This happens because of the high printing speed, high friction in the printing nozzle, and the printing peculiarities (printing filament pulling while changing the printing direction), as carbon fiber tends to break. Different printing speeds from 1 to 10 mm/s were tested during study. The best qualitative results in terms of the printing time and process stability were obtained with the printing structures being at 3 mm/s regardless of the carbon fiber in use.

The heating element and the printing platform temperature: the recommended values for PLA material are as follows: the heating element: 180 °C, and the printing platform: 60 °C (as recommended by producers); however, during experimental printing, the parameter settings and the development of the composite structure printing technology, it was noted that PLA tends to suffer from poorer adhesion to carbon fiber at standard temperatures, and its fluidity and bonding to the printing platform decreased. Therefore, the following most appropriate temperatures in the range of thermoplastic were determined: the heating element temperature: 200–220 °C, and the printing platform temperature: 80 °C.

Cooling is an important parameter when printing CCF reinforced composite structures. The timely and sufficient cooling of the matrix material prevents or reduces the pulling effect of the printing filament due to the printhead direction changes or when printing a new layer. While searching for the best cooling, in the testing phase, the cooling fan speed was changed in the range from 0% to 100%. During the experiment, it was determined that the most efficient cooling range is 60–90%.

In summary, the experimentally determined and recommended printing parameters are provided in Table 2.4.

Table 2.4 Recommended printing parameters

Parameters	1K	3K
Layer height, mm	0.3/0.4	0.5/0.6
Print line spacing, mm	1/1.2	1.4/1.6
Extrusion multiplier, %	60/80	40/60
Printing nozzle, mm	1.6	
Printing speed, mm/s	0.3	
Head temperature, °C	220	
Platform temperature, °C	80	
Cooling, %	60–90	

2.3.5. The Printing Process

The printing of continuous carbon fiber reinforced composite structures is a complex process which requires knowledge of the most effective printing parameters, a suitable modified printing module, and a properly prepared printer along with the understanding of the printing process itself. A principal scheme of the printing process is provided in Fig. 2.10.

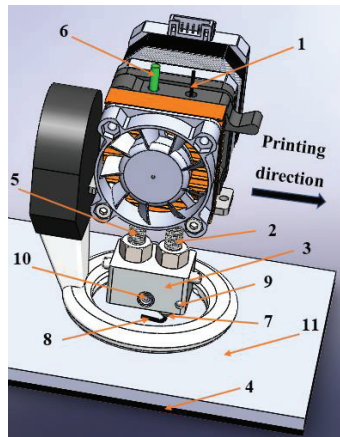


Fig. 2.10 Scheme of the printing process: 1 – impregnated CCF; 2 – CCF feeding channel; 3 – heating element; 4 – printing platform; 5 – thermoplastic feeding channel; 6 – thermoplastic; 7 – printing nozzle; 8 – homogenous composite filament; 9 – thermocouple; 10 – heater; 11 – borosilicate glass

Firstly, impregnated carbon fiber (1) is passed through the printhead until it protrudes the printing nozzle (7). As the principal scheme indicates, the carbon filament enters the hot zone of the printhead through the carbon fiber feeding channel (2). After the carbon fiber has been passed, the heating element (3) is heated to the operating temperature of 220 °C. When the heating element reaches the set temperature, thermoplastic (6) is fed through the thermoplastic feeding channel (5) to the heating element. Thermoplastic is fed until the heating element fills with thermoplastic, and the carbon fiber that is fed through the printing nozzle is covered with it and becomes homogenous composite filament (8). When the filament becomes homogenous, the printing platform (4) on which borosilicate glass (11) is

placed is heated to 80 °C. For better adhesion between the printing platform and the composite filament, the glass surface is coated with a layer of 3D LAC adhesive in order to increase adhesion. When the printhead temperature remains constant (which is measured by the thermocouple (9) and maintained by the heater (10)), the printhead is moved to the beginning of the x and the y axes. Afterwards, the printhead is placed near the starting point of the printed structure, and the printing platform is placed at the starting point of the z axis. The printing process is started in the last stage. Since continuous carbon fiber is printed, after the structure printing is finished, the printer lowers the printing platform vertically by 20 mm. Then, the carbon fiber filament is cut. After the printing platform has cooled down, the printed structure can be removed from the printing platform. Since this prototype printing device has no carbon fiber cutting unit, only one piece can be printed at a time.

After the development of 3D printing process and the determination of the optimal printing parameters, various groups of samples were produced. As it was mentioned above, the printing layer height and the print line spacing were changed in the course of experiments in order to achieve the optimal mechanical performance of composite structures. The main parameters of the printed groups can be found in Table 2.5.

Table 2.5 Main parameters of printed sample groups

	Group 1	Group 2	Group 3	Group 4	Group 5
Line width, mm	1	1	1.2	1.2	1.6
Layer height, mm	0.3	0.4	0.3	0.4	0.5
Fibers in the tow	1000 (1K)				3000 (3K)
Printing speed, mm/s	3				

It can be seen that most of the experiments were performed with samples produced by using the 1K carbon fiber tow; however, one group of samples reinforced with the 3K carbon fiber tow was used as well. This group was made in order to test the suitability of the impregnation process and to check the mechanical properties of the composite structures reinforced with the 3K carbon fiber tow.

2.3.6. Evolution of the Printing Process

Four years of continuous research and development of the printing process created significant changes and improved the qualitative and mechanical characteristics compared to the state-of-the art level at the start of the study. The experimental development of the printing technology began with the printing of the impregnated carbon fiber while using an early heating element prototype without additional thermoplastic insertion. The entire printing process development and evolution with an early printing element is demonstrated in Fig. 2.11. The next step was to incorporate an additional amount of thermoplastic in order to improve adhesion between the layers and lines, and to improve the adhesion of the composite structure to the printing platform. After the inclusion of thermoplastic in the printing process, new challenges were being faced, and, while handling them, the experimental printing technology was introduced to improve the understanding of

the process. After the development of the printing technology, the first samples were printed for the analysis of mechanical characteristics.

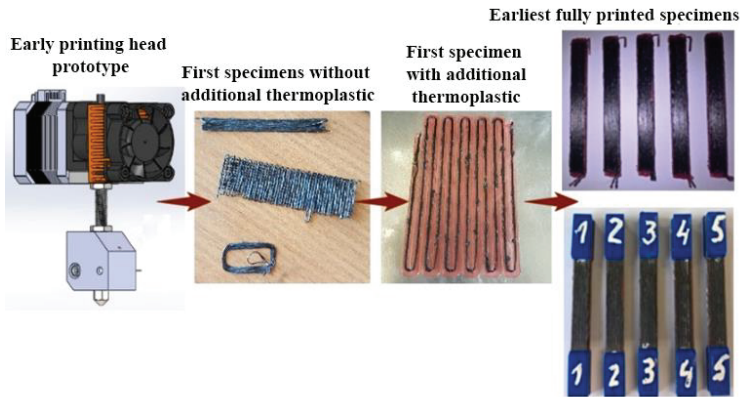


Fig. 2.11 Experimental printing with the early printing module prototype

The samples were printed by using the following parameters: layer height 1 mm, print line spacing 0.75 mm, printing speed 1 mm/s, heating element temperature 200 °C, printing platform temperature 70 °C. When printing with an early prototype, the carbon fiber tended to break, and the printing nozzle tended to get blocked. The early mechanical tests also did not indicate any expected improvement in comparison to the pure PLA. The tensile strength was only about 90 MPa, which is twice as high as the samples printed from the matrix material only (PLA) which featured a tensile strength of about 45 MPa.

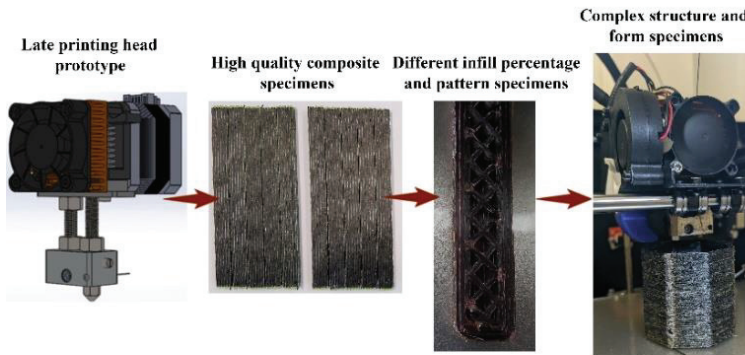


Fig. 2.12 Experimental printing with improved printing module prototype

A significant breakthrough was achieved when printing continuous carbon fiber reinforced composite structures when the earlier printhead prototype was replaced with the improved one (Fig. 2.12). When using the prototype, the printing technology was significantly improved, the recommended printing parameters for 1K and 3K carbon fiber printing were determined, and high-quality samples for

tensile and flexural tests were printed. Their tensile strength reached 320 MPa, which is 7 times more than the values for PLA printed samples. The improved prototype and the precisely determined printing parameters allowed printing complex composite structures. A significant advancement in the development of the FDM printing process was achieved with the improved printing module. Examples are provided in Fig. 2.12.

2.4. Pre-processing of Continuous Carbon Fibers²

1.75 mm diameter PLA DR3D filament was used as the matrix material in this investigation. The material of this matrix was used to print all of the samples used in the experiment. *Toray T300B-1000* (1000 fibers) and *T300B-3000* (3000 fibers) nonwoven continuous carbon fiber was used as the reinforcing material. According to the manufacturer, the diameter of one fiber is 7 micrometres regardless of the number of fibers in the tow. Three different materials were used for the impregnation of the carbon fiber: PLA, ABS and PC. The first material is *NatureWorks* biopolymer *PLA 3D850* created for the 3D printing industry. The *PLA 3D850* tensile strength is 51 MPa, its Young's modulus is equal to 2315 MPa, and the density is equal to 1.24 g/cm³. The second material is *ABS P400*; it is a standard industrial thermoplastic from *Stratasys*. The *ABS P400* tensile strength is equal to 22 MPa, its Young's modulus is equal to 1627 MPa, and the density is equal to 1.05 g/cm³. Standard 3D printing material PC from *Ultimaker* was used as a third alternative for impregnation. The PC material tensile strength is 76.4 MPa, its Young's modulus is equal to 2134 MPa, and the density is equal to 1.18–1.20 g/cm³. *Eurochemicals* methylene chloride was used as the solvent (CH₂Cl₂). The material suppliers provided the characteristics of the materials described in this section.

2.4.1. Carbon Fiber Impregnation

It was decided to use various impregnation materials and investigate their influence on the characteristics of the 3D printed samples. It was decided to analyze the influence of three different materials on the characteristics of the printed structures, the impregnation qualities, and the influence of the thermoplastic content on the characteristics of the printed samples. PLA was used in the form of granules, and ABS and PC were mechanically crushed and prepared from filaments used in 3D printing. The aim was to maintain granules of a similar size (3–5 mm) as PLA. Solutions with concentrations of 2, 4, 6, 8 and 10 wt% were used for the test. The polymer granules were completely dissolved by using a magnetic stirrer *LBX H01*. During dissolution, no heating was used. The impregnation technology and equipment in use did not change regardless of the thermoplastic used for impregnation, and the process is described in the section *Impregnation Process*.

The cross-sectional surface analysis of the impregnated carbon fiber was performed by using a *Nikon Eclipse LV100ND* (*Nikon*, Japan) motorized microscope and a high-resolution colour camera *DS-Ri2* (*Nikon*, Japan). The maximum allowable sample size for microscopic analysis is 150×150 mm, and the maximum

² The material in this section was previously published in [100]

display resolution of the camera is 4908×3264 pixels. The image processing software *NIS Elements D* was used for the image analysis, which allowed preparing and processing data for further work.

2.4.2. Additive Manufacturing of Composite Samples

A *MeCreator 2 FDM* printer was used to produce composite samples. This system is designed to print only from thermoplastic; hence, the printhead was modified by using the improved prototype developed and described in Section 2.3. The printer was chosen due to its simplicity and feasibility to easily adapt to the printing of CCF reinforced composite structures. Fig. 2.13 indicates the printing process and samples.

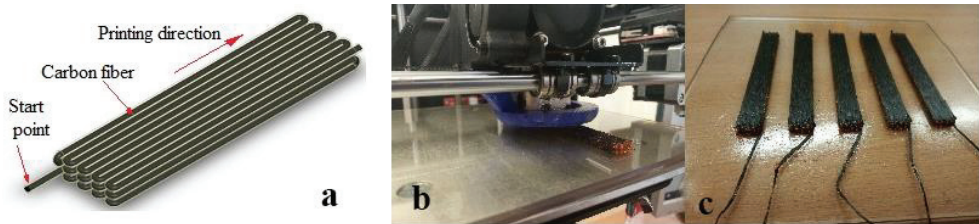


Fig. 2.13 Scheme of the designed printing head and printing process: a – 3D printing path; b – Printing process; c – Printed samples

Unidirectional 0° rectangular profile samples were chosen for the experiments. It should be mentioned that all the samples were printed with the same printer under the same conditions and parameters. The printing parameters were adjusted according to the carbon fiber type. All the printing parameters are provided in Table 2.6.

Table 2.6 Printing parameters

Printing parameter/Carbon fiber tow	Group 4	Group 5
Extrusion multiplier	0.6	0.6
First layer speed, mm/s	1.20	1.20
Fan speed, %	50 first/80 second/100 following layer	50 first/80 second/100 following layer
Extruder temperature, °C	200	200
Bed temperature, °C	70	70

2.4.3. Mechanical Tests

In order to determine the strength and elastic characteristics of printed composite materials, analysis of their mechanical properties was performed. Firstly, the testing of carbon fiber was performed, i.e., strength testing was conducted for all the impregnating materials and impregnated fibers that were impregnated at various concentrations. After impregnation, the fiber was cut to a length of 150 mm, and each sample was clamped at a distance of 25 mm from the end of each fiber. 8 samples were prepared for each case; thus, 240 samples were produced in total. A

Universal Two columns testing machine *Tinius Olsen H25KT* (limit: 25kN) (*Tinius Olsen*, United Kingdom) was used for the experiments. A loading rate of 2 mm/min was used during the tensile tests. This experiment aimed to analyze if the concentration of the impregnation solution influences the mechanical properties of impregnated CCF tows. Meanwhile, composite samples were printed according to the recommendations of the ASTM D 3039 Standard. According to the presently mentioned standard, at least five samples must be used to determine the properties of the material. It was therefore decided to prepare 5 samples under the same printing conditions and with the same materials. It is important to note that the composite samples used for tension were printed by using only the carbon fiber that was impregnated in the largest concentration solutions (8–10%), i.e., 60 pieces in total were obtained. The geometry of the samples is not strictly regulated by the Standard, thus samples of rectangular cross-sections with dimensions of 100×10×5 mm were used. Even though the Standard does not require to use a tab, missing tabs can significantly influence the mechanical properties, the nature and the location of a break. It was decided to use a 3D printed PLA material tab with the dimensions of 30×11×1.5 mm, 1K carbon fiber reinforced samples and 40×11×1.5, respectively, for 3K carbon fiber reinforced samples for this experiment. The slope angle used for both types of the tab was 30°, and tabs were attached to the samples by using cyanoacrylate glue.

2.5. Evaluation of Impregnated Carbon Fiber Tow Quality

This research aims to analyse how the impregnation conditions, such as the concentration, the impregnation speed, or the drying time of carbon fiber before printing, affect the number of air voids in the printed structure, the adhesion between the matrix and the reinforcing material, and the quality of the impregnated fiber. *Toray T300-1000* nonwoven continuous carbon fiber was used in the test. Before the testing, carbon fiber was impregnated in a 10% solution of PLA and methylene chloride. The impregnation process and its quality depend on a variety of parameters, such as the pulling (winding) speed, the solution preparation, the drying temperature, the chemical substances used, the inlet and outlet nozzle diameters, etc. During the testing, the parameters of the impregnation process were kept constant: the pulling speed was 30 rev/min, the drying temperature was 220 °C, and the inlet and outlet opening diameters were 0.6 mm. The appropriate impregnation process and the precisely chosen parameters have significant influence not only on the air void volume and the strength of impregnated carbon fiber, but also on the high-quality printing process. Microscopic image processing software *NIS Elements D* was used for the image analysis of carbon fiber, and an automated *Nikon Eclipse LV100ND* microscope with a high-resolution camera *DS-Ri2* was used for CCF cross-section analysis. Samples of fiber of 30 mm in length were taken at random and cut out of impregnated carbon fiber reel. Six continuous carbon fiber samples were prepared for visual analysis, which was carried out by using the *ImageJ2x* image processing software package. The quality of the impregnated fiber can be described by the ratio of the area of the impregnated inner area to the area of the air voids inside. Fig. 2.14 reveals the stages of the testing of visual analysis that are

necessary for the calculation of the impregnated fiber cross-section area and air voids.

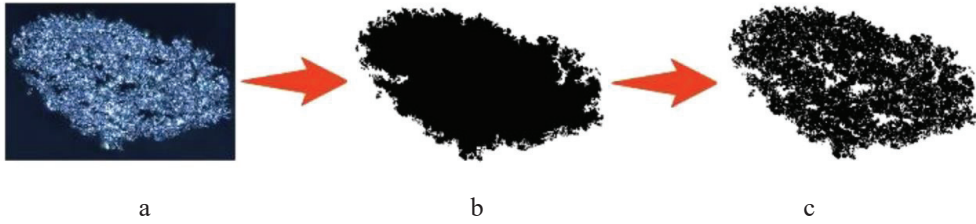


Fig. 2.14 Procedure of visual analysis: a – photo of cross-section; b – total area; c – impregnated area

Firstly, a cross-sectional image of impregnated carbon fiber (a) is inserted in the program, and the total cross-sectional area (b) is calculated. In this case, the total cross-sectional area of the impregnated fiber is ~ 0.6 megapixels. In the third step, the adjustment of the image contrast and the visual threshold help eliminate the air voids of the total area, thus obtaining the impregnated area image (c). In this case, the total cross-sectional area of the impregnated fiber is ~ 0.5 megapixels. After this analysis, the numerical value is calculated which describes the impregnation quality and reliability. This method can also be used to determine the number of air voids and their location in the fiber.

Another important material performance characteristic determined in this research is the pull-out force of the impregnated continuous carbon fiber from the matrix. This size allows the evaluation of the adhesion between the matrix and the reinforcing material. The samples for this test were prepared by covering the carbon fiber attached in the middle of the cylindrical shape with the matrix material. This method was selected for the determination of adhesion due to its simplicity, repeatability and the more accurate results. The adhesion testing procedure is illustrated in Fig. 2.15.

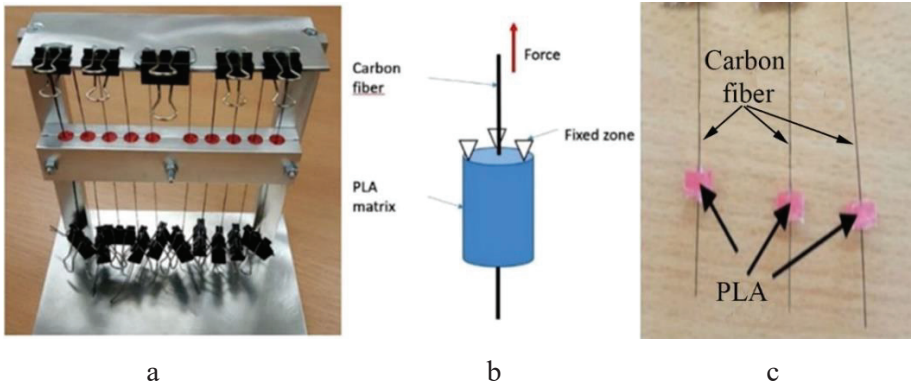


Fig. 2.15 Adhesion testing procedure: a – sample preparation; b – testing scheme; c – prepared samples

The pull-out of the impregnated fiber from the matrix material was performed by using Tinius Olsen H25KT at a 2 mm/min loading rate. Ten samples were used to determine the adhesion force with the impregnated carbon fiber filament in the cylindrical sample. In order to compare the influence of the impregnation, 10 samples of untreated carbon fiber were also produced to pull out the carbon fiber filament from the matrix material.

2.6. Investigation of Influence of Printing Parameters³

This investigation aims to characterize the internal defects of 3D printed CCF reinforced composite structures, specifically, voids: their formation and characterization, as well as the influence of voids on the mechanical properties. X-ray computed tomography and the matrix dissolution method were used during the investigation with the objective to determine the carbon content and the voids volume in the composite structures. During the mechanical testing, the voids volume influence on the strength performance, the adhesion properties and the breakdown nature were investigated. The basic scheme of the research is presented in Fig. 2.16.

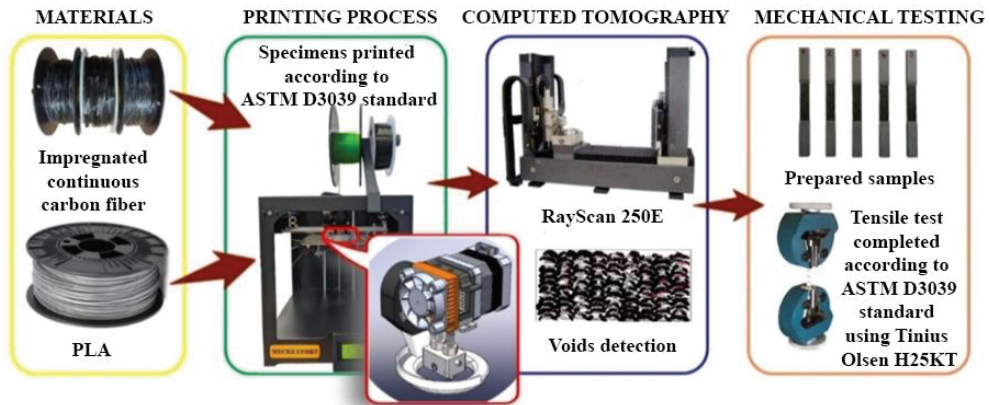


Fig. 2.16 Research workflow for void volume determination by using XCT

Carbon fiber is known to possess excellent mechanical properties and is a good electrical conductor. During the experiments, *Toray T300-1000* carbon fiber was used. The second part of the composite structure is thermoplastics; in this case, *DR3D polylactide* (PLA) 1.75 mm filament was used.

During the experiments, it was decided to investigate the influence of micro voids and their content on the tensile and bending properties in 3D printed composite structures.

The samples were printed by using 1K impregnated continuous carbon fiber. The fiber was impregnated in a 10% solution of *NatureWorks* PLA biopolymer and CH_2Cl_2 solvent. As previous research demonstrated, impregnation improves the mechanical properties of the printed composite structures, as well as the adhesion between layers, and facilitates the printing process. All the samples were printed by

³ The material in this section was previously published in [101]

using a *MeCreator2* printer with a modified printhead which allows printing composite structures. This printhead was developed to ensure the optimum printing process of composite structures of thermoplastic and continuous carbon fiber. CAD software *Solidworks 2019* was used to prepare 3D models of the samples. *Simplify 3D* software was used for the preparation of models and the printing process control which would allow choosing the location of the object, the printing speed, the layer height, the extrusion multiplier, etc. Unidirectional 0° samples were selected for printing according to the recommendations and requirements of the *ASTM D3039* Standard. All the samples with dimensions 135×11×5 mm were printed by using the same FDM machine, parameters and materials. Four groups of 5 samples each were printed for the investigation, and they were different in terms of the layer height and the print line spacing. These variables were chosen to evaluate how their variation changes the volume of air voids and the mechanical properties of the composite structures. Although it is well known that the tensile strength and the Young's modulus decrease with the increasing volume of the voids in the traditional composite structures, however, the influence of the voids in 3D printed composite structures has rarely been studied in the AM research community. The printing parameters of our research are provided in Table 2.7.

Table 2.7 Printing parameters

Groups of samples	Group 1	Group 2	Group 3	Group 4
Extrusion multiplier	0.6	0.6	0.6	0.6
First layer printing speed, mm/s	1.20	1.20	1.20	1.20
Fan speed, %	50 first/80 second/100 following layer	50 first/80 second/100 following layer	50 first/80 second/100 following layer	50 first/80 second/100 following layer
Extruder temperature, °C	200	200	200	200
Printing bed temperature, °C	70	70	70	70

Before further tests, a hypothesis has been put forward that, while decreasing the height of the printed layer and the print line spacing, the volume of air voids can decrease, and the mechanical properties, such as strength and stiffness, of the structure can increase.

Tensile tests were performed at a 2 mm/s loading rate on *Tinius Olsen H25KT*. Each group of samples consisted of five samples with tabs attached at their ends. Non-contact *VEM 300* video extensometer was used for the displacement measurement of the sample to the break. The samples were measured and weighed before the tests.

2.6.1. X-ray Defectoscopy of Printed Structures

The volume of the voids was evaluated by using two different methods. In the first case, 20 samples for mechanical tests were scanned by using the computed microtomography method. It was performed by using *Rayscan 250E* (*RayScan Technologies GmbH*, Germany). *RayScan 250E* is a 3D computed tomography system with two X-ray sources: a 10–230 kV X-ray source for the operation in the micro-focus mode (focus point: Ø3–250 µm) and the 50–450 kV macro-focus mode (focus point: Ø400 µm). The X-ray source and the X-ray detector can move up and down depending on the size of the object under investigation. The active area of the X-ray detector is 410×410 mm², 2048×2048 pixels. The measurements were performed by using the 10–230 kV X-ray source in the micro-focusing mode with the following parameters: 100 kV voltage, 200 µA current, ISO 2000 exposure time. 1800 projections (scanned images) of 11 µm resolution were created in total. For each scanned sample data set, a volume closure procedure using *Avizo* software was applied to separate air voids from the air around the sample (Fig. 2.17). The samples were analysed in perpendicular planes along with the longest measurement. The full and the filled area were calculated for each plane, and the difference between them represents the amount of air voids in the plane.

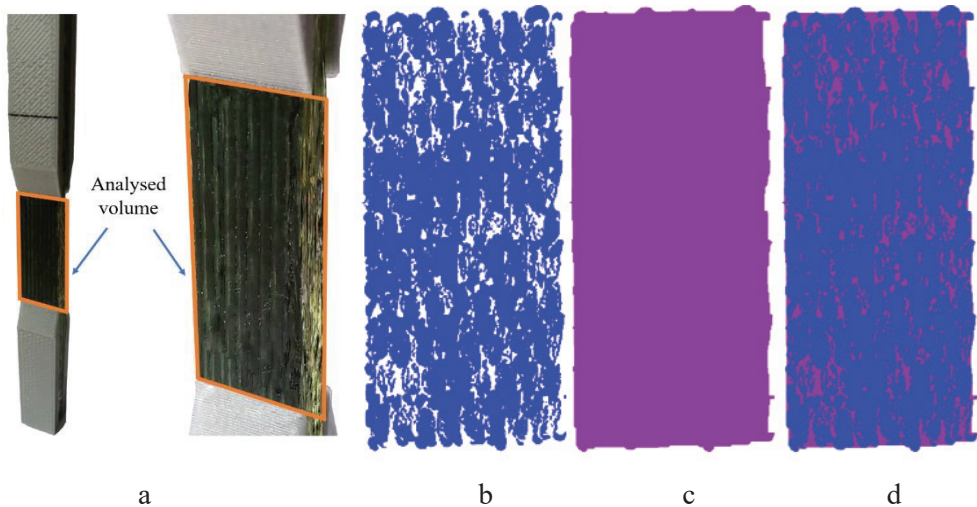


Fig. 2.17 CT analysis: a – analyzed volume; b – binary threshold; c – mask from the closing procedure; d – detected air voids

2.6.2. Air Voids Investigation Using *ASTM D 3171* Standard

In order to evaluate the effectiveness of computed tomography in the microstructural analysis of 3D printed structure research, the methodology defined in the *ASTM D 3171* Standard was used. Square cross-sectional samples were printed by using the same printing parameters. To determine the content of carbon in the composite structure, 3 samples with dimensions 30×10×10 mm for one type of structure were used as required in the Standard. To determine the effect of the surface roughness on the volume of air voids in the structure, it was decided to

perform the test with sanded and untreated samples. Samples of both types were weighed with an analytical balance *GR-200* with an accuracy of ± 0.1 mg. The samples were placed into a *Memmert UFB 40* furnace at a constant temperature of 40°C for 4 hours before weighing. The samples were measured with a *Mitutoyo SERIES 293* micrometer (accuracy $\pm 1\ \mu\text{m}$) to calculate the density of the composite structure. Procedure A2, according to the *ASTM D 3171* Standard, was used for matrix dissolution: the matrix is dissolved from the composite structure by using a solution of sulfuric acid and hydrogen peroxide. The process workflow is provided in Fig. 2.18.

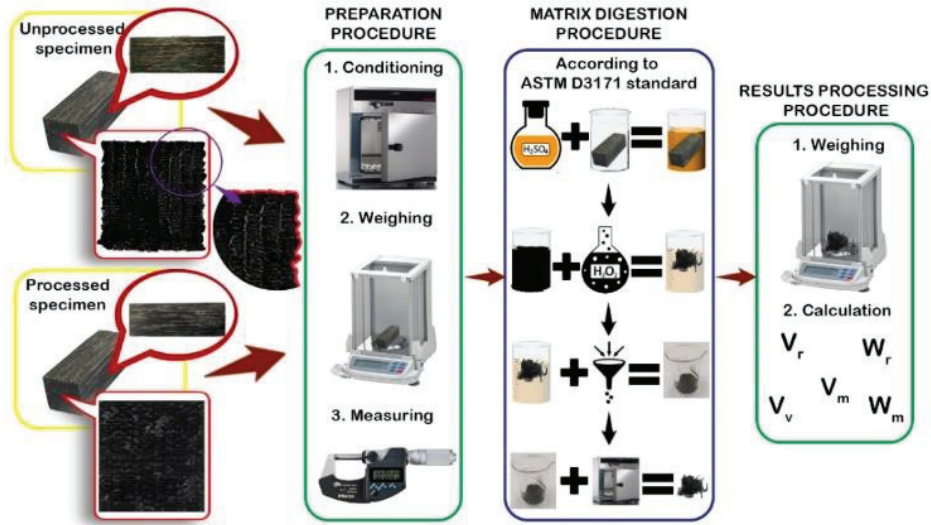


Fig. 2.18 Research workflow for void determination using matrix dissolving procedure

After dissolving the matrix material, the solution was filtered to separate the carbon fiber that was later washed with distilled water and dried at 100°C temperature for an hour. The dried carbon fiber was weighed with an analytical balance *GR-200*. The density of the carbon fiber and the matrix material (PLA) is provided by the manufacturers. The volume of carbon in the composite structure is calculated as:

$$V_r = (M_f/M_i) \cdot 100 \cdot \rho_c/\rho_r; \quad (1)$$

M_f – the mass of the weighed sample after dissolution;
 M_i – the mass of the composite sample before the investigation;
 ρ_c – the density of the composite structure;
 ρ_r – the density of the carbon fiber.

The density of the matrix material is calculated as:

$$V_m = (M_i - M_f)/M_i \cdot \rho_c/\rho_m \cdot 100; \quad (2)$$

Since the densities of the materials forming the composite structure differ, often, the percentage by mass of the matrix and the reinforcing material needs to be

calculated. The percentage by mass of the matrix material in the composite is calculated according to the formula:

$$W_m = (M_i - M_f)/M_i \cdot 100; \quad (3)$$

The percentage by mass of the carbon fiber in the composite structure is calculated according to the following formula:

$$W_r = (M_f/M_i) \cdot 100; \quad (4)$$

The amount of air pores determining the quality of the composite structure is calculated as:

$$V_v = 100 - (V_r + V_m); \quad (5)$$

V_v – the volume of pores in the composite structure.

2.7. Determination of Delamination Force and Shear Strength⁴

At present, in scientific articles investigating the mechanical properties of continuous carbon fiber reinforced 3D printed composite structures, the main object of the research is usually the tensile strength and the flexural strength; yet, other mechanical properties are no less important. Since AM is based on the production of the object layer by layer, it is essential to evaluate the adhesion between the layers and the fusion between the matrix and the reinforcement. During this research, the shear strength and the separation force required to separate the two independent layers of the CCF reinforced structures and their dependence on the printing parameters and the overlap length shall be investigated.

The research consists of three stages: the printing process, the mechanical testing, and the visual analysis. The workflow is provided in Fig. 2.19.

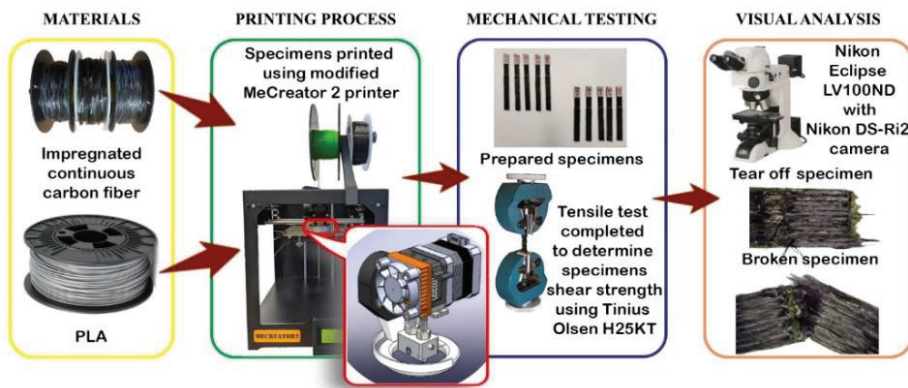


Fig. 2.19 Experiment workflow for delamination force and shear strength

All the composite samples were printed by using PLA filament and impregnated 1K CCF. *MeCreator2* was chosen for the printing of composite samples. The sequence of the printing process is provided in Fig. 2.20 a. It is

⁴ The material in this section was previously published in [102]

important to note that all the samples for this test were printed by using the improved prototype. It is marked in the scheme with the number (1). During the printing process, thermoplastic (2) and continuous carbon fiber (3) enter the heating element at the same time through two different input channels (4). The matrix and the reinforcing material mix in the heating element just before the composite filament is placed onto a borosilicate glass plate (6) on the metal printing platform (7) through the nozzle (5). It is important to consider that the matrix material is fed into the printhead by using a feeding device.

The carbon fiber is supplied through the movement of the printhead and the force of adhesion to the printing platform. The constant heating head temperature is maintained by using an electric heating element (8) and controlled by a thermocouple (9). To increase the adhesion of the composite filament with the printing platform and to reduce the pulling effect (Fig. 2.20 b), the glass surface is coated with a thin layer of adhesive *3DLAC* before printing. The above mentioned pulling effect occurs when the printhead changes its direction. During this pulling, the length of the sample decreases (as indicated in Fig. 2.20 b and 2.21 b where the blue line marks the actual length of the sample after the printing: the orange color represents the designed length of the sample, A is the length change after the filament pulling).

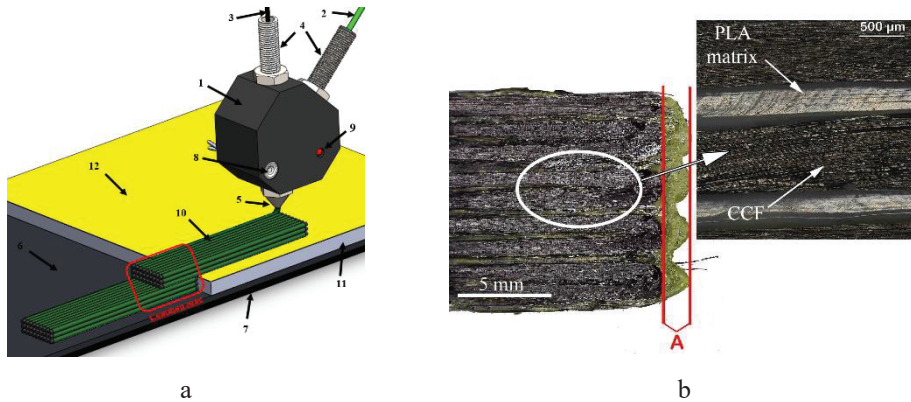


Fig. 2.20 Printing process: a – scheme of the printing process; b – pulling effect; 1 – improved heating element; 2 – thermoplastic; 3 – impregnated CCF; 4 – guiding tubes; 5 – nozzle; 6 – borosilicate glass plate; 7 – metal printing platform; 8 – heater; 9 – thermocouple; 10 – overlap area; 11 – steel plate; 12 – Kapton tape

It is impossible to eliminate this effect completely; however, it can be reduced by increasing the cooling of the area, by decreasing the printing speed, or by using additional substances to increase adhesion between the platform and the printing structure. As mentioned above, before the printing process, extruded plastic bonds to the printing platform together with the carbon fiber. When the printhead moves in the x/y axis directions, the composite filament replicates the tool path and forms the object. However, if the movement direction changes (by more than 60°), the pulling effect may be observed since carbon fiber is not able to adhere to the platform, and the tensile force moves it slightly along with the moving printhead. This effect can

be reduced by increasing the cooling of the extruded material, by increasing the adhesion of the matrix material to the platform and decreasing the printing speed, or by performing compensation of the item dimensions.

In order to determine the shear strength, single lap-joint samples were selected for printing. This type of sample was chosen due to its simplicity and its wide use in determining the adhesion and shear strength in composite structures. To print these samples with a modified printer, during the printing process on the platform, a steel plate (11) of the appropriate thickness is added (depending on the height of the printed sample layer). Kapton tape (12) is glued to the surface of the plate to increase the adhesion between the printed sample and the platform. Kapton tape is also covered with a thin layer of *3D LAC* adhesive before the printing process. All the samples used in the tests were printed by using the same printer, the same materials, and constant printing parameters. The parameters are provided in Table 2.8.

Table 2.8 Printing parameters

Nozzle diameter, mm	1.6
Extrusion multiplier, %	70
Print line spacing, mm	1/1.2
Layer height, mm	0.3/0.4
Printing speed, mm/s	3
Cooling, %	80
Platform temperature, °C	80
Head temperature, °C	210

In order to perform statistical evaluation of the results, five samples were obtained (Fig. 2.21) while maintaining the constant sample length (100 mm), and the three layers were printed; however, it was decided to modify four parameters: the layer height Z (from 0.3 to 0.4 mm), the print line spacing K (from 1 to 1.2 mm), the overlap length Y (from 10 to 20 mm, while increasing in increments of 5 mm), and the number of printing lines in width L (9 and 11 filaments). 120 samples were printed in total. Details of the printed samples are given in Table 2.9 and Table 2.10.

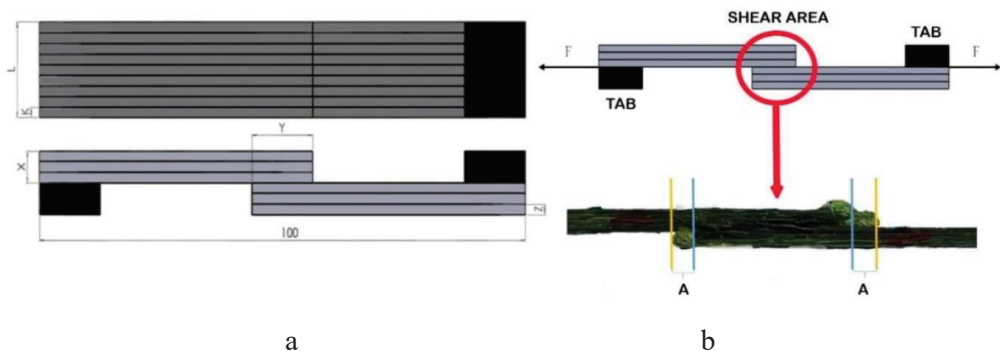


Fig. 2.21 Printed sample: a – schematic view of the sample; b – shear area after print; A – length change after pulling

All the printed samples were divided into two main groups by the number of printing lines in their width. Like the length of the overlap, the number of printing lines has a direct effect on the shear area width and the separation force. Each group consists of 12 subgroups with different layer heights, print line spacing and overlap lengths. The details of sample groups with 9 printing lines are provided in Table 2.9.

Table 2.9 Printed samples with 9 printing lines

Group of the sample	G1	G2	G3	G4	G5	G6	G7	G8	G9	G10	G11	G12
Line number Y	9	9	9	9	9	9	9	9	9	9	9	9
Layer height Z, mm	0.3	0.3	0.3	0.4	0.4	0.4	0.3	0.3	0.3	0.4	0.4	0.4
Print line spacing K, mm	1	1	1	1	1	1	1.2	1.2	1.2	1.2	1.2	1.2
Length of the shear area Y, mm	10	15	20	10	15	20	10	15	20	10	15	20
Shear area, mm ²	38	76	129	38	76	129	39	89	146	39	89	146

The details of the sample groups with 11 printing lines are provided in Table 2.10. As the provided data indicates, the actual total area increases by 30% on average by increasing the number of lines from 9 to 11. The maximum increase of the shear area is recorded when the overlap length is 10 mm, and it increases by about 41%.

Table 2.10 Printed samples with 11 printing lines

Group of the sample	G1	G2	G3	G4	G5	G6	G7	G8	G9	G10	G11	G12
Line number Y	11	11	11	11	11	11	11	11	11	11	11	11
Layer height Z, mm	0.3	0.3	0.3	0.4	0.4	0.4	0.3	0.3	0.3	0.4	0.4	0.4
Print line spacing K, mm	1	1	1	1	1	1	1.2	1.2	1.2	1.2	1.2	1.2
Length of the shear area Y, mm	10	15	20	10	15	20	10	15	20	10	15	20
Shear area, mm ²	53	89	152	53	89	152	59	116	176	60	116	176

The bigger increase in the shear area in these sample groups appears due to the pulling of the printing filament during the printing process. This effect is indicated in Fig 2.21 b and marked with the letter *A*. In order to print the sample of 100 mm, the length of the model is designed to be 5 mm longer, i.e., 105 mm. This principle

applies to the length of the sample, but not to the overlap length. The actual (after printing) overlap length is provided in Table 2.11.

Table 2.11 Shear area overlap length difference

Nominal length, mm	Real length of the shear area, mm	Difference, %
10	4.8	52
15	9.7	35
20	15.1	24.5

The overlap length for adhesion testing was chosen experimentally. It is not possible to print with a nominal length of less than 10 mm or to delaminate more than 20 mm. Samples produce fracture before they are delaminated. Therefore, when determining the shear strength, the length was changed within the interval from 10 to 20 mm.

2.7.1. Shear strength test

The shear strength size was determined by performing a tensile test. The shear strength was calculated by using the following formula:

$$\tau = \frac{F}{A}; \quad (6)$$

τ – shear strength;

F – shear force;

A – shear area.

The tensile test was performed with *Tinus Olsen H25KT* with mechanical clamps at a loading rate of 2 mm/min. It was decided to use additional plates for the testing. The additional plates decrease the influence of the flexural and rotating forces which appear during the testing. A sketch of the prepared sample is presented in Fig. 2.21 b. The additional plate dimensions are as follows: thickness 0.9 or 1.2 mm depending on the height of the sample layer, length 15 mm (regardless of the sample parameters), the width depends on the width of the sample, the material is PLA.

The plates are glued to the sample by using universal ethyl 2 cyanoacrylate glue after removing any plastic deposits left after the printing with sandpaper and rubbing the contact surface of the sample for better adhesion between the plate and the sample.

After the shear strength test, visual analysis of the samples was performed to determine the nature of delamination. A *Nikon Eclipse LV100ND* optical microscope was used for the visual analysis.

2.8. Improvement of Mechanical Properties by Secondary Impregnation

The test aims to investigate the possibilities of the improvement of mechanical properties of 3D printed composite structures impregnated with epoxy resin. The research process consists of three main stages: printing, impregnation, and mechanical testing (Fig. 2.22).

Thermoplastic filament and 1K continuous carbon fiber, which was impregnated in a 10% solution of methylene chloride and PLA, were chosen for printing. All the samples were printed by using the material extrusion based FDM technology. Some of the printed samples were impregnated in epoxy resin. After the impregnation, the samples were prepared for the mechanical tensile and flexural tests. After the analysis of the obtained results, the values of the tensile and flexural strength, the Young's modulus, the Poisson's ratio, and the effectiveness along with the benefits of the impregnation process in improving the mechanical properties of the printed composite structures were determined.

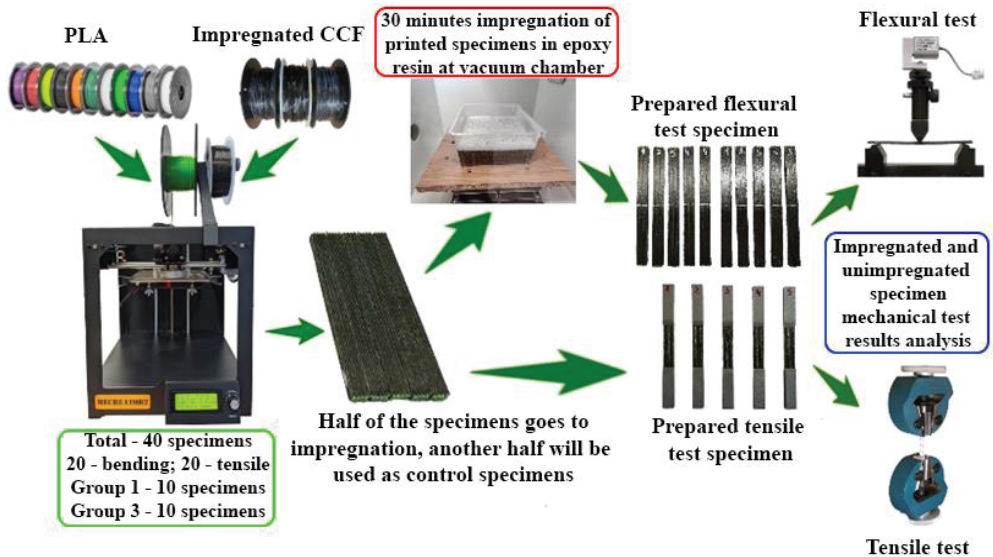


Fig. 2.22 Research workflow for the improvement of mechanical properties of 3D printed CCF composite structures by secondary impregnation

All the samples were printed by using 1.75 diameter *DR3D Filament* (PLA) thermoplastic filament which was used as a matrix for composite samples. Before the printing process, carbon fiber was impregnated in a 10% solution of PLA and dichloromethane. Some of the printed composite samples were impregnated in the *R&G Faserverbundwerkstoffe GmbH* manufactured epoxy resin *Epoxy Resin L* while using the hardener *L*. This combination of the epoxy resin and the hardener was selected by considering its mechanical characteristics and temperature properties. The tensile strength of this epoxy resin is 69 MPa, and the flexural strength is 111 MPa. Resin *L* features a curing time of 40 minutes. At this stage, the printed samples shall be immersed in the resin in a vacuum chamber and thoroughly cleaned afterwards. The low viscosity of the hardener and resin system allows better penetration of the impregnating material into the air voids inside the sample and filling them. The low reaction temperature and hardening at the ambient temperature allow avoiding the possible matrix damage or sample deformation. The resin is also transparent and resistant to UV; it features a glass transition temperature similar to

that of the matrix material ~ 76 °C; the resin is also highly resistant to static and dynamic effects.

2.8.1. Printing Process

According to the *ASTM D 3039 Standard Test Method for Tensile Properties of Polymer Matrix Composite Materials* and *ASTM D 7264 Flexural properties testing of polymer matrix composite materials*, 40 samples were taken (20 samples for each mechanical testing). The dimensions of the tensile samples are $150 \times 13 \times 2$ mm (L×W×H), respectively, meanwhile, the flexural sample designed dimensions are $4 \times 13 \times 150$ mm. It is important to note that, during designing, the sample length was extended to 155 mm because, during the printing of composite structures with a modified device, the printed sample shortens to the designed 150 mm. Experiments demonstrated that the shrinkage of the printed composite structure stems from the improper adhesion between the thermoplastic matrix and the glass surface of the printing platform when the printhead transitions (loop) from one print line to the other.

For increased adhesion of the printing platform and the printed composite structure, a clean glass surface is coated with *3D LAC* adhesive. The printing time depends on the sample height (which varies from 2 to 4 mm) and on the print line spacing (which varies from 1 to 1.2 mm). All the samples used in the testing were printed by using the same printer, the same materials, and the constant printing parameters. The parameters are provided in Table 2.12.

Table 2.12 Printing parameters

Sample group	Group 1	Group 3
Nozzle diameter, mm	1.6	
Extrusion multiplier, %	70	
Cooling, %	70	
Platform temperature, °C	80	
Head temperature, °C	210	

40 samples were printed in total: 20 samples for tensile and 20 samples for flexural tests. The ‘tensile’ and ‘flexural’ samples were divided into two groups (10 samples each) according to the print line spacing. Each group was divided in half; five samples were selected before secondary impregnation in order to define the mechanical properties of unimpregnated composite structures. The other samples were left for the impregnation with epoxy resin. All the samples were measured by using a caliper (in terms of their height, width and length) and weighed. To achieve a more accurate measurement, the overall dimensions were measured three times at different points (at both ends and at the center) of the sample.

2.8.2. Secondary Impregnation Process

Impregnation in epoxy resin was performed on twenty printed composite samples (10 tensile and 10 flexural) to evaluate the effect of impregnation on their mechanical properties. When printing, air voids appear between the print lines and the printing layers (Fig. 2.23). Air voids appear not only because of the print process

of the composite structures, but, also, due to the peculiarities of the FDM technology, air voids always appear between 4 printing lines in two layers. The number of air voids in the printed structure can be reduced by adjusting three parameters of the printing process: by reducing the layer height, the print line spacing, and the percentage of plastic in the sample. By changing any of these parameters, the amount of the reinforcing material in the composite structure changes accordingly. The amount of CCF in the samples used in this experiment varied from 18% (the print line spacing was 1.2 mm) to 22.4% (the print line spacing was reduced to 1 mm); the layer height remained constant at 0.3 mm. A larger number of air voids in the structure exerts direct influence on the reduced mechanical properties, the decreased adhesion between the print layers and the lines. In addition, moisture can accumulate in the air voids of the structure, which can significantly shorten the service life of the printed composite structures. The main purpose of impregnation is to reduce the number of these air voids by filling them with epoxy resin and impregnating them in a vacuum chamber. The quality of the process directly depends on the viscosity of the epoxy resin. The more viscous it is, the harder the epoxy resin fills the voids inside. It is necessary to ensure that, during impregnation, the outer surface of the structure is also covered. This outer shell of epoxy resin is also useful. The covered surface protects the composite structure from adverse environmental factors, rapid ageing, and mechanical wear. The ideal impregnation of the cross-section of the composite structure is indicated in Fig. 2.23. The ideal impregnation is achieved when all air voids inside the structure are filled with epoxy resin, and the outer surface is covered with a thin layer which helps to smoothen the surface; however, it has no significant effect on the mechanical properties.

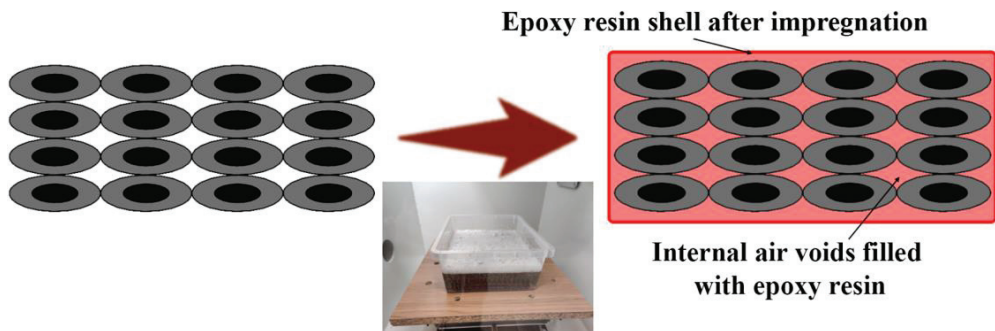


Fig. 2.23 Cross-section image of sample before and after impregnation

10 tensile and 10 flexural samples (five samples each of Group 1 and Group 3) were placed in a container for impregnation. Then, the container was filled with a mixture of *Epoxy Resin L* and hardener *L* at a ratio of 100:40 (tolerance: $\pm 2\%$). Since the total weight of the mixture in use was greater than 20 g, the resin and the hardener were dosed according to the weight ratio. It is important to mix the epoxy resin and the hardener at the most accurate ratio; otherwise, the curing time may be shortened or extended, the mixture may not cure at all, or it may exhibit poorer mechanical characteristics than the ones specified by the manufacturer. This can also

affect the viscosity of the resin, which can lead to the insufficient filling of air voids in the printed composite structure. Another important factor is the impregnation process temperature. The most suitable temperature is between 20–25 °C; quantities of more than 100 g of the mixture cannot be stirred at a lower temperature, as this affects the viscosity of the mixture and the reaction time. When the temperature rises by 10 degrees, the reaction time decreases by half, but the amount of heat released during the reaction is doubled. In our case, the samples were filled with a mixture of 500 g of the epoxy resin and the hardener, and the whole system was placed in a vacuum chamber. To eliminate as much air from the samples as possible, the pressure inside the vacuum chamber was decreased to 0.5 kPa. The system remained in this environment for 30 minutes. The most active elimination of air was performed at the ends of the sample, which indicated that the greatest penetration of the resin into the air voids of the sample occurred through the openings at the ends. After half an hour, the samples were removed from the epoxy resin and thoroughly dried, cleaned and left to cure for 24 hours at room temperature. After 24 hours, all the impregnated samples were measured again. The efficiency of the impregnation process for cavity filling was evaluated by calculating the percentage change in the sample mass and cross-section. One of the major parameters to evaluate the efficiency of the impregnation process and the filled voids inside the sample is the change in the mass of the impregnated and unimpregnated samples. The higher is the value, the higher is also the amount of the epoxy resin that got inside the sample and reduced the number of air voids. However, this value only relatively indicates the efficiency of the air voids filling, as the epoxy resin also remains on the outside of the sample as well. In order to assess how well the epoxy resin was removed from the surface of the sample and its deposits, the cross-sectional area of the sample after impregnation is calculated. The smaller is the difference between the impregnated and the unimpregnated sample cross-sectional areas, the better is the cleaning of the composite structure after the impregnation process.

2.8.3. Flexural and Tensile Testing

Both impregnated and unimpregnated tensile and flexural samples were tested by using *Tinius Olsen H25KT*. Different force sensors were used (a 25 kN sensor for the tensile test, and 1 kN sensor for the flexural test) depending on the tensile and flexural forces influencing the samples.

The flexural test was carried out according to the procedure specified in the *ASTM D 7264* Standard. Printed composite structures were bent by using the 3-point bending method. The loading rate was 1 mm/s, and the distance between the supports was 128 mm. All the samples were numbered prior to the test, and the center of each sample was marked. The prepared samples and the flexural scheme are provided in Fig. 2.24. The samples were placed on 10 mm-diameter support rollers, and the force was transmitted to the sample through a 10 mm roller.

The flexural test was carried out until the resistance force suddenly decreased; during the testing, a significant change in force was observed during the tenth minute of the test, after which, it decreased dramatically.

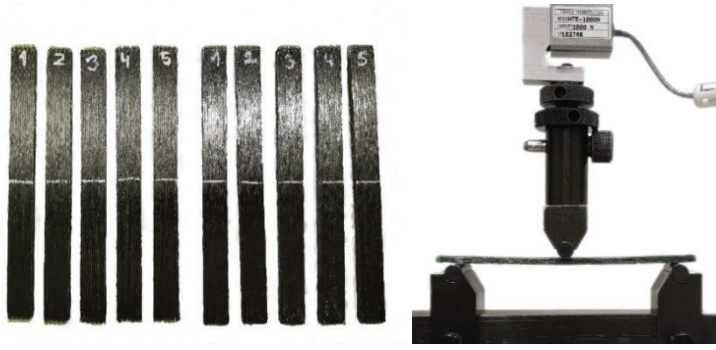


Fig. 2.24 Samples ready for the test; the principal flexural test scheme

Flexural stresses were calculated by using the following formula:

$$\sigma = \frac{3PL}{2bh^2}; \quad (7)$$

σ – stress on the outer surface at the centre, MPa;
 P – force at the sample, N;
 L – distance between the supports, mm;
 b – sample width, mm;
 h – sample height, mm.

The flexural modulus is calculated by using the following formula:

$$E^{chord} = \frac{\Delta\sigma}{\Delta\varepsilon}; \quad (8)$$

E – flexural modulus, MPa;
 $\Delta\varepsilon$ – change of bending stresses between two points of deformation, MPa;
 $\Delta\sigma$ – change between two selected deformation points (nominal: 0.20%).

The tensile test was carried out according to the test procedure specified in the *ASTM D 3039* Standard. When preparing the samples for the tensile experiment, additional plates with the dimensions 50×13.6×2 were printed of PLA and glued to both ends of the sample. One end of the plate had a 60° bevel. The main purpose of the plates is to evenly distribute the force resulting from the attachment of the sample, thus reducing the possibility of damage to the sample during tension. In addition, before the testing, the central part of the sample between the additional plates is painted white, and six points are marked that will be used to determine the transverse and the longitudinal deflection during tension. The sample is painted to make the marked points clearer during the test. The prepared samples and the tensile test scheme are presented in Fig. 2.25. Deflections were measured by using a video extensometer. The loading rate of the printed composite structures was 2 mm/s.

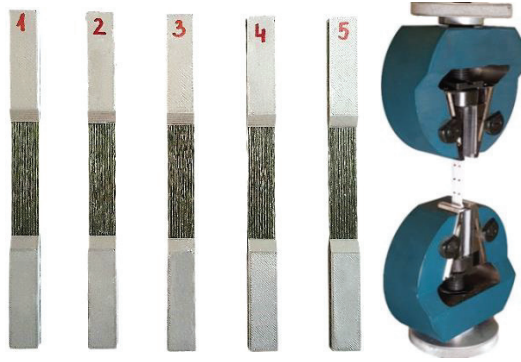


Fig. 2.25 Prepared tensile sample; scheme of the tensile test

The tensile stresses were calculated by using the following formula:

$$\sigma = \frac{F}{A}; \quad (9)$$

σ – tensile stress, MPa;

F – force acting on the sample, N;

A – cross-sectional area of the sample, mm.

The tensile modulus was calculated by using the following formula:

$$E = \frac{\sigma_2 - \sigma_1}{\varepsilon_2 - \varepsilon_1}; \quad (10)$$

E – tensile modulus, MPa;

σ_1 – tensile stresses at the strain of 0.25%;

σ_2 – tensile stresses at the strain of 0.05%;

ε_1 – strain point 1;

ε_2 – strain point 2.

Poisson's ratio was calculated by using the formula:

$$\nu = -\frac{\varepsilon_l}{\varepsilon_a}; \quad (11)$$

ν – Poisson's ratio;

ε_l – lateral strain;

ε_a – axial strains.

2.9. Chapter Conclusions

Following the planned research, a novel additive manufacturing technology for the rapid fabrication of CCF reinforced structures was developed based on FDM. Recommendations for the manufacturing parameters were presented: the layer height from 0.3 to 0.4 mm for the 1K carbon fiber and from 0.5 to 0.7 mm for the 3K carbon fiber tow, while the print line spacing from 1 to 1.2 mm and from 1.4 to 1.6 mm for 1K and 3K carbon fiber tow, respectively, was suggested. An improved printing module with the effective design of the input/output channels and co-extrusion was designed, fabricated and successfully demonstrated for 3D printing of composite structures reinforced with 1K and 3K CCF. The methodology was

implemented, and the equipment was designed for CCF impregnation before printing at 10 wt% PLA and treating with the methylene chloride solution. The impregnated carbon fiber is denoted by a lower void volume, superior mechanical properties and higher rigidity, which improves printability. The methodology for the tensile and flexural strength, the Young's modulus, the Poisson's ratio and other material characterizations was described. For the air void volume determination, two different methods were used: dissolving of the matrix and defectoscopic analysis of the printed composite structures by means of X-ray computed tomography. The methodology for the improvement of mechanical properties of 3D printed composite structures by secondary impregnation with epoxy resin was developed and tested.

3. CHARACTERIZATION RESULTS

3.1. Carbon Fiber Tow Impregnation⁵

The dissolution time depends on the stirring speed, concentration and the materials in use. The dissolution time is provided in Table 3.1. As the data in the table indicates, the dissolution duration highly depends on the material(s) in use. The test showed that PC dissolves most rapidly, and that there is a linear relationship between the dissolution time and the concentration of the substance in the solution. Meanwhile, the duration of PLA and ABS material dissolution was extended when the concentration increased to 8%. These increases in the dissolution duration are explained by the material behavior during dissolution. As the concentration increased to 8–10%, granular agglomeration formed in the solution, which significantly increased the dissolution time of the thermoplastic.

Table 3.1 Dissolution time of materials

Concentration, %	2	4	6	8	10
Time, min (PLA)	20	25	30	90	120
Time, min (ABS)	15	20	40	50	55
Time, min (PC)	15	20	23	25	28

After material impregnation in solutions of different concentrations, the impregnated fiber was cut into samples of 1 m long and weighed. The results are provided in Fig. 3.1.

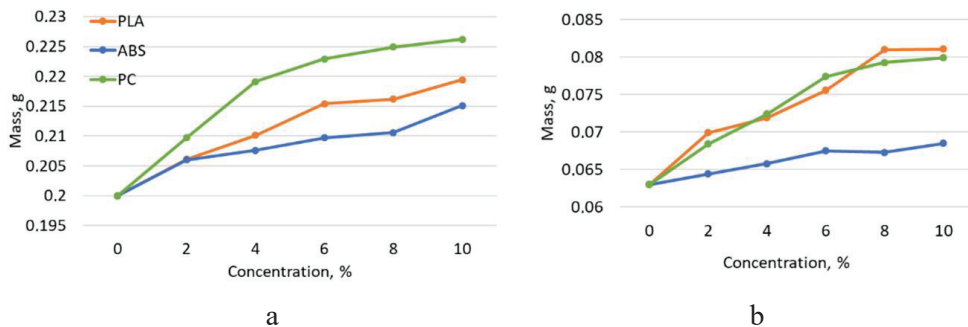


Fig. 3.1 Mass of carbon fiber after impregnation at different concentrations: a – 3 K carbon fiber; b – 1 K carbon fiber

As shown by the presented data, the least prominent change in the mass of the carbon fiber was observed in the carbon fiber impregnated with the ABS solution, and this can be explained by the lower density of the ABS material. Meanwhile, the density of PLA and PC thermoplastic is similar, hence, the masses of 1K PLA and

⁵ The material in this section was previously published in [100]

PC impregnated carbon fiber are also similar. In order to explain the differences in the mass between PC and PLA using 3K carbon fiber, a solution viscosity test is required. In this case, it can be assumed that, due to the differences in viscosity, PC is better absorbed in the carbon fiber. The results provided in Fig. 3.1 with 0% concentration demonstrate the mass of unimpregnated carbon fiber.

The concentration of the PLA solution was shown to have a significant effect on the quality of the carbon fiber impregnation (Fig. 3.2). As the concentration of the solution increases, the number of air voids in the impregnated carbon fiber tow decreases. After the visual analysis, it can be observed that the adhesion between the carbon fiber filaments soaked in 2–4% solutions is insufficiently low. This concentration of the solution cannot ensure the proper adhesion between separate fibers. Meanwhile, when the concentration of the solution changes from 6% to 10%, only slight changes in the impregnated carbon fiber are detected.

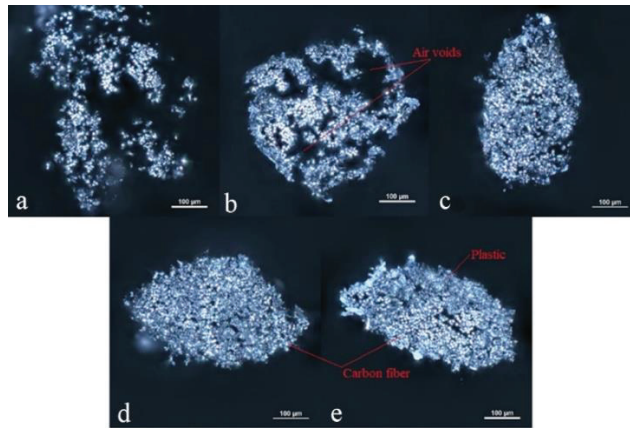


Fig. 3.2 Optical micrographs of the cross-section of impregnated carbon fiber tow: a – 2%; b – 4%; c – 6%; d – 8%; e – 10%

Tensile tests of the impregnated carbon fiber were performed to determine the mechanical properties of the impregnated fibers and the effect of impregnation on printed composite structures.

The tests were performed at all concentrations (2–10%) and different impregnation materials (ABS, PLA, PC). The impregnation results are highly dependent on different parameters, including those that are hard to control, e.g., the impregnation device nozzle blockage. It was decided to reject two tensile test results with the maximum and minimum values. Fig. 3.3 indicates the tensile results of PLA impregnated carbon fiber (1K and 3K). As expected, the mechanical properties of carbon fiber tend to increase when impregnating with a solution of a larger concentration, i.e., the tensile force increases with a higher concentration of the solution.

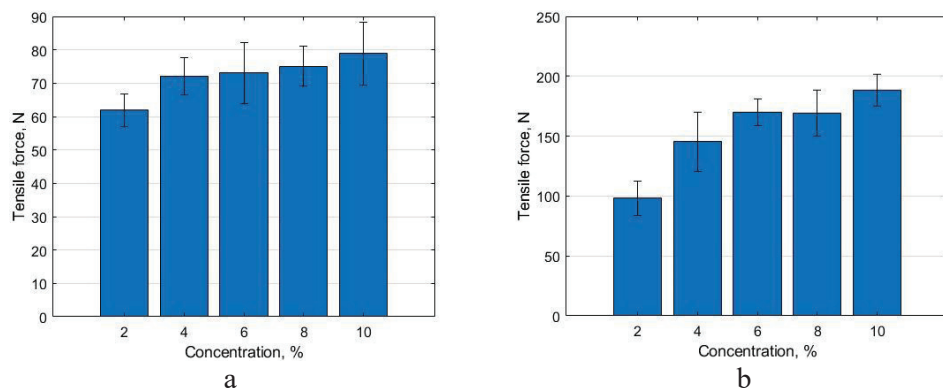


Fig. 3.3 Tensile properties of PLA impregnated carbon fiber: a – 1K carbon fiber; b – 3K carbon fiber

It is important to evaluate the relation between the impregnated carbon fiber mass and the tensile force during the tension. The mass difference indicates how much the impregnation material adheres to CCF. For this reason, the correlation coefficient between the impregnated carbon fiber mass and the tensile force results was calculated. Based on the obtained results, a strong relationship between the impregnated carbon fiber mass and the tensile force was found. The calculated PLA impregnated 1K and 3K carbon fiber correlation coefficients were determined as 0.82 and 0.97, respectively. These results indicate a significant linear relationship between the impregnated carbon fiber mass and the tensile force.

As mentioned above, the scattering of the results that can be influenced by various reasons, such as the nozzle blockage, the ambient temperature, the viscosity of the solution; also, some other parameters of the impregnation process were observed. On the other hand, it is also possible that, during the impregnation process, when a larger amount of carbon fiber filaments is impregnated, the nozzle tends to clog more frequently, and a large number of carbon fiber filaments is damaged. In terms of other properties, it should be noted that 1K carbon fiber impregnated with a 10% solution of PLA becomes fairly brittle. This causes problems when winding this fiber on the spool, and it is more difficult to feed it to the printing device. No such difficulties were observed after impregnation with PC and ABS solutions. Fig. 3.4 outlines the tensile results of PC impregnated carbon fiber.

It should be noted that the trends remain similar to the impregnation with the PLA solution. When the concentration of the solution increases, the tensile force also increases. The calculated correlation coefficients for PC impregnated 1K and 3K carbon fiber are 0.89 and 0.98, respectively.

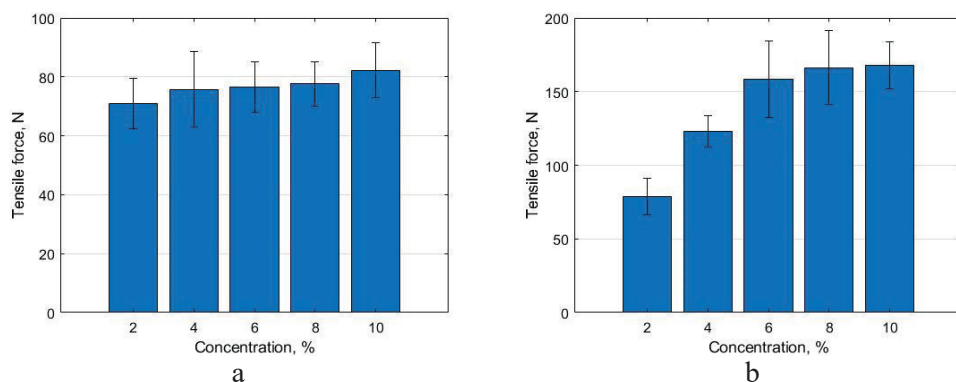


Fig. 3.4 Tensile properties of PC impregnated carbon fiber: a – 1K carbon fiber; b – 3K carbon fiber

Fig. 3.5 indicates ABS solution impregnated carbon fiber test results. There is also a trend of the increased tensile force of the impregnated carbon fiber as the concentration of the solution increases. A significant increase in the tensile force is demonstrated in Fig. 3.5 when the concentration changes from 2% to 4%. The cause may be the insufficient adhesion between the fibers, as this may be due to the low concentration of the polymer in the solution. However, the correlation coefficient confirms the strong positive relationship between the impregnated carbon fiber mass and the tensile force. The lowest correlation coefficient of 0.82 was obtained in the 1K fiber impregnated with the PLA solution. Another correlation coefficient was 0.89 for the 1K fiber impregnated with PC solution.

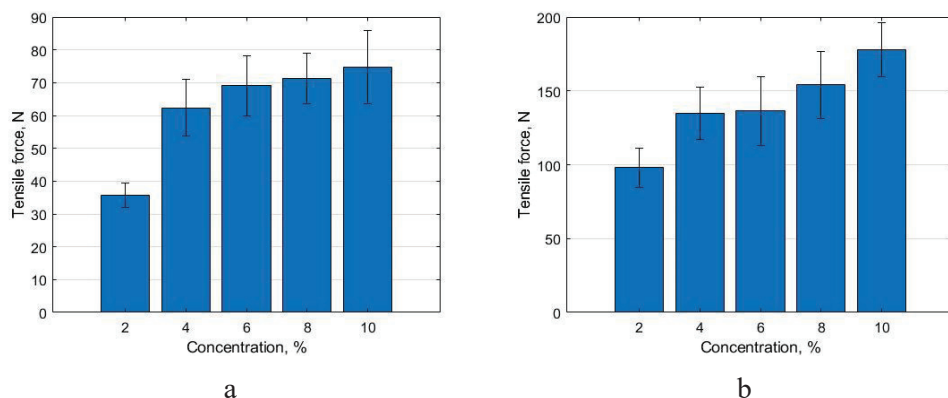


Fig. 3.5 Tensile properties of ABS impregnated carbon fiber: a – 1K carbon fiber; b – 3K carbon fiber

All other correlation coefficients significantly exceeded the previously mentioned values. The strongest relationship (correlation coefficient: 0.99) between the variables was determined in the 3K carbon fiber impregnated with the polycarbonate solution. Based on the obtained results, it can be stated that the results of the carbon fiber tensile tests using 3K carbon fiber for impregnation reveal a

higher correlation with the amount of plastic than with 1K carbon fiber. This happens because 3K CCF is denoted by a larger specific surface area. It can be assumed that, by changing the impregnation process parameters and impregnating with solutions of different concentrations, the tensile strength of the carbon fiber reinforced structures will change, respectively. The results also indicate that 1K carbon fiber impregnated with PC offers the best qualities during the tensile test. Yet, when using 3K carbon fiber, the best results were obtained when using impregnation with the PLA polymer solution.

3.1.1. Mechanical Properties of 3D Printed Composite Structures

The tensile force values of the carbon fiber do not reflect the actual mechanical properties of the composite structure because the adhesion of the impregnated carbon fiber, the matrix material and the impregnated carbon fiber tow behavior during the printing are not evaluated. It is also necessary to appreciate that different impregnating materials were used, and adhesion properties between the matrix and the reinforcing materials are unknown. Hence, in order to investigate the mechanical properties of the composite material, the carbon fiber impregnated in 8% and 10% solutions of ABS, PLA and PC was used. Five samples were printed with 1K and 3K carbon fiber, and different concentrations of impregnation solution were applied. The dimensions and the mass averages of the printed samples are provided in Table 3.2.

Table 3.2 Dimensions of 3D printed samples

Material	Length, mm	Width, mm	Thickness, mm	Mass, g
Samples reinforced with 1K carbon fiber				
PLA 8	99.87±0.36	10.94±0.09	4.98±0.05	4.68±0.13
PLA 10	100.58±0.46	11.1±0.02	5.08±0.01	4.7±0.09
PC 8	100.77±0.63	11.09±0.20	5.11±0.03	4.73±0.04
PC 10	101.32±0.08	10.81±0.06	5.07±0.03	4.76±0.05
ABS 8	101.2±0.52	11±0.04	5.11±0.02	4.85±0.03
ABS 10	101.16±0.17	10.9±0.04	5.07±0.02	4.79±0.09
Samples reinforced with 3K carbon fiber				
PLA 8	100.17±0.23	11.63±0.02	5.25±	5.6±0.03
PLA 10	99.57±0.63	11.54±0.03	5.29±	5.62±0.08
PC 8	99.91±0.41	11.64±0.05	5.34±	5.6±0.07
PC 10	100.12±0.4	11.58±0.06	5.31±	5.63±0.1
ABS 8	99.76±0.56	11.53±0.03	5.31±0.03	5.53±0.07
ABS 10	100.1±0.53	11.59±0.05	5.35±0.05	5.54±0.02

The tensile strength test results are provided in Fig. 3.6. Based on the results of mechanical tests of the impregnated carbon fiber tow and compared to the properties of the printed samples, it appears that impregnation affected the mechanical properties

of the material. Also, the parameters of the printing process have a significant effect on the repeatability of the results.

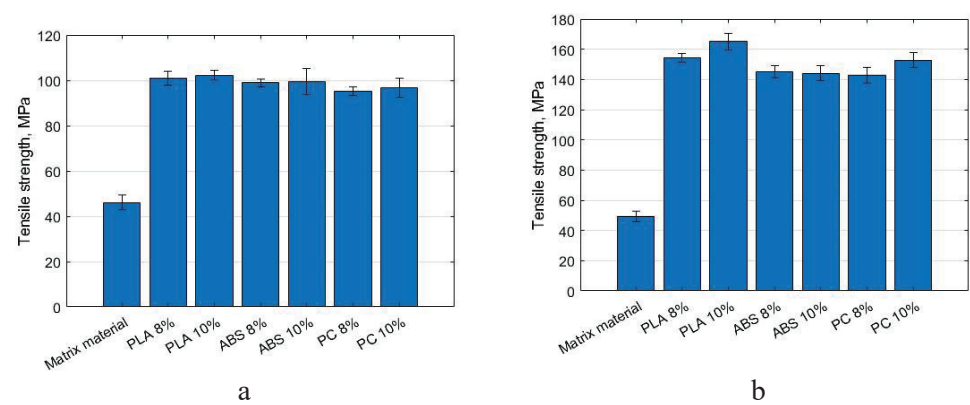


Fig. 3.6 Values of the tensile strength of samples produced by using 3D printed unidirectional composite materials: a – 1K carbon fiber; b – 3K carbon fiber

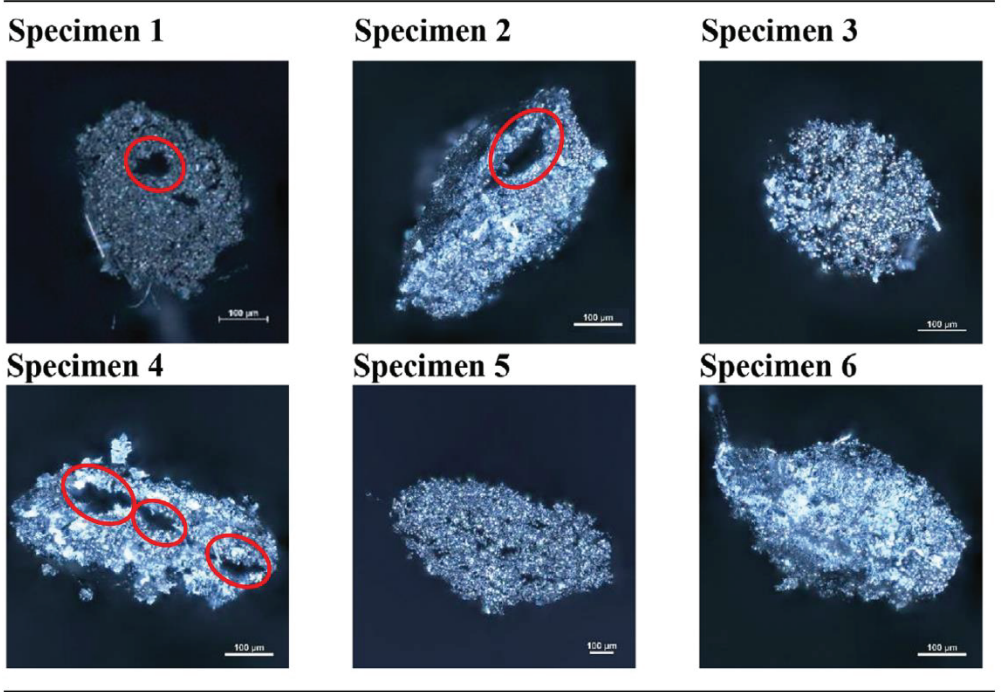
This is especially evident for the samples reinforced with the 1K carbon fiber filament. On the other hand, when evaluating PLA and PC materials, an increasing trend of the strength was observed when increasing the concentration of the solution. In addition, an assumption can be made that the modification of the carbon fiber surface with the thermoplastic dissolved in methylene chloride increases the mechanical properties and adhesion. However, the experiments did not reveal the influence of impregnation on the composite structures printed by using ABS material. 1K carbon fiber impregnated with 10% solutions was characterized by a wider scattering of results. When using 3K carbon fiber filaments and the 10% concentration impregnation solution, the obtained results were lower than when using the fiber impregnated with the 8% solution. It can be assumed that these results were influenced by the adhesion difficulties between the impregnating material and the matrix. It is known that the mechanical properties of the composite materials reinforced with carbon fiber highly depend on the content of carbon in the material. During the printing process, the carbon fiber tow is printed according to the default path. In this case, the content of carbon was calculated by estimating the path of the printhead and the carbon mass per unit length. It should be noted that all samples used for the tensile test were weighed before the experiments. Therefore, when using 1K carbon fiber, the maximum content of carbon in the sample calculated analytically was 15.5%. Meanwhile, the minimum content of carbon in the samples of the same type was 14.6%. When using 3K carbon fiber, the maximum and minimum content of carbon in the sample was 25.2% and 23.8%, respectively.

3.2. Quality of Carbon Fiber Tow

Cross-section images of six samples cut from the same impregnated carbon fiber are given in Table 3.3. The images indicate that the impregnation process is not consistent throughout the whole length of the impregnated filament. In samples 2

and 4, large accumulations of air voids can be observed. These results confirm the hypothesis that the impregnation process is non-uniform and difficult to control. However, quantitative analysis helps to assess the quality and repeatability of impregnation more accurately. The dark spots observed in the cross-sectional images are air gaps or voids, the small dots are CCF threads, and the glossy surface is PLA thermoplastic. An ideally impregnated carbon fiber tow cannot have any cavities or air voids. In this case, air voids can appear in between fibers, impregnation material or fiber and impregnation material. However, the impregnation process depends on various factors, such as the concentration of the solution, the thermoplastic in use, the rotation speed, the heating temperature, etc. Air voids appear due to these factors. Another important factor can be the sample preparation method. During the sample preparation process, when the sample is being cut from the impregnated fiber filament, air cavities or other structural discontinuities may appear. When cutting, after contact between scissors and the fiber, a part of the fragile PLA thermoplastic matrix can crumble due to the resulting deformation.

Table 3.3 Cross-sections of impregnated CCF tow and large accumulations of air voids



The area of internal air cavities was calculated after performing cross-sectional analysis of the samples with *ImageJ2x* software. The visual analysis was performed on all 6 samples, and the results of the impregnated carbon fiber cross-sectional area vary from 77% to 89%. All the results are provided in Table 3.4.

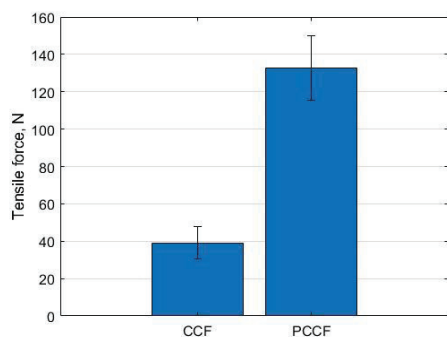
Table 3.4 Quantitative results of visual inspection

Sample	1	2	3	4	5	6
Impregnated area, %	81.3	80.4	78.6	77.2	83.7	88.9
Area of internal air voids, %	18.7	19.6	21.4	22.8	16.3	11.1

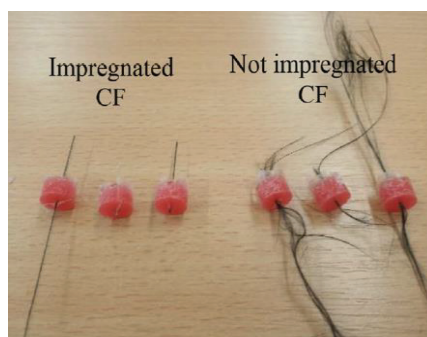
When comparing sample 4 with sample 6, the impregnated area increased by 14%, whereas the area of internal voids decreased by 69%. The biggest issue with this experimental test is that the results may vary, and they depend on the threshold level which has been chosen. When performing this type of test and evaluation of the results, the same researcher must analyze the samples and use the same clearly described methods and rules. Visual analysis of the cross-section of the impregnated continuous carbon fiber shows that the impregnation process used to prepare CCF is of appropriate and acceptable quality, and it can be used to prepare the carbon fiber for printing.

3.2.1. Adhesion between CCF and Polymer Matrix

The results demonstrated in Fig. 3.7 suggest that the average pulling force of unimpregnated carbon fiber of the PLA thermoplastic matrix is 38 N. The tensile force increases more than 4 times and reaches 130 N with an attempt to pull impregnated carbon fiber from the matrix. It is necessary to highlight that unimpregnated CCF was easily pulled out from the matrix material. During the test, when drawing the impregnated carbon fiber, the fiber broke before pulling it out from the PLA matrix. Therefore, it can be assumed that the actual adhesion force is even higher than the value provided in Fig. 3.7. The results confirm the hypothesis that the preparation and impregnation of the continuous carbon fiber significantly improves the bonding strength (adhesion) between the matrix and the reinforcing material.



a



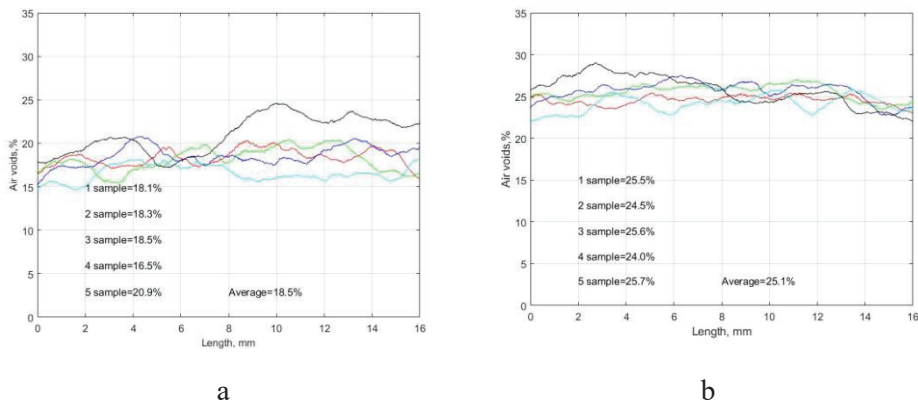
b

Fig. 3.7 Adhesion test results and samples after test: a – pullout test results; b – samples after test

The results indicate that the scattering of data is slightly higher when using the impregnated CF. Because of this behavior, it has been suggested that this difference in results depends on the impregnation process. As it was mentioned above, internal voids are formed after CF impregnation, and they can affect the results of tensile strength and adhesion. On the other hand, the actual force required to extract impregnated continuous carbon fiber from the PLA matrix was not determined in the experiments because the fiber broke before being pulled out from the matrix. This trend was detected with all the impregnated samples. Another important parameter that can influence the adhesion between impregnated CF and the matrix material is the geometric shape of the filament. As Table 3.3 reveals, the geometric cross-sectional shape of the filament changes after the impregnation from a circle to an ellipse. It is clear that the relative contact surface area between the matrix and the impregnated CCF will be different in all samples, hence, this parameter can influence the tensile strength and the scattering of results.

3.3. Quality of 3D Printed Composite Structures⁶

In order to evaluate the properties of 3D printed composite structures, it is important to calculate the volume of the carbon fiber and air voids because it influences the strength of printed structures. Two methodologies were chosen to evaluate the reliability and effectiveness of printed composites for the analysis of 3D printed structures. Prior to the tensile tests, all four groups of samples (5 samples each) were scanned by using the XCT system. The relative volume of voids determined by using the X-ray computed tomography is provided in Fig 3.8. Each figure indicates a different scan result for each group of samples. The relative volume of air voids slightly differs in the individual sample in all groups. The inconsistent volume of air voids in the samples of the same group is observed due to the inconsistency of the printing process or due to the voids that appear during the impregnation of the fiber or during the printing process.



⁶ The material in this section was previously published in [101]

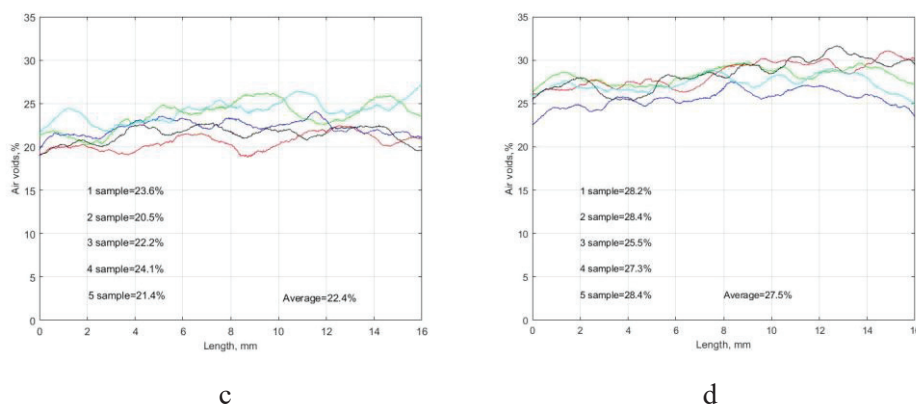


Fig. 3.8 Content of air voids in samples: a – Group 1; b – Group 2; c – Group 3; d – Group 4

The obtained results show a clear trend of the relative volume of air voids: as the height of the layer and the print line spacing decrease, the volume of voids decreases as well. For example, the average relative volume of air voids in the first group of samples was 18.5% (Fig. 3.8 a); however, when the print line spacing increased from 1 to 1.2 mm (Group 3), the average air void volume increased to 22.4% (Fig. 3.8 c), i.e., by 3.9 percentage points. When evaluating the results in the second (Fig. 3.8 b) and fourth (Fig. 3.8 d) sample groups, it is indicated that the relative void volume increased by about 2.4 percentage points with the increase of the print line spacing. When evaluating the influence of the printing parameters on the relative volume of voids, it can be observed that, when the layer height decreases but the print line spacing remains constant, the volume of the pores decreases more, i.e., by 6.6 percentage points when the print line spacing is 1 mm (Fig. 3.8 a and b) and 5.1 percentage points when the spacing is 1.2 mm (Fig. 3.8 c and d). When the print line spacing changes from 1 to 1.2 mm, the relative void volume in the samples is increased by 3.9 percentage points on average with a layer height of 0.3 mm, and by 2.4 percentage points for the samples with a layer height of 0.4 mm. Therefore, the assumption which we put forward earlier that printing parameters, i.e., the layer height and the line width, influence the number of air voids in the samples is correct.

Matrix dissolution was chosen as the second method of composite structure analysis. Three square cross-sectional samples were printed for each group. During experimental tests, the matrix material was dissolved according to the A2 procedure of the *ASTM D 3171* Standard, and the amount of the reinforcing material was weighed. It is necessary to note that both treated and untreated samples were used. The average carbon fiber content after the dissolution is provided in Fig 3.9 a. It reveals that the percentage of carbon fiber by weight in the treated composites is higher than the percentage by volume due to the influence of the material's density. After separate evaluation of the results of each group of samples, it can be concluded that, after reducing the layer height and the print line spacing, the content of carbon in the printed composite structure increases. This trend can be easily explained by the fact that the lower layer height allows increasing their number, and, similarly, by

decreasing the line width, the number of printed lines in the layer can be increased. The dissolution results demonstrated that the samples with the line spacing of 1.2 mm and a layer height of 0.4 mm are of lower quality, i.e., they have the lowest share of carbon and the maximum volume of air voids. These samples (Group 4) had 13% carbon fiber content by weight and 7.2% carbon fiber by volume on average.

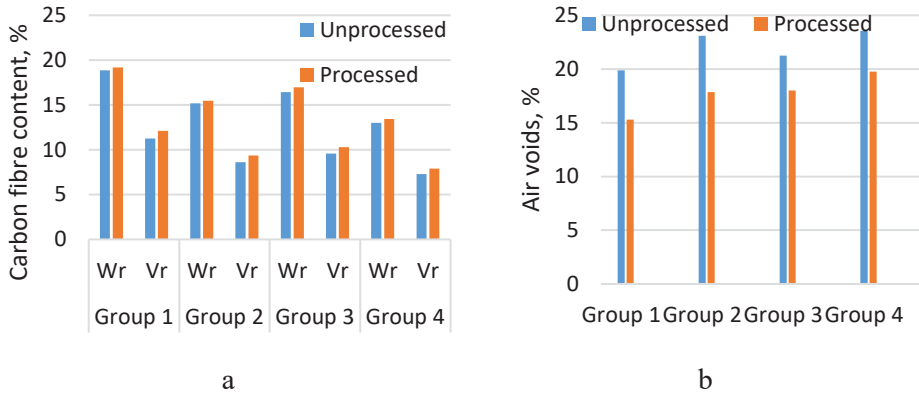


Fig. 3.9 Results after matrix dissolving: a – carbon fiber content in processed composite; b – volume of air voids in the structure

By reducing the layer height to 0.3 mm, the carbon content increases to 16.4% by weight and 9.5% by volume. The highest content of carbon was detected in the samples which were printed by using the following parameters: the layer height of 0.3 mm and the 1 mm print line spacing (Group 1). In this case, the content of carbon fiber by weight was 18.8%, and it was 11.2% by volume. It is important to remark that the results of the carbon content in the samples directly correlate with the tensile strength determined during the tensile tests. It is clear that when the carbon content in the sample increases, the mechanical properties of the composite structure change significantly. One more important parameter of the structural quality is the air void volume which indicates how stable the printing and impregnation processes were. Fig 3.9 demonstrates the averages of the air void volume which were calculated for the 4 groups of treated and untreated samples. The obtained results confirm that the most important parameter of the printing process for a smaller volume of the air void in the sample is the layer height. During the test, it was determined that, when the width of the line in the samples is 1 mm and the layer height is 0.3 mm (Group 1), the void volume in the untreated sample is 19%, and, due to the layer height being increased up to 0.4 mm, the void volume increases to 23% (Group 2) in the untreated samples (Fig. 3.9 b). Respectively, when the width of the line is 1.2 mm, and the layer height is 0.3 mm (Group 1), the void volume in the untreated samples is 21.4%, and, after the layer height is increased to 0.4 mm, the void volume increases to 23.5%. When evaluating the results for the treated and untreated samples (Fig. 3.9 b), it was determined that the air void volume in the treated samples is significantly lower. For example, the air void volume decreases from 3% (Groups 3 and 4) to 5% (Groups 1 and 2). This trend can be explained by the fact that untreated 3D printed samples have incurred

damage stemming from the process of printing, as well as some micro irregularities which directly influence the calculation of the air void volume.

A comparison of the results obtained by X-ray computed tomography and the results obtained by using the standard ASTM D3171 procedure indicates that the volume of the air void determined by computed tomography is on average higher by 3 percentage points. The main reason for that may be the irregular surface of the samples which may have influenced the closing process of the scanned surface, by connecting the voids on the outer surface of the sample to the voids inside the sample being investigated. There may several reasons for this distribution of results: inaccuracies caused by weighing, measurement, or setting thresholds in the image processing algorithm.

Tensile tests were carried out with all the samples after XCT scanning. The results provided in Fig. 3.10 indicate that the printing parameters (the layer height and the print line spacing) exert huge influence on the mechanical properties of 3D printed composite structures. Fig. 3.10 a reveals how the tensile strength changes by changing the printing parameters. The diagrams indicate the averages of the results for the printed sample group and their standard deviations. As expected, the best result (the tensile strength: 184 MPa) was achieved in the samples which were printed with the 0.3 mm layer height and the 1 mm print line spacing (Group 1).

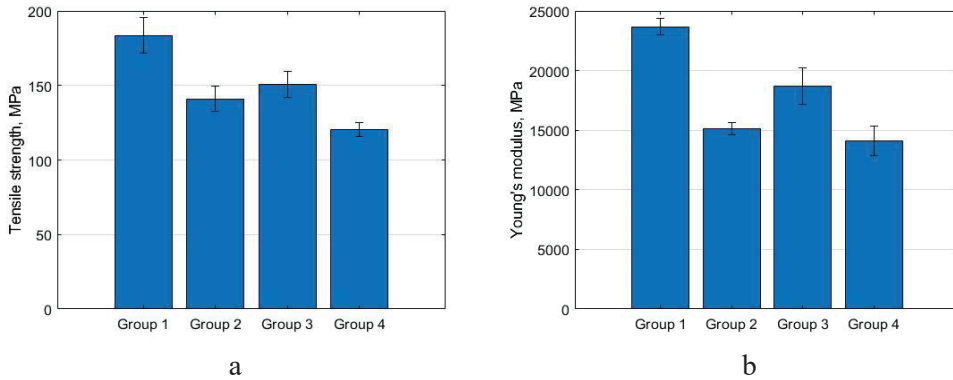


Fig. 3.10 Results of mechanical testing: a – tensile strength, b – Young's modulus

Respectively, we note that the lowest result (the tensile strength: 120 MPa) was achieved when the printed layer height was 0.4 mm, and the line width was 1.2 mm (Group 4). The results also clearly reveal that the layer height has more influence on the mechanical properties of the printed composite structures than the print line spacing.

When reducing the layer height from 0.4 mm to 0.3 mm and maintaining the same line width of 1 mm, the tensile strength increases by 30% (Group 2 and Group 1). Respectively, if the line width is 1.2 mm, the tensile strength increases by 25.6% (Group 4 and Group 3). When changing the print line spacing from 1.2 mm to 1 mm, the tensile strength increases by 21.7% when the layer height is 0.3 mm, and by 17.5% when the layer height is 0.4 mm. This can be explained by the fact that, by reducing the height of each layer, the total amount of layers and the content of

carbon fiber increase. This has a decisive effect on the tensile strength. The Young's modulus evaluation (Fig. 3.10 b) also indicates that the highest value of 23.8 GPa was determined during the testing of the samples with the layer height of 0.3 mm and the line width of 1 mm. In addition, after the evaluation of the relative volume of air voids in the samples and their mechanical properties, it can be observed that the results correlate, i.e., the samples (Group 1) with the lowest relative volume of voids are also denoted by superior mechanical properties; respectively, the samples with the maximum volume of air voids have inferior mechanical properties. However, the exact influence of air voids on the mechanical properties cannot be evaluated because a different carbon content is used for the samples.

The defects induced during the fracture of all 20 samples were determined visually according to the *ASTM D 3039* Standard recommendations. Fig. 3.11 provides the most common defects that occur after the tensile test. The obtained results cannot suggest a clear conclusion that the failure mode of 3D printed composites after a tensile test is constant. However, it was noticed that many samples cracked near the mounting points in the clamps. This is the common issue when performing tensile tests with composite samples of a rectangular cross-section.

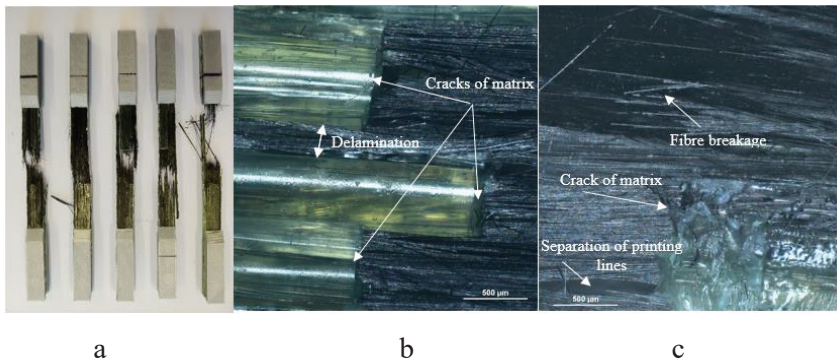


Fig. 3.11 Failure modes: a – the most common failure modes; b – delamination of layers; c – breaking of carbon fiber

Fig. 3.12 indicates the stress-strain curves for the four sample groups demonstrating the behavior of the printed composite samples which were printed by using different parameters during the tensile test. It may be assumed that the structures that have a larger CCF content have more stiffness. Some of the curves demonstrate sudden changes, especially before the failure. This behavior can be explained by the formation of micro irregularities or delamination-related defects in the composite structure of the sample.

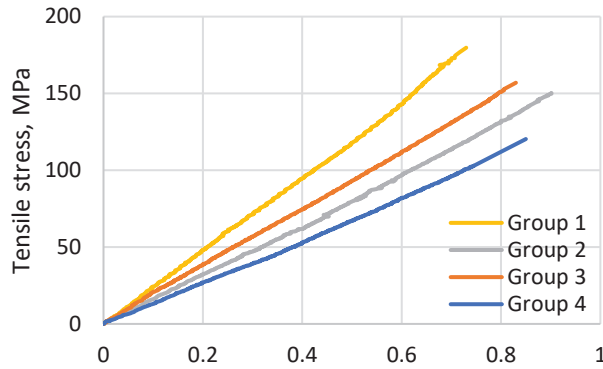


Fig. 3.12 Stress-strain curves of 3D printed samples

The designed printing and impregnation processes and equipment do not guarantee that the printed structures do not have micro or macro voids or any other defects that were found during the experiments. Due to the observed defects, the nature of the fracture and the mechanical properties may change, and pores may influence the fracture of the sample at other locations and significantly reduce the mechanical properties. By evaluating the results of the mechanical tests, it can be assumed that the assumption is true, i.e., when the layer height and the print line spacing decrease, the mechanical properties of the printed composite structures increase significantly.

3.4. Delamination Force and Shear Strength in Printed Composite Structures⁷

During the experiment, all the samples were successfully delaminated. No sample broke above or below the joint area. This means that the average tensile strength of the test structure was not exceeded during the test. The force necessary for the delamination and shear strength was determined. The obtained results are provided in Fig. 3.13 by grouping them according to the print line spacing and the printed layer height.

As the plots in Fig. 3.13 indicate, the major factors influencing the delamination force value are the layer height, the print line spacing and the overlap length. It is clear that these three parameters directly influence the delamination force, but the change in the overlap length exerts bigger influence. Considering the change in results when the layer height of the sample decreases from 0.4 mm to 0.3 mm, it can be observed that the force needed for delamination increases significantly. The delamination force of the 10 mm joint area width of the samples of 9 lines of Group 4 is equal to 236 N, whereas the reduction of the layer height increases the delamination force up to 470 N. In other words, when the layer height is reduced by 100 μm , the force is doubled. A similar trend was also noted in the samples printed in Group 1 and Group 2 9 lines, 10 mm groups; in this case, the delamination force increases to 279 N, or by 88%. This upward trend does not

⁷ The material in this section was previously published in [102]

depend on the total area, the number of printing lines, or the shear area length and remains approximately the same for all the sample groups.

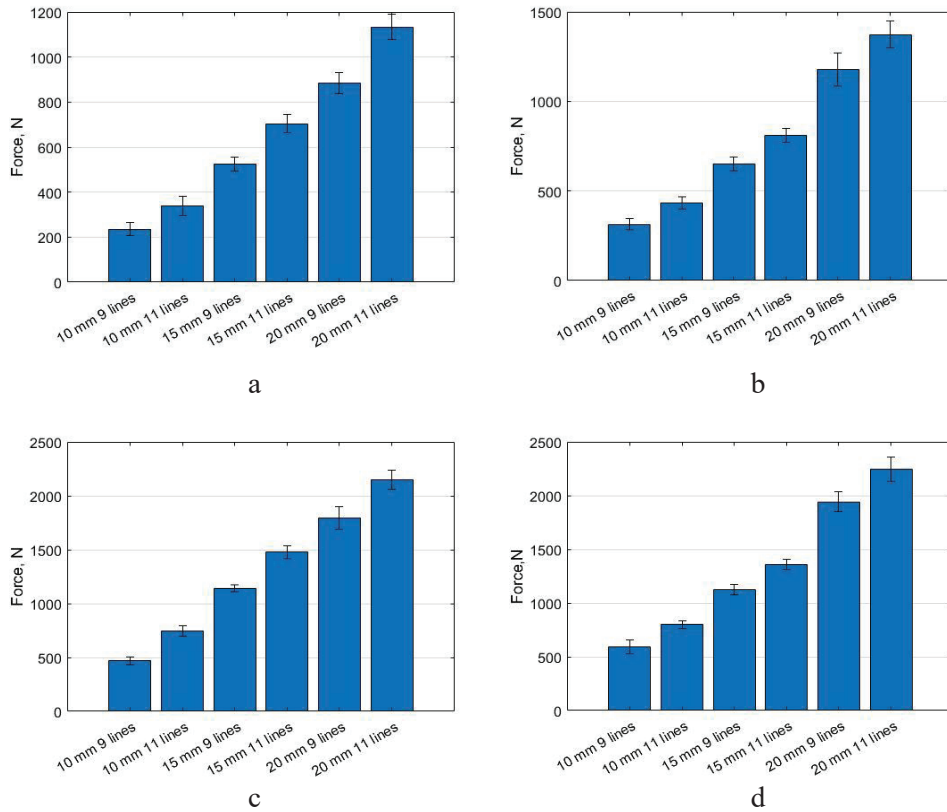


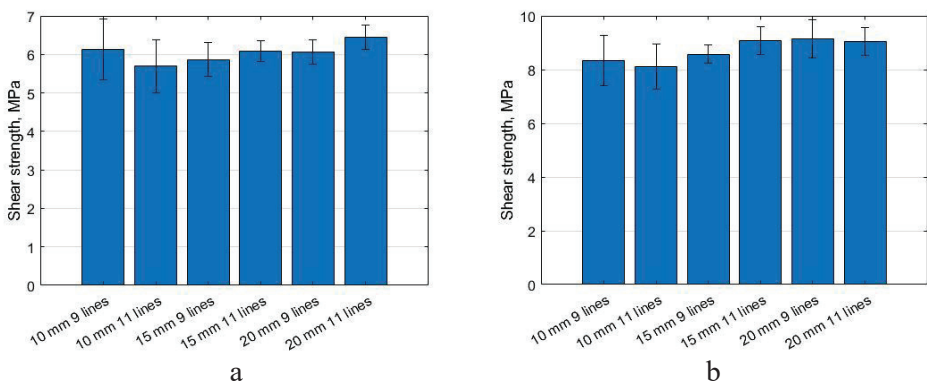
Fig. 3.13 Shear force of samples in the groups with different print line spacing and layer height: a – Group 4; b – Group 2; c – Group 3; d – Group 1

Another important printing parameter is the print line spacing, and the influence of this parameter on the composite delamination force needs to be determined. When the print line spacing was reduced from 1.2 mm to 1 mm, the lower delamination force increase was noted, i.e., 30% on average. Comparing the values of the force required to delaminate the samples with the overlap length of 20 mm of 11 lines, which are 1134 N Group 4 and 1373 N Group 2, respectively, an increase of 239 N (or 21%) is observed.

A brief discussion of the increase in the force required for delaminating from the total joint area is provided further. In the samples of Group 4, the area increasing from 38.5 mm² to 176 mm² also increased the force from 236 N to 1134 N. In other words, when the area increased 4.6 times, the delamination force increased 4.8 times. In the samples of Group 2, the force changed from 314 N to 1373 N when the area increased from 37.7 mm² to 152 mm². In this case, the force needed for delaminating increased 4.4 times when the shear area increased 4.1 times. In the samples of Group 3, the force increased from 470 N to 2151 N, whereas the area

increased from 38.5 mm² to 176 mm². Respectively, the force increased by 4.6 times when the area increased 4.6 times. The same trend is detected in Group 1 samples. When the area increased from 37.7 mm² to 152 mm², the force increased from 593 N to 2247 N. Therefore, when the total shear area increased 4 times, the delamination force increased 3.8 times. The comparison of these results suggests that, if the shear area increases, the tearing force also equally increases. It can be stated that there is a linear relationship between the force and the shear area.

A conclusion can be made that of the two printing parameters (the print line spacing and the layer height), the latter exerts more significant influence on the value of the delamination force. It can be assumed that, when the layer height and the print line spacing decrease, the percentage of air voids in the sample also decreases. This assumption is based on the widely reported and discussed plastic printing behavior when using the FDM method in the scientific literature. It is clear that the decrease of these printing parameters allows a significant increase in adhesion between the layers. These investigations are important because they allow the prediction of the behavior of 3D printed composite structures with varying cross-sections and different loads. It can be assumed that, when the shear area increases, the delamination force increases linearly. When the number of lines increases from 9 to 11 in the sample, the force in Group 4 increases to 179.6 N on average, whereas, in Group 2, it increases to 211.8 N. When the layer height is reduced in the relevant sample groups to 0.3 mm, the average delamination force increases to 336.1 N in Group 3, and to 330.8 N in Group 1. The same trend can be observed when increasing the nominal overlap length. When this parameter increased in Group 4 samples, the force increased to 360.9 N on average, while the increase in Group 2 was 451.2 N. In the corresponding samples with a layer height of 0.3 mm, the increase in the force required for delamination was equal to 681.4 N in Group 3 and to 699.2 N in Group 1. These results also indicate that the lower layer height increases the printing reliability, the parameters of the printed structure become more predictable, and the scattering of the results becomes less prominent. Respectively, printing with a lower layer thickness allows ensuring better adhesion between the layers and the printing lines. Therefore, if we seek to print more reliable composite structures with superior mechanical properties, the layer height has to be as low as possible.



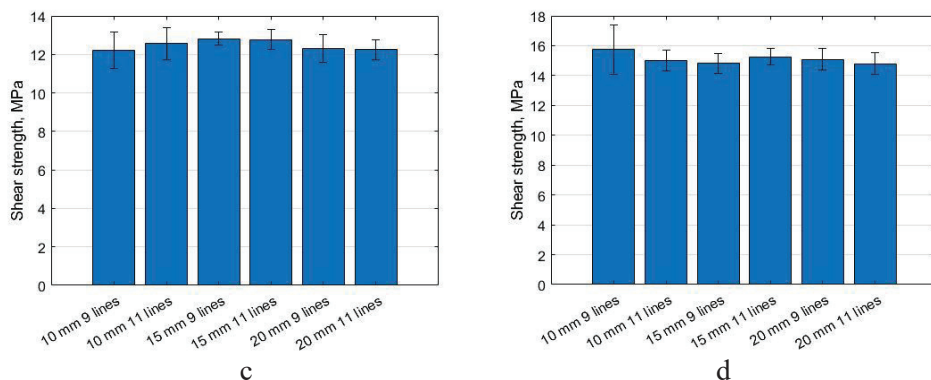


Fig. 3.14 Shear strength of samples in the groups with different print line spacing and layer height: a – Group 4; b – Group 2; c – Group 3; d – Group 1

As it can be observed from the diagrams in Fig. 3.14, the shear strength does not depend on the shear area. However, this mechanical property is highly influenced by the layer height and the print line spacing. For example, the shear strength of the samples printed with a layer height of 0.4 and a print line spacing of 1.2 mm is 6.1 MPa, whereas the reduction between the lines to 1 mm increases the shear strength up to 8.7 MPa, i.e., an increase of 42.6% is observed. If the effect of the print line spacing on the samples printed with the 0.3 mm layer height were compared, it would be noted that the shear strength increases from 12.5 MPa in Group 3 samples to 15.1 MPa in Group 1 samples (by about 21%). The change in the layer height has a higher influence on the printed structures. When the layer height decreased by 100 μm , the shear strength roughly doubled on average, both in the samples printed with 1 mm or 1.2 mm print line spacing, respectively, to 12.5 MPa and 15.1 MPa. The scattering of the results is another important aspect. As it can be observed from the diagrams in the Fig. 3.14, the largest data scattering is observed when the nominal overlap length is 10 mm (it does not depend on the layer height or the print line spacing). This is because the actual reduction in the length of the shear area due to the pulling of the filament is larger and more variable than in the larger lengths of the shear area. The larger variation and shortening occur due to the shorter printing path and a shorter cooling time of the printed area (loop).

3.4.1. Microscopic Inspection of Test Samples

After determining the shear strength of the samples, visual analysis of the pulled off samples was performed. When determining the delamination force, it was observed that the samples with the up to 20 mm nominal shear area length, regardless of the printing parameters, tended to delaminate. Fig. 3.15 indicates the image of the sample from the G3 sample group with 11 lines after the investigation of the delamination force. As the figure reveals, the delamination of the sample is clean, with no breaks or cracks, no significant tear of the carbon fiber from the matrix or any other visual structural changes. This trend was noticed in all the groups of samples.

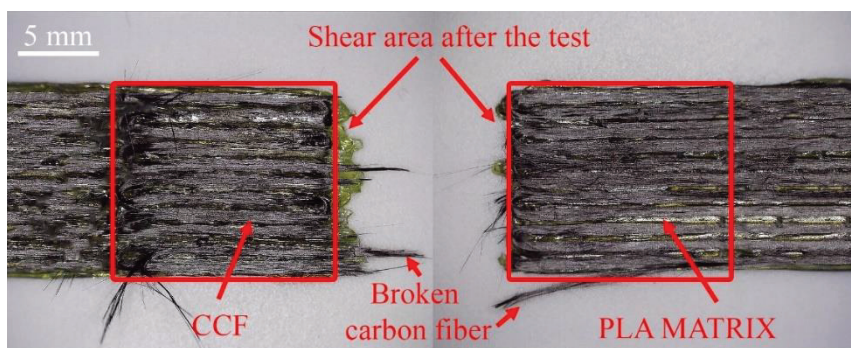


Fig. 3.15 11 printing lines of G3 group sample after the shear test

This suggests that, during the test, the sample was exposed mainly to the shear forces. When evaluating the adhesion between the layers, the lines of plastic and the impregnated carbon fiber are visible on the surface of the layers.

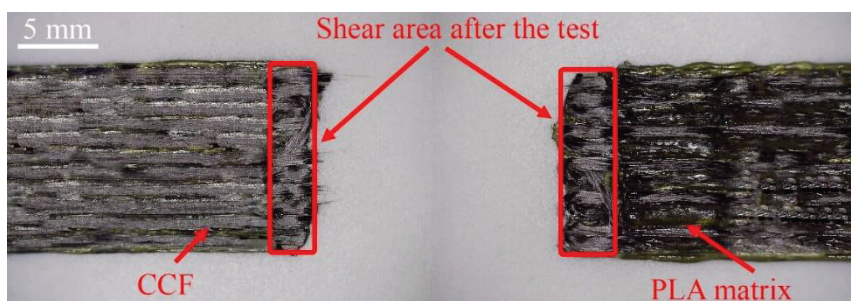


Fig. 3.16 11 printing lines of G4 group sample after the shear test

It is clear that the larger is the content of the matrix material in the area, the lower is the printing layer height or the print line spacing, which led to superior adhesion. When these parameter values are lower, carbon fiber is more tightly embedded in the thermoplastic matrix during the process. Some samples with an overlap length of 20 mm had a tendency to delaminate at different failure modes. Therefore, it was decided to analyze the failure modes after the shear strength tests according to the *ASTM D 5573* Standard. The results demonstrated that most of the samples delaminated according to the light-fiber-tear failure modes described in the standard.

Examples of failure modes determined after the test are demonstrated in Fig. 3.17. The fiber-tear failure mode occurs exclusively in between the fiber-reinforced polymer matrix and is explained by the appearance of reinforcing fibers on both delaminated surfaces. The light-fiber-tear failure mode occurs in the fiber-reinforced polymer substrate near the surface and is characterized by a polymer matrix layer reinforced with a thin layer visible on one of the delaminated surfaces with several carbon fiber filaments or without them on another delaminated surface. However, no clear failure trend was noticed during the analysis, i.e., both failure modes were recorded in several sample groups. These groups of samples were made of different printing parameters when the shear area length was 20 mm, and both Light-fiber-tear

and Fiber-tear failure modes were noted. Although there was no clear trend, it is necessary to highlight that many of the samples of the 0.3 mm layer height and the 1 mm line width are denoted by the more straightforward fiber-tear mode. This trend can be explained by the improved layer adhesion, which is noticed when evaluating the shear strength analysis.

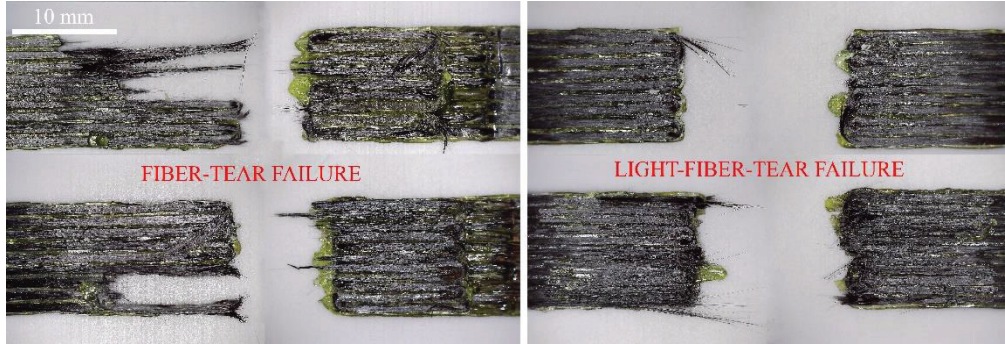


Fig. 3.17 Observed failure modes after the shear test

The samples with a shear area length exceeding 20 mm tended to break earlier during the test before they could delaminate. Two different types of breakage were observed, specifically, a breakage near one of the additional plates and a crack near the shear area. The schematic nature of the sample breakage is provided in Fig. 3.18.

No effect of the printing parameters was observed on the breakage of the samples, or regarding the nature of delamination. While evaluating the testing results of such samples, it can be stated that the tensile force of the sample exceeded the force required to break a sample; however, it still was lower than the delamination force. In order to investigate the samples of a bigger joint area and determine the trends, samples of a higher thickness should be printed.

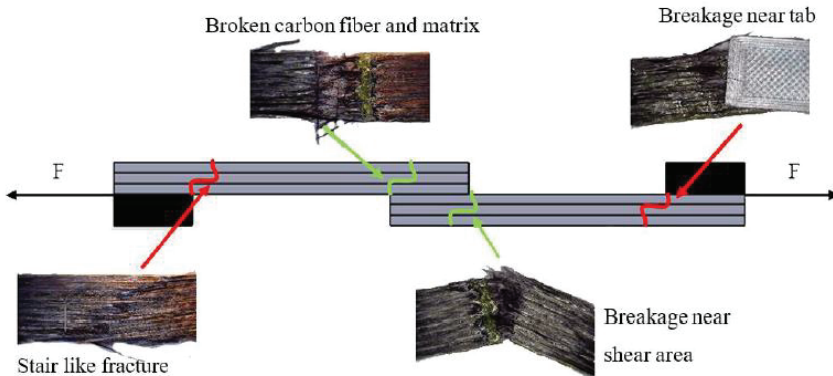


Fig. 3.18 Examples of sample fracture patterns

3.5. Improvement of Mechanical Properties by Secondary Impregnation

The obtained measurement results are summarized, and the average values are calculated. The cross-sectional area of the sample is calculated as it will be later used for the determination of the mechanical properties of composite structures and

the evaluation of the change of the cross-sectional area of the sample after impregnation. The results of the flexural and tensile measurements and calculations are summarized in Tables 3.5 and 3.6.

Table 3.5 Flexural sample dimensions before impregnation

Sample number	Width, mm	Height, mm	Length, mm	Mass, g	Area of cross-section, mm ²
Group 1 (reference samples)					
1	13.83	4.48	151.29	9.30	61.93
2	13.78	4.36	151.17	9.33	60.11
3	13.71	4.38	150.31	9.08	60.04
4	13.83	4.47	150.64	9.58	61.85
5	13.92	4.57	148.85	9.40	63.68
Five sample average	13.81	4.45	150.45	9.44	61.52
Group 1 (samples for impregnation)					
1	13.59	4.42	150.69	9.43	60.02
2	13.62	4.37	150.30	9.25	59.49
3	13.71	4.47	150.41	9.11	61.33
4	13.71	4.49	150.95	9.37	61.57
5	13.74	4.38	150.95	9.33	60.24
Five sample average	13.67	4.43	150.66	9.29	60.24
Group 3 (reference samples)					
1	13.56	4.52	150.44	9.36	61.29
2	13.66	4.50	150.18	9.45	61.44
3	13.74	4.52	149.75	8.91	62.04
4	13.60	4.48	149.24	8.91	60.99
5	13.65	4.50	149.49	8.93	61.43
Five sample average	13.64	4.5	149.82	9.11	61.43
Group 3 (samples for impregnation)					
1	13.61	4.48	150.63	9.40	60.91
2	13.63	4.48	150.02	9.19	61.11
3	13.59	4.49	149.92	9.30	61.08
4	13.60	4.52	149.85	9.37	61.52
5	13.71	4.49	150.03	9.12	61.57
Five sample average	13.64	4.50	149.82	9.11	61.44

ASTM D 7264 Standard specifies the overall dimensions of a flexural sample, specifically, 150×13×4. When summarizing the measurement results of the printed samples, an increase in the dimensions was observed. The average change in the height of 20 samples is about 11.8%, the change in width equals to 5.7% and 4.9% (at 1 mm and 1.2 print line spacing), and there is virtually no change in the length (only up to 0.2%). The only difference between the overall dimensions of the

flexural and tensile samples is the lower height of the sample. According to the *ASTM D 3039* tensile Standard, the sample dimensions can be 150×13×2 mm. However, the values of the actual measurements as in the case of the tensile sample are slightly bigger. The sample measurement results are provided in Table 3.6.

Table 3.6 Tensile sample dimension before impregnation

Sample number	Width, mm	Height, mm	Length, mm	Mass, g	Area of cross-section, mm ²
Group 1 (reference samples)					
1	13.59	2.25	150.64	4.66	30.57
2	13.63	2.29	150.87	4.65	31.16
3	13.57	2.26	150.96	4.63	30.62
4	13.64	2.26	150.88	4.69	30.82
5	13.54	2.21	150.89	4.69	29.98
Five sample average	13.59	2.25	150.85	4.66	29.98
Group 1 (samples for impregnation)					
1	13.52	2.50	150.45	5.64	33.79
2	13.65	2.42	150.51	5.62	33.03
3	13.74	2.41	149.91	5.59	33.08
4	13.71	2.37	149.93	5.55	32.53
5	13.64	2.33	150.52	5.52	31.74
Five sample average	13.65	2.41	150.26	5.58	32.83
Group 3 (reference samples)					
1	13.58	2.36	150.29	4.45	32.06
2	13.39	2.35	150.33	4.52	31.46
3	13.46	2.33	149.98	4.57	31.40
4	13.42	2.29	150.30	4.49	30.73
5	13.33	2.42	149.85	4.53	32.25
Five sample average	13.44	2.35	150.15	4.51	31.58
Group 3 (samples for impregnation)					
1	13.41	2.33	150.26	4.51	31.25
2	13.41	2.37	150.24	4.51	31.73
3	13.47	2.26	150.44	4.50	30.49
4	13.56	2.35	149.77	4.45	31.86
5	13.45	2.32	149.54	4.47	31.15
Five sample average	13.46	2.33	150.05	4.49	31.29

The average height deviation in the twenty flexural samples from the one specified in the standard is about 16.5%. The width deviates from the standard width by 4.8% and 3.5% (1 and 1.2 mm), respectively, with the lowest change in the length being as little as 0.2%.

The measurement results of the dimensions after impregnation are provided in Tables 3.7 and 3.8.

Table 3.7 Flexural sample dimensions after impregnation

Sample number	Width, mm	Height, mm	Length, mm	Mass, g	Mass difference, %	Cross-section area, mm ²	Cross-section difference, %
Group 1							
1	13.62	4.45	151.30	10.46	10.92	60.55	0.88
2	13.74	4.41	150.46	10.44	12.86	60.61	1.88
3	13.77	4.54	150.96	10.83	18.88	62.49	1.88
4	13.73	4.55	151.13	10.70	14.19	62.41	1.36
5	13.78	4.42	151.10	10.54	12.97	60.86	1.03
Five sample average	13.73	4.47	150.99	10.59	13.96	61.38	1.41
Group 3							
1	13.62	4.52	150.80	10.56	12.34	61.59	1.12
2	13.73	4.54	150.13	10.86	18.17	62.27	1.91
3	13.51	4.55	150.18	10.56	13.55	61.49	0.67
4	13.57	4.60	150.07	10.65	13.66	62.39	1.42
5	13.73	4.55	151.05	10.80	18.42	62.53	1.56
Five sample average	13.63	4.55	150.45	10.69	15.23	62.05	1.34

The average change in the mass of the flexural samples in the Group 1 samples is 14%, and in the Group 3 samples, it is 15.2%, the mean percentage change in cross-section is 1.4% and 1.3%, respectively. The highest change in the mass was observed in Group 1 samples: 18.9%, and, in Group 3 samples, it is 18.4%. The lowest impregnation rate, i.e., change in mass in Group 1, was 10.9%, and, in Group 3, 12.3%.

The measurement results suggest that the large part of the epoxy resin penetrated inside the sample and filled the air voids, and, on the outside of the samples, only a small amount of epoxy resin was left. This can be observed from the slight change in the cross-section of the sample which is 3% on average in Group 1 samples and 2% in Group 3 samples.

As it can be observed from the measurement results of the samples for the tensile test after the impregnation process (Table 3.8), the average percentage change in mass in Group 1 samples is 22.4%, whereas, in Group 3, it is 21.6%. The average cross-sectional percentage change is 3% and 2%. The maximum change in mass was noticed in Group 1, i.e., 24%, while, in Group 3 samples, it was 23%. The lowest impregnation rate in the samples of Group 1 was 21% in comparison to 20% in Group 3.

Table 3.8 Tensile sample dimension after impregnation

Sample number	Width, mm	Height, mm	Length, mm	Mass, g	Mass difference, %	Cross-section area, mm ²	Cross-section difference, %
Group 1							
1	13.52	2.50	150.45	5.64	23.68	33,79	3,04
2	13.65	2.42	150.51	5.62	22.98	33,03	3,28
3	13.74	2.41	149.91	5.59	22.05	33,08	2,99
4	13.71	2.37	149.93	5.55	21.98	32,53	3,26
5	13.64	2.33	150.52	5.52	21.32	31,74	2,65
Five sample average	13.65	2.41	150.26	5.58	22.4	32.83	3.04
Group 3							
1	13.60	2.36	150.32	5.45	22.47	32.05	0.02
2	13.46	2.40	150.51	5.53	22.35	32.26	2.54
3	13.54	2.37	150.20	5.48	19.91	32.13	2.32
4	13.47	2.33	150.95	5.40	20.27	31.39	2.15
5	13.44	2.48	150.45	5.57	22.96	33.28	3.19
Five sample average	13.50	2.39	150.49	5.49	21.59	32.22	2.04

A summary of the measurement results after the impregnation process suggests that Group 3 samples were impregnated better. This confirms the previous hypothesis that such samples contain more air voids due to the higher print line spacing, and epoxy resin penetrates the sample easier.

In order to evaluate the effectiveness and the influence of epoxy resin impregnation on the mechanical properties, tensile and flexural tests were performed on both impregnated and not impregnated continuous carbon fiber reinforced composite structures, and the tensile strength, the flexural strength, the Poisson's ratio, the tensile and flexural modulus were determined.

3.5.1. Tensile Testing

During the experiment, the tensile strength of the printed composite samples was determined at first. Fig. 3.19 presents the tensile stress-strain curves of the samples of Group 3 and Group 1. It can be observed that the impregnated samples are denoted by higher tensile strength than the unimpregnated samples, regardless of the print line spacing. The lowest stress value in Group 3 impregnated samples is 249 MPa, whereas, in the unimpregnated samples of the same group, the value is 189 MPa. After the impregnation, the stress increased by 60 MPa. The maximum stress value in the same group in the impregnated samples is 281 MPa, whereas, in the unimpregnated samples, it is 218 MPa. Therefore, after the impregnation, the stress of the printed composite structures is increased by 63 MPa. It can be observed

that, between the maximum and the minimum strain values in this group, the impregnation with epoxy resin increases the tensile strength by about 61.5 MPa on average. The curves also indicate that the impregnated samples tended to break when elongation at break reaches 1.2%, whereas not impregnated samples broke before the strain reached 1%.

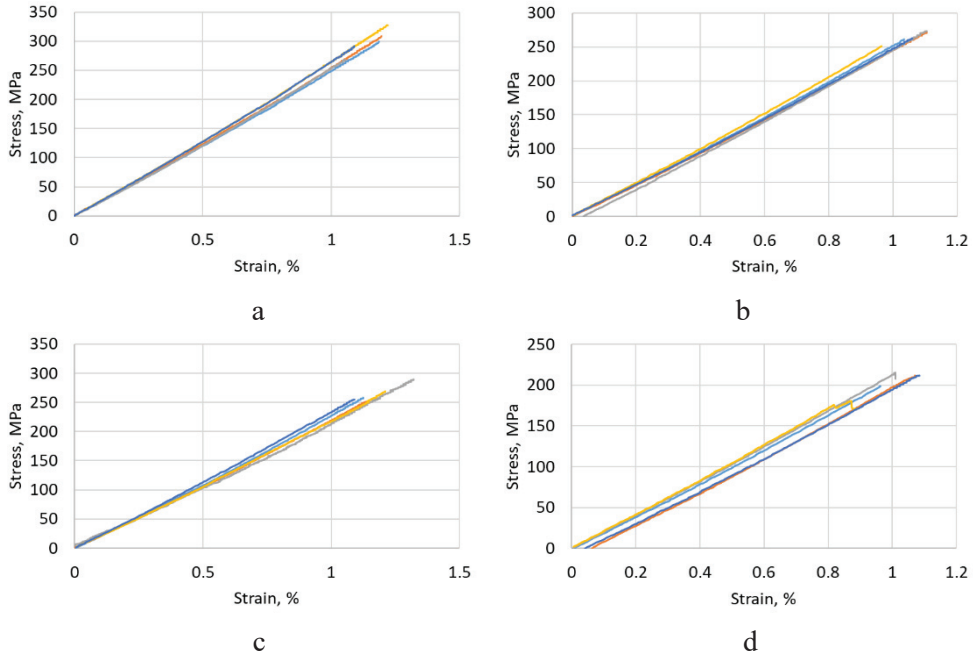


Fig. 3.19 Tensile stress-strain curves: a – Group 1 impregnated; b – Group 1 unimpregnated; c – Group 3 impregnated; d – Group 3 unimpregnated sample

The same trend is clear in the Group 1 sample group as well. The minimum stress value in Group 1 impregnated samples is 276 MPa, whereas, in unimpregnated samples, it is equal to 255 MPa. The difference between the minimum values is about 21 MPa. The maximum stress value in the impregnated samples is 321 MPa, whereas, in the unimpregnated samples, it is equal to 273 MPa. In this case, the difference between the impregnated and the unimpregnated Group 1 sample group stresses is 48 MPa. Therefore, after impregnation, the tensile strength of this group of samples increased by 34.5 MPa on average. As in the Group 3 sample group, the impregnated samples in Group 1 broke at larger strains, respectively, 1.3% and 1% strains. Hence, the conclusion may be drawn that the impregnation with epoxy resin increases the tensile strength and the stiffness of the composite structure. It is also clear that impregnation exerts bigger influence on the Group 3 group samples. This is because the larger print line spacing in the sample increases the number of air voids that are filled with epoxy resin during the impregnation. The difference between the stresses in the samples of Group 3 and Group 1 after the impregnation is about 27 MPa. As a result, impregnating at a greater print line spacing allows increase of mechanical properties almost two times.

It is important to note that impregnation does not change the failure mode: both impregnated and unimpregnated samples break after reaching the maximum stress value, and this leads to the sudden, brittle failure rupture of both impregnated and unimpregnated samples. These curves are inherent for composite materials under tensile load.

The summary of the tensile strength results is provided in Fig. 3.20 a. It indicates that the impregnation with epoxy resin exerts higher influence on the samples of Group 3. The average tensile strength in the impregnated samples of Group 3 is 265 MPa, whereas, in Group 1, it is 299 MPa. The difference between the impregnated groups is about 13%. Comparing the unimpregnated groups with one another, when the average tensile strength in Group 3 reaches 203 MPa, and 264 MPa in Group 1, it can be observed that the difference is about 31%. The difference between the tensile strength of the groups after impregnation decreases due to its greater influence on the samples of Group 3. The best evidence of this is obtained by comparing the impregnated and unimpregnated samples from the same group. As it was mentioned above, the average tensile strength in Group 3 is 203 MPa, and, after impregnation, it increases to 265 MPa. Hence, impregnation results in a 31% increase. Meanwhile, in Group 1, the tensile strength of unimpregnated tensile samples is 264 MPa, whereas, the value of the impregnated samples is 299 MPa; the increase accounts for about 13% after impregnation. It can be concluded that the impregnation of samples with a larger print line spacing achieves an even 18% higher increase regarding the tensile strength. The graph also indicates that the scattering of the results is not high, especially in the unimpregnated samples, which suggests that the printing process is stable and consistent. Higher scattering of results is observed in the impregnated groups of samples. The highest scattering of results is detected in the impregnated samples of Group 1. It can be assumed that the higher scattering of results after impregnation is observed due to uneven cleaning or void filling of the samples after the impregnation process or because of uneven penetration of the epoxy resin into the air pockets in the sample.

Another characteristic of the material determined during the tensile test is the Poisson's ratio.. For most materials, the Poisson's ratio is between 0 and 0.5. The results of the test are provided in Fig. 3.20 b for printed composite structures. After the ratio was calculated, it varied from 0.39 in Group 1 samples to 0.30 in Group 3 samples on average. After the impregnation, this value increased to 0.41 in the Group 1 and 0.38 in Group 3 sample groups. The Poisson's ratio increase after impregnation in the sample groups was 5% in Group 1 and 27% in Group 3. It is clear that the trend is the same: the impregnation exerts higher influence on the samples with a larger print line spacing. When comparing impregnated and unimpregnated samples from different groups, the difference between the Poisson's ratio is 8% and 30%, respectively. As follows, after the impregnation, the difference between Group 3 and Group 1 samples in the Poisson's ratio decreased by 22%. The graph also indicates that the scattering of the calculated ratios is low, i.e., the printing and impregnation of the samples was of sufficient quality.

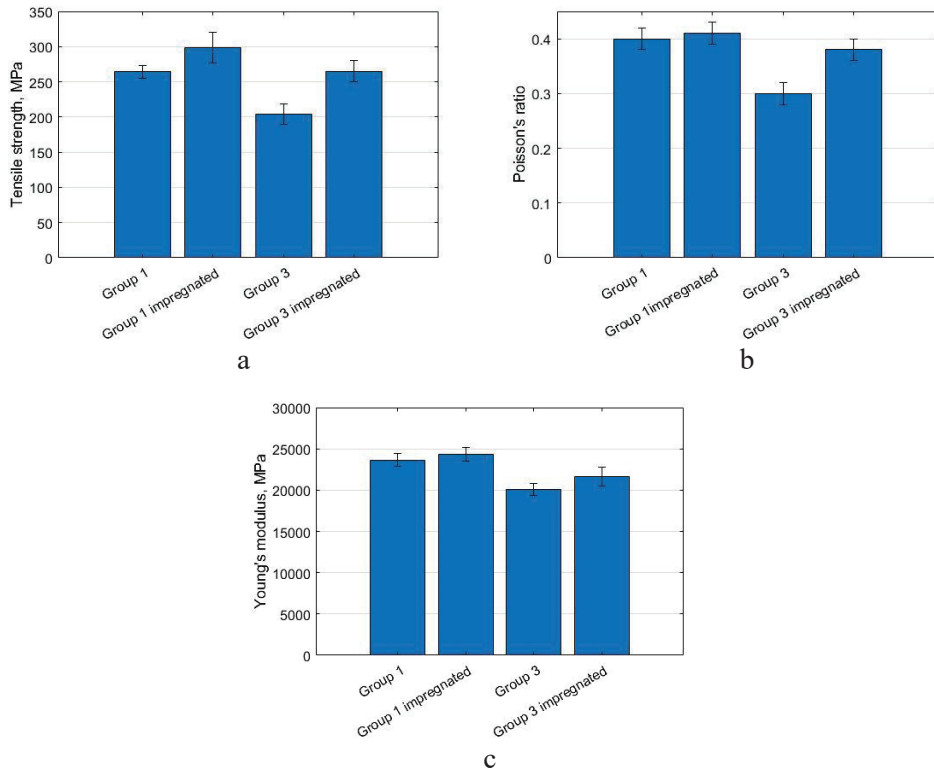


Fig. 3.20 Mechanical properties: a – Tensile strength; b – Poisson's ratio; c – Young's modulus

One more physical property describing the printed composite material is the Young's modulus. The results obtained during the experiment are provided in Fig. 3.20 c. The graph reveals that the average Young's modulus of unimpregnated continuous carbon fiber reinforced 3D printed composite structures is 24 GPa in the Group 1 samples and 20 GPa in the Group 3 samples. The difference between the modulus of elasticity of these groups is 17%. After impregnation, the modulus of elasticity increases in the corresponding groups up to 24 GPa and 22 GPa, respectively. The difference between the modulus of elasticity of these groups is 17%. A comparison of the results of the samples of the same groups, before and after the impregnation, indicates that the Young's modulus increases to 2.8% in Group 1 and 7.5% in Group 3. The same trend is observed as in the above discussed experiments: impregnation exerts higher influence on the samples with 1.2 mm print line spacing, and it is almost 5% more effective compared to Group 1 samples. This is because this group of samples contains more air voids that may be filled with epoxy resin during the impregnation process. Another important aspect is the low scattering of the results. This means that the test and investigations were carried out accurately, and the preparation of the samples was of high quality.

3.5.2. Flexural Testing

In the course of the 3-point bending test, the flexural strength of the printed composite samples was tested first. Fig. 3.21 indicates the stress-strain curves of samples Group 3 and Group 1. This reveals that the impregnated samples are characterized by higher flexural strength than the unimpregnated samples, regardless of the print line spacing. The tensile test demonstrated the same trend. The minimum stress value in the Group 3 impregnated samples was 281 MPa, while, in the unimpregnated samples of the same group, it was 132 MPa. The strength increased by 149 MPa after impregnation. In other words, the samples withstand two times higher loads before fracture. The maximum stress value of the same group of samples in the impregnated samples is 308 MPa, whereas, in the unimpregnated samples, they yield 150 MPa. Therefore, after impregnation, the flexural strength of the printed composite structure increased by 158 MPa or 69%. It is clear that, between the maximum and minimum stress values in this group, impregnation with epoxy resin increases the flexural strength by about 154 MPa on average. The values also indicate that the maximum stress of the impregnated samples during flexural is reached when the strain reaches 1.5%, while the strain of the unimpregnated samples does not reach 1.8%. The same trend is observed in the Group 1 sample group. The minimum stress value in the Group 1 impregnated samples is 238 MPa, whereas, in the unimpregnated samples, it is 138 MPa. The difference between the minimum values is 100 MPa, or 53%. The maximum stress value in the impregnated samples is about 309 MPa, whereas, in the unimpregnated samples, it is 168 MPa. In this case, the difference between the stresses of the impregnated and the unimpregnated samples in Group 1 is 141 MPa, or 59%. Therefore, after impregnation, the flexural strength in this group of samples increased by 120.5 MPa on average. However, unlike in the case of the samples of Group 3, the samples of this group, both impregnated and unimpregnated, reach maximum flexural stresses at similar strains. In summary, the impregnation with epoxy resin increases the mechanical properties of the composite structure and its flexural strength by 137 MPa on average. There is also a trend alike the one observed in the tensile test: impregnation has more influence on the Group 3 group samples. This is because, at a greater print line spacing, more air voids appear in the sample which are filled with epoxy resin during impregnation. The difference between the average flexural strength in the Group 3 and Group 1 sample groups after impregnation is about 33 MPa. However, there is a clear difference between the flexural and tensile tests. If the material behavior in tensile samples does not change after impregnation, then, the nature of fraction during the flexural test is already different between the impregnated and the unimpregnated samples. After the impregnation, regardless of the sample group, the curves were vertical, which suggests higher stiffness of the composite material and the flexural strength.

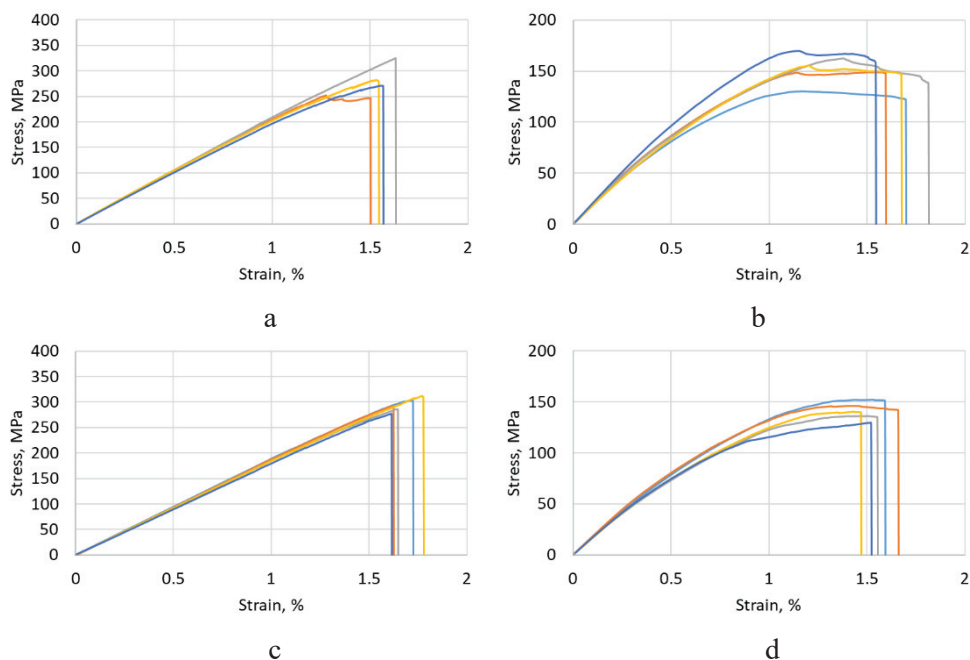


Fig. 3.21 Flexural strength dependency from strain: a – Group 1 impregnated; b – Group 1 unimpregnated; c – Group 3 impregnated; d – Group 3 unimpregnated sample

When unimpregnated thermoplastic CCF composite is subjected to the flexural test, it passes various stages before fracture; see Fig. 3.21 b and d. The curves which are fairly similar to pure thermoplastic, elastic and plastic regions can be observed. The stress-strain curves (Fig. 3.21 a and c) of tested samples (after the secondary impregnation with epoxy resin) replicate the composite behavior typical for carbon/epoxy composites. Only the elastic region is observed. This change of a material's behavior occurs because, after the second impregnation with epoxy resin, printed composite structures become more homogenous. Air voids, cracks and other defects which developed in the course of CCF composite printing are filled with epoxy resin. This is because, in the impregnated samples, not only the matrix but also the reinforcing material breaks during the bending test. In the unimpregnated samples, the matrix breaks first, the gradual delamination starts, and the reinforcing material breaks. This change in the fracture indicates successful penetration of epoxy resin into the air voids inside the sample.

Summarized results of the flexural strength testing are provided in Fig. 3.22 a. These graphs, as well as the stress-strain curves, indicate that impregnation with epoxy resin exerts higher influence on the Group 3 sample group. However, unlike in the tensile test, the difference in the influence between the different groups is not so prominent. The average flexural strength in the impregnated samples of Group 3 is 294 MPa, whereas, in Group 1, it is 273 MPa. The difference between the impregnated groups is about 7.7%. Meanwhile, the tensile test yielded the difference of 13%. A comparison between the unimpregnated groups, where the average

flexural strength in Group 3 is 140 MPa, which compares against 153 MPa in Group 1, indicates that the difference is about 9.3%. The difference between the groups decreases after impregnation due to the higher influence on the samples of Group 3. Strong evidence supporting this assumption is the comparison between the impregnated and the unimpregnated samples of the same group. As mentioned above, the average flexural strength of Group 3 is 140 MPa, and, after impregnation, it increases to 294 MPa. The impregnation accounts for an increase of 110%. Meanwhile, in the Group 1 group of unimpregnated samples, the flexural strength is 153 MPa, while the impregnated samples yield the value of 273 MPa. The increase after impregnation is about 78%. It can be assumed that, by impregnating samples with greater print line spacing, the tensile strength increases by 32%. The comparison of the impregnation influence on the flexural and tension strengths indicates a clear advantage and a higher increase of the level of flexural properties. The tensile strength increased in the Group 1 samples after impregnation only by 30.5%, whereas the flexural strength increased by 110%. Respectively, in the Group 1 samples, the tensile strength increased by 13%, and the flexural strength increased by 78%. The higher influence on the flexural strength is achieved not only because of the internal penetration of epoxy resin into the air voids, but also due to the external shell that forms after impregnation. Although the surface of all the samples is thoroughly cleaned after the impregnation, however, a small amount of resin remains on the surface of the samples, thereby forming a shell on the sample.

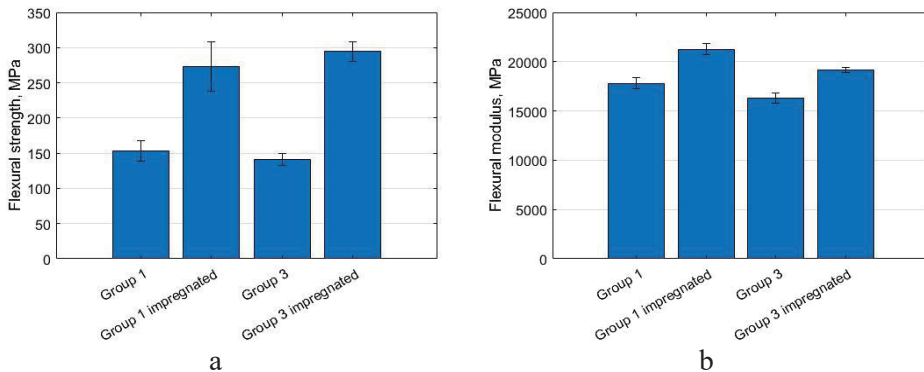


Fig. 3.22 Mechanical properties: a – Flexural strength; b – Flexural modulus

Moreover, Fig 3.22 indicates that the low scattering of the results, particularly in the unimpregnated samples, indicates a reliable and consistent printing process. The higher scattering of results is observed in the impregnated sample groups, except for Group 1 of the impregnated samples. As well as in the tensile test, the same assumption is made regarding the scattering of the results in this group. This is influenced by the uneven cleaning and/or impregnation of the samples after the impregnation process or the uneven penetration of the epoxy resin into the air voids in the sample.

The flexural modulus of 3D printed continuous carbon fiber reinforced composite material was also determined during the flexural test. The modulus

determined during the test is demonstrated in Fig. 3.22 b. The graph of unimpregnated continuous carbon fiber reinforced 3D printed composite structures indicates that the average flexural modulus is 18 GPa in the Group 1 and 16 GPa in the Group 3. The difference between the flexural modulus of these groups is 1480 MPa, or around 9%. After the impregnation, the flexural modulus increases in the relevant groups to 21 GPa and 19 GPa. In this case, the difference in the flexural modulus is 2097 MPa, or 11%. A comparison of the sample results of the same groups, before and after impregnation, indicates that the flexural modulus increases by 19% in Group 1 and 17% in Group 3. In this case, unlike before, the higher influence of impregnation on the flexural strength is noted in Group 1, and the difference between the impregnated samples printed with different print line spacing is around 2%. However, these two percentage values do not contradict the fact that impregnation exerts higher influence on the tensile and flexural strength in the Group 3 sample group. This deviation from the previous trend can occur due to measurement or due to poor sample cleaning after the impregnation process. Another important aspect is the low scattering of results. In the Group 3 sample group, it is hardly observed at all, especially in the impregnated samples, whereas, in the Group 1 impregnated samples, the scattering is the most prominent of any of the sample groups, which also influences the flexural modulus.

3.6. Chapter Conclusions

In this section, 3D printed CCF thermoplastic composites were analysed. The main focus was on the pre-processing for the better printability of carbon fiber. It is known that the impregnation of carbon fiber tow improves the quality of printed structures. Three impregnating materials (PLA, PC, ABS) and solutions of various concentrations (2–10%) by dissolving in methylene chloride were used. The tensile test with impregnated carbon fiber revealed that, when the concentration of the solution increases, the fiber resistance against breakage increases as well. Correlation analysis demonstrated strong relationship between the tensile force of the impregnated carbon fiber and the impregnated carbon fiber mass. The correlation coefficient varied from 0.82 in the case with 1K PLA impregnated carbon fiber to 0.99 in the case of PC impregnated carbon fiber. In order to investigate if these results apply to 3D printed composite materials, the samples were printed for tensile tests by using 3 different impregnation materials (PLA, PC, ABS) and different carbon fiber impregnating solution concentrations (8–10%). The obtained results revealed the dependence between the solution concentration and the tensile strength, i.e., the higher is the concentration of the impregnating solution, the larger is the tensile strength of the composite structure. This trend is evident in 3K carbon fiber impregnated in PLA and PC solutions, where the tensile strength increases from 154 MPa to 165 MPa and from 142 MPa to 152 MPa depending on the material used. Meanwhile, by impregnating carbon fiber in ABS solution, the change in results was insignificant, and, when using 3K carbon fiber, the tensile strength of the samples even decreased from 145 MPa to 144 MPa. The difference in the results confirmed that the impregnation process is complex and depends on many factors. To decrease the scattering of results, the influence of these factors must be evaluated and

controlled. Moreover, the content of CCF in the samples was determined: it varied from 15% when using 1K carbon fiber to 25% when 3K carbon fiber was used.

The microscopic inspection of impregnated 1K CCF demonstrated that the percentage of the impregnated area varies in the range ~80–90%. Whereas the percentage of air voids varies in the range ~12–23%, respectively. To evaluate the adhesion between the matrix and CCF, the carbon fiber extraction test on the matrix material was performed. This experiment was carried out using both impregnated and unimpregnated CCF. The results indicated that the extraction force from the matrix of untreated CCF is 38 N on average. After CCF impregnation, the adhesion between the reinforcing material and matrix material can increase more than four times. After the impregnation of the fiber, the tensile force average value increases up to 138 N.

During the mechanical tests, it was determined how the strength and elastic characteristics of 3D printed composite structures change when modifying the printing parameters, i.e., the printed layer height and the print line spacing. Four groups of samples were investigated and printed by using different parameters: line widths of 1.0 and 1.2 mm and layer heights of 0.3 and 0.4 mm. These parameters were selected due to their influence on the mechanical properties and quality characteristics of the printed structures. Tensile tests demonstrated that, when the layer height and the printing line width decrease, the tensile strength increases. Samples with a layer height of 0.3 mm and a line width of 1.0 mm demonstrated the best results, i.e., 183 MPa tensile strength and the Young's modulus of 23.8 GPa. The CCF content revealed that the results of the mechanical tests correlate with the carbon fiber content in the samples, i.e., a higher carbon fiber content ensures a higher strength and modulus of elasticity. The same trend was also confirmed when using X-ray computed tomography: the obtained results indicated that, when printing the samples with a layer height of 0.3 mm and a line width of 1.0 mm, the minimum volume of air voids is ~19%. When using XCT analysis, it was determined that the altered printing parameters change the volume of voids. During the evaluation of the results of the dissolution of the matrix of treated and untreated samples, it was noted that, due to sample surface irregularities, the volume of air voids can increase to ~5%.

The force required for the delamination of printed CCF reinforced composite structures was determined experimentally. It appeared to directly depend on the layer height, the print line spacing and the shear area. With the layer height being reduced from 0.4 mm to 0.3 mm, the delamination force increases twice on average. With the print line spacing getting reduced from 1.2 mm to 1.0 mm, the force increases by 30% on average. When the shear area increases, the delamination force also increases. When the number of lines increases from 9 to 11 in the sample, the force in the samples printed with Group 4 parameters increases to 180 N on average, whereas, in the Group 2, it increases to 212 N. If the layer height is reduced to 0.3 mm in the respective sample groups, the average delamination force increases to 336 N in Group 3 and to 330 N in Group 1. The shear strength was also calculated during the test, and it depends only on the printing parameters, but does not depend on the shear area; the Group 4 sample shear strength is 6.1 MPa on average, and,

when the print line spacing was reduced to 1 mm, the shear strength increased to 8.7 MPa. The shear strength of the respective sample groups printed with the 0.3 mm layer height is 12.5 MPa for the Group 3 samples and 15.1 MPa for Group 1. After the visual analysis of the samples, it was determined that all samples were delaminated cleanly, without breaks, cracks, carbon fiber tearing from the matrix or other visual structural changes regardless of the printing parameters or the joint area length. This trend was confirmed in all sample groups.

The influence of secondary impregnation with epoxy resin was analysed. During the experiment, two groups of samples with a different print line spacing were printed (the layer height remained the same, respectively, in Group 3 and Group 1). Half of the samples were impregnated with epoxy resin, and all the samples were tested by performing the tensile and flexural tests, investigating the tensile and flexural strength of the material, the Poisson's ratio, the modulus of elasticity and the Young's modulus. After the experiments, it was determined that impregnation exerts higher influence on the mechanical properties of the composite structures which are printed with a greater print line spacing, i.e., on the Group 3 samples. After the impregnation of this group, an increase of 31% in the tensile strength and an increase of 110% in the flexural strength was observed. In Group 1, the increase of the strength was lower: 13% for the tensile strength and 78% for the flexural strength, respectively. The Poisson's ratio is equal to 0.39 in the Group 1 samples and 0.30 in the Group 3. After the impregnation, this value increased to 0.41 in Group 1 and 0.38 in Group 3. The average Young's modulus of the composite structures is 23 GPa in Group 1 and 20 GPa in Group 3. After the impregnation, the Young's modulus increased in the respective groups to 24 GPa and 22 GPa. The average flexural modulus is 18 GPa in Group 1 and 16 GPa in Group 3. After the impregnation, the flexural modulus increased in the relevant groups to 21 GPa and 19 GPa.

CONCLUSIONS

Literature analysis revealed insufficient reported research work on the CCF impregnation methods, and lack of comprehensive analysis of the potential impregnation materials for CCF impregnation, concentrations, drying time, temperature and the impregnation speed. The scientific literature covering CCF printing processes lacks in-depth analysis of the ways how various printing parameters (e.g., the layer height, the print line spacing, the printing speed) and the differently impregnated CCF impact the mechanical properties, adhesion, or the void content.

1. The technology and equipment for the impregnation of 1K and 3K CCF in PLA, ABS, PC thermoplastics and solvent (methylene chloride) solution have been developed and described. When the concentration increases from 2% to 10%, the tensile force at break increases by 20% with 1K and 105% with 3K fiber tow. After the examination of various impregnation materials, it was found that carbon fiber tow acquires the best properties after impregnation in 10 wt% PLA and CH_2Cl_2 . After impregnation, the adhesion force between the PLA matrix and the CCF reinforcement material increased by ~240%. Microscopic inspection demonstrated that the percentage of air voids contained in the impregnate fiber tow ranges from 11% to 23% depending on the impregnation concentration.
2. Extrusion-based additive manufacturing process and technological equipment capable of printing composite structures reinforced with impregnated CCF have been developed. An improved FDM printing module with an efficient design of the input/output channels for the co-extrusion process was designed, fabricated and successfully applied for 3D printing of composite structures reinforced with 1K and 3K CCF with the recommended layer heights from 0.3 to 0.6 mm, with the print line spacing ranging from 1.0 to 1.6 mm and the extrusion multiplier ranging from 40% to 60% depending on the tow.
3. Defectoscopic analysis of printed composite structures was carried out by means of X-ray computed tomography and the experimental matrix dissolving method to determine the relative volume of air voids. The air volume in the structure directly depends on the layer height and the print line spacing. The air void volume can be decreased by minimizing these printing parameters. The amount of air voids determined by both methods is very similar and ranges from ~19% to ~28% depending on the layer height and the print line spacing. It was determined that the air void volume more significantly depends on the layer height if compared against the print line spacing.
4. The main mechanical properties of printed composite structures reinforced with CCF have been experimentally determined. The tensile strength

reaches 264 MPa and 204 MPa in sample Groups 1 and 3, respectively. The flexural strength of the same groups samples is 153 MPa and 140 MPa, while the Poisson's ratio is 0.39 and 0.30. The Young's modulus of the materials is equal to 23.6 GPa and 20.0 GPa, and the flexural modulus is equal to 17.0 GPa and 16.3 GPa, respectively for the above mentioned sample groups. The shear strength depends only on the printing parameters but does not depend on the shear area. The shear strength of Group 4 is 6.1 MPa on average, and, after the print line spacing was reduced to 1 mm, the shear strength increased to 8.7 MPa. The shear strength of the sample groups printed with the 0.3 mm layer height is 12.5 MPa and 15.1 MPa for sample Groups 3 and 1, respectively.

5. After the secondary impregnation in epoxy resin, the tested structures demonstrated significantly improved mechanical properties in comparison with the unimpregnated counterparts. The tensile strength increased by 30.5%, while the flexural strength grew by 110% in sample Group 3. A smaller increase of the tensile strength by 13% and a flexural strength of 78% was observed in sample Group 1. As it can be observed from the obtained data, impregnation with epoxy resin exerts greater impact on the sample groups printed with a higher layer height and print line spacing. This is related to the dependence of the volume of air voids from these printing parameters, i.e., there is relationship between air voids and the influence of epoxy resin impregnation on the mechanical properties of structures. A higher air void volume means that more epoxy resin could be absorbed.

SANTRAUKA

IVADAS

Temos aktualumas

Šiuo metu pramonei žengiant ketvirtosios revoliucijos link, adityviosios gamybos (AG) technologijos vaidina vis svarbesnį vaidmenį vienetinėje ir negausių serijų gaminių gamyboje. Dėl lengvo integravimo į gamybos procesą, beveik neribotos gaminamo modelio formos ir geometrijos bei mažų gamybos atliekų šios technologijos tampa vis populiareesnės. Didėjant jų panaudojimui, gamintojai ir mokslininkai ieško naujų, tvarių, geras mechanines savybes turinčių ir inovatyvių spausdinimo medžiagų. Prieš nepilnus dešimt metų pagrindinės spausdinimo medžiagos buvo termoplastikai ir fotopolimerai, tuo tarpu pramonė ir mokslas vis dažniau gręžiasi į įvairias kompozitines, plataus naudojimo medžiagas, kurios gali būti pasitelktos automobilių ar aviacijos pramonėje. Kompozitinės konstrukcijos pasižymi maža mase ir puikiomis mechaninėmis savybėmis, lyginant su metalinėmis konstrukcijomis. Šiuo metu ypatingas dėmesys skiriamas kompozitinėms medžiagoms, armuotoms ištisiniu pluoštu, kurios gali būti naudojamos automobilių ir aviacijos pramonėje. Lydžiosios masės formavimo technologija (LMF) yra viena iš plačiausiai naudojamų ir sparčiausiai tobulėjančių AG technologijų. Šios technologijos lankstumas, universalumas, sparčiai besiplečianti spausdinamų medžiagų (kurios gali būti naudojamas kaip matricos medžiaga) įvairovė, pažangi technologinė ir programinė įranga bei prieinamumas leidžia šią technologiją pritaikyti ištisiniu anglies pluoštu (IAP) armuotų kompozitinių konstrukcijų gamybai.

Tokių medžiagų spausdinimas naudojant LMF technologiją yra sudėtingas procesas, kurio metu reikalinga tinkama ir tam pritaikyta įranga, optimizuoti spausdinimo parametrai ir nustatyta jų įtaka gamybos procesui. Taip pat reikia paminėti, kad anglies pluošto impregnavimo efektyvumas ir jo įtaka spausdinimo proceso stabilumui ir spausdintos konstrukcijos mechaninėms savybėms turi būti nustatyta norint užtikrinti gaminamų kompozitinių konstrukcijų mechaninių savybių atkartojamumą. Impregnavimo procesas turi labai reikšmingą įtaką adhezijai tarp sluoksnių bei termoplastiko matricos ir IAP armuojančios medžiagos, oro ertmių tūriui ir kompozitinės medžiagos takumui. Visi šie veiksniai turi įtakos spausdintos kompozitinės konstrukcijos mechaninėms savybėms.

Tyrimo aktualumą lemia vis populiarėjančios adityviosios gamybos technologijos, kylanti ištisiniu anglies pluoštu armuotų 3D spausdintų konstrukcijų paklausa pramonėje, neišsamus impregnavimo, spausdinimo proceso, spausdinimo įrangos, spausdintų kompozitinių konstrukcijų mechaninių savybių analizavimas ir supratimas.

Darbo tikslas ir uždaviniai

Pagrindinis daktaro disertacijos tikslas yra sukurti ir validuoti ištisiniu anglies pluoštu armuotų 3D spausdintų sudėtingos geometrijos kompozitinių konstrukcijų gamybos technologiją. Šiam tikslui pasiekti iškelti šie uždaviniai:

1. Sukurti anglies pluošto impregnavimo technologiją ir ištirti impregnavimo tirpalo koncentracijos ir tirpinamos medžiagos įtaką spausdintoms ištisinio anglies pluošto ir termoplastiko matricos kompozitinėms konstrukcijoms.
2. Sukurti LMF technologija pagrįstą, ištisiniu pluoštu armuotų kompozitinių konstrukcijų spausdinimo procesą.
3. Ištirti spausdintų kompozitinių konstrukcijų kokybę įvertinant oro ertmių ir anglies pluošto procentinį tūrį.
4. Nustatyti pagrindines 3D spausdintų kompozitinių konstrukcijų mechanines savybes; tempimo, lenkimo ir šlyties stiprumo ribą, tempimo ir lenkimo modulius, Puasono koeficientą.
5. Ištirti antrinio impregnavimo epoksidinėje dervoje įtaką 3D spausdintų ištisiniu anglies pluoštu armuotų kompozitinių konstrukcijų mechaninėms savybėms.

Metodai ir priemonės

Šio mokslinio darbo metu buvo naudojami teoriniai, technologiniai-praktiniai, analitiniai ir eksperimentiniai tyrimai, skirti impregnavimo ir spausdinimo procesams bei spausdinimo įrangai sukurti ir konstrukcijų mechaninėms savybėms ištirti. Mokslinio darbo metu buvo naudojama ši programinė įranga: „MatLab“, „Simplify3D“, „PrusaSlicer“, „SolidWorks“, „Avizo“, „ImageJ2x“ ir „NIS Elements D“. Tyrimai atlikti Kauno technologijos universiteto Mechanikos inžinerijos ir dizaino fakultete, Gamybos inžinerijos katedroje, Mechatronikos bei Ultragarso institutuose. Sukurta technologija buvo eksperimentiškai išbandyta tiriant atspausdintų ištisiniu anglies pluoštu armuotų 3D spausdintų kompozitinių konstrukcijų mechanines savybes. Mechaninės savybės tirtos naudojant universalią „Tinius Olsen H25KT“ mašiną, oro ertmių kiekis nustatytas dviem metodais: naudojant „ImageJ2x“ vaizdo apdorojimo programinės įrangos paketą ir automatinį „Nikon Eclipse LV100ND“ mikroskopą su didelės skiriamosios gebos kamera „DS-Ri2“ ir naudojant kompiuterinę tomografiją – „RayScan 250E“.

Mokslinis naujumas

1. Sukurtas inovatyvus metodas, skirtas ištisinio anglies pluošto impregnavimui.
2. Sukurtas naujas spausdinimo modulis, galintis spausdinti ištisiniu anglies pluoštu armuotas kompozitines konstrukcijas.
3. Sukurtas ir išbandytas spausdintų konstrukcijų mechaninių savybių tempiant ir lenkiant gerinimo procesas, jas impregnuojant epoksidinėje dervoje.

Praktinė vertė

Mokslinio darbo metu sukurtos technologijos ir įranga gali būti naudojama gaminant sudėtingos formos, lengvas ištisiniu anglies pluoštu armuotas kompozitines konstrukcijas moksliniams tyrimams ar automobilių, aviacijos, medicinos pramonėje, bei kitose sparčiai besivystančiose srityse tokiose kaip autonominių robotų, žmogui reikalingų inovatyvių pagalbinių priemonių gamyboje. Sukurtos technologijos ir įrenginiai gali būti naudojami su įvairaus gijų skaičiaus

pluoštu. Atlikti mechaniniai ir kokybiniai spausdintų kompozitinių konstrukcijų tyrimai suteikia vertingos informacijos ir žinių tolimesniam technologiniam proceso vystymui.

Ginamieji teiginiai

1. Sukurtas ištisinio anglies pluošto impregnavimo technologinis procesas gali sumažinti oro ertmių kiekį, padidinti adheziją tarp sluoksnių ir sukibimą tarp matricos ir armuojančios medžiagos, bei užtikrinti stabilesnį spausdinimo procesą.
2. Sukurtas technologinis procesas ir originalus spausdinimo modulis, pagrįstas LMF technologija, gali užtikrinti nepertraukiamą anglies pluoštu armuotų kompozitinių konstrukcijų spausdinimą.
3. Spausdintų kompozitinių konstrukcijų mechaninės savybės gali būti pagerintos antriniu impregnavimu epoksidinėje dervoje.

Darbo aprašymas

Disertacijos tyrimo rezultatai buvo paskelbti 4 mokslinėse publikacijose tarptautiniuose žurnaluose. Iš jų trys publikacijos žurnaluose turinčiuose Web of Science citavimo indeksą ir viena neindeksuojamame moksliniame žurnale.

Disertacijos tema buvo sudalyvauta septyniose tarptautinėse mokslinėse konferencijose: „Mechanika 2018“ (Kaunas, Lietuva), „iCAT 2018“ (Mariboras, Slovėnija), „Conference on 3D printing technology and innovations 2019“ (Roma, Italija), „Advanced materials and technologies 2019“ (Palanga, Lietuva), POLCOM 2020 (Bukareštas, Rumunija), „International conference on composite structures 2021“ (Portu, Portugalija), MECHCOMP7 2021 (Portu, Portugalija).

Disertacijos struktūra

Disertaciją sudaro įvadas, trys skyriai (literatūros apžvalga, metodologija, rezultatai), išvados, naudotos literatūros sąrašas, autoriaus publikacijų disertacijos tema sąrašas. Pagrindiniai skyriai: literatūros apžvalga, kurioje analizuojami pagrindiniai lydžiosios masės formavimo technologijos principai kartu su pagrindinėmis šioje technologijoje naudojamomis medžiagomis. Analizuoti šiuo metu egzistuojantys kompozitinių medžiagų ir spausdinimo metodai. Metodikoje aprašoma, atliktų eksperimentų eiga, naudotos medžiagos ir įranga. Aprašoma, sukurta spausdinimo technologija ir spausdinimo modulis skirtas ištisiniu anglies pluoštu armuotų kompozitinių konstrukcijų spausdinimui. Rezultatų skyriuje pateikiami pagrindiniai eksperimentų rezultatai, pvz., oro ertmių procentinis kiekis ir kompozitinės medžiagos mechaninės savybės bei antrinio impregnavimo metodo efektyvumas ir poveikis spausdintų konstrukcijų stiprumui.

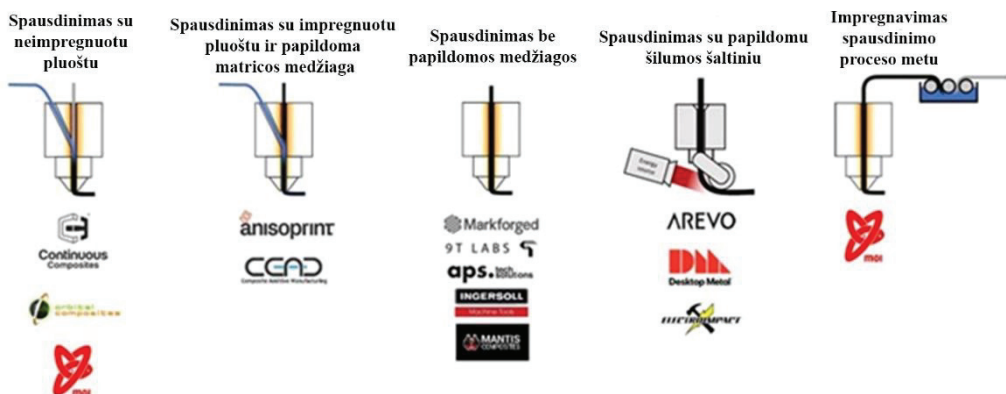
1. LITERATŪROS APŽVALGA

1.1. Ištinio anglies pluošto spausdinimas LMF Technologija

Šiuo metu mokslinėje literatūroje galima surasti ir išskirti penkis pagrindinius ištisinių anglies pluoštu armuotų LMF technologija spausdintų kompozitinių konstrukcijų būdus:

1. Spausdinimas su neimpregnuotu pluoštu – neparuoštas pluoštas patenka į spausdinimo antgalį, tuo tarpu matricos medžiaga tiekiamas per vieną ar kelis įėjimo kanalus. Pluoštas impregnuojasi kaitinimo elemente prieš pat kompozitinei gijai išeinant iš spausdinimo antgalio ant spausdinimo platformos [66].
2. Spausdinimas su impregnuotu pluoštu ir papildoma matricos medžiaga – vietoje neparuošto pluošto į spausdinimo antgalį patenka prieš spausdinimą paruoštas ištisinis anglies pluoštas, tuo pačiu metu kaip ir matricos medžiaga. Dažniausiai anglies pluošto impregnavimo ar paruošimo medžiaga yra tokia pati kaip ir spausdinamos kompozitinės konstrukcijos matricos medžiaga [20, 55].
3. Spausdinimas be papildomos medžiagos – impregnuotas anglies pluoštas ekstruduojamas be jokios papildomos matricos medžiagos [53].
4. Spausdinimas su papildomu šilumos šaltiniu – technologija paremta automatinio pluošto išdėstymo termoplastiko matricoje modeliu. Šiuo atveju paruoštas ar neparuoštas anglies pluoštas yra tiekiamas per spausdinimo antgalį į darbo zoną. Darbo zonoje išorinis šilumos šaltinis kaitina darbo zoną ar anksčiau spausdintus sluoksnius, o volelis įpresuoja pluoštą į matricą [66].
5. Impregnavimas spausdinimo proceso metu – pluoštas impregnuojamas spausdinimo proceso metu, prieš pat anglies gijai patenkant į spausdinimo galvutę.

Schematinis kiekvienos technologijos vaizdas pateikiamas 1.1 pav.



1.1 pav. Galimi ištisinių anglies pluoštu armuotų kompozitinių konstrukcijų spausdinimo metodai [67]

1.2. Literatūros apžvalgos apibendrinimas

Šiuo metu kompozitinių ir kitų inovatyvių spausdinimo medžiagų paklausa sparčiai auga. Taip pat į adityviosios gamybos technologijas pradedama žiūrėti ne vien kaip į skirtas prototipavimui, bet ir kaip į realiai pramonėje galinčias įsitvirtinti technologijas. Šios dvi priežastys skatina tyrėjus ieškoti galimybių ir naujų inovatyvių sprendimų, pritaikyti adityviasias technologijas pramonės poreikiams. Anglies pluoštu armuoti kompozitai yra viena plačiausiai šiuo metu naudojamų kompozitinių medžiagų grupių aviacijos ir automobilių pramonėje. Tuo tarpu LMF technologija yra viena plačiausiai naudojamų adityviosios gamybos technologijų spausdinant ištisiniu anglies pluoštu armotas konstrukcijas. Taip yra dėl šios technologijos lankstumo, universalumo, plataus medžiagų pasirinkimo, tobulėjančios techninės ir programinės įrangos. Taip pat pastebėta labai didelė nauda mechaninėms spausdintų konstrukcijų savybėms. Įterpus ištisinį anglies pluoštą į spausdintą polimerinę matricą stiprumo ribą tempiant galima padidinti nuo 3 iki 7 kartų lyginant su grynu termoplastiku. Pirmieji tyrimai ir mokslinės publikacijos susijusios su ištisinio pluošto spausdinimu LMF technologija atsirado 2016 metais. Tais pačiais metais susikūrė ir du pagrindiniai šios rinkos lyderiai, t. y. įmonės „Markforged“ ir „Anisoprint“. Ilgą laiką „Markforged“ spausdintuvai, medžiagos ir jais atspausdintos konstrukcijos buvo vieninteliai tyrimo objektai šioje srityje. Tačiau norint geriau suprasti patį ištisiniu anglies pluoštu armuotų kompozitinių konstrukcijų spausdinimo procesą, atskirų spausdinimo parametrų, anglies pluošto kiekio, jo paruošimo ir impregnavimo įtaką mechaninėms, cheminėms, fizikinėms ir kokybinėms savybėms tyrėjai pradėjo ieškoti ir kurti alternatyvias spausdinimo, impregnavimo technologijas ir įrangą. Naudojant komercinius spausdintuvus to padaryti neįmanoma dėl komercinių paslapčių, o tai stabdo šios srities progresą ir plėtrą. Todėl šioje disertacijoje buvo kuriama ir vystoma spausdinimo ir anglies pluošto impregnavimo technologija bei įranga, tirama spausdinimo bei impregnavimo procesų parametrų įtaka spausdintų konstrukcijų mechaninėms ir kokybinėms savybėms.

2. METODOLOGIJA

Disertacijos tikslas yra sukurti 3D spausdinimo technologiją ir išanalizuoti ištisiniu anglies pluoštu (IAP) armotas 3D spausdintas kompozitines konstrukcijas. Visus disertacijos metu atliktus tyrimus galima suskirstyti į tris pagrindines dalis:

1. Pasiruošimas. Šio etapo metu buvo sukurtos: ištisinio anglies pluošto impregnavimo technologija bei IAP armotas kompozicines konstrukcijas galinti spausdinti spausdinimo galvutė.
2. Spausdinimas. Šio etapo metu sukurtas, LMF technologija paremtas, ištisiniu anglies pluoštu armotas konstrukcijas galintis spausdinti, procesas. Taip pat naudojant šį procesą pagaminti bandiniai tolesniam mechaninių charakteristikų nustatymui.
3. Testavimas. Šiame etape atlikti visi suplanuoti eksperimentai ir tyrimai, reikalingi 3D spausdintų kompozitinių konstrukcijų analizei ir pagrindinių mechaninių savybių nustatymui.

2.1. Medžiagos

Kompozitines konstrukcijas sudaro dvi arba daugiau skirtingomis mechaninėmis savybėmis pasižyminčios medžiagos. Rišančioji medžiaga vadinama matrica, o suteikianti stiprumą – armuojančia medžiaga. Šiame darbe aprašomos kompozitinės konstrukcijos yra sudarytos iš termoplastiko matricos ir ištisinio anglies pluošto armuojančios medžiagos.

3D spausdinant kompozitines konstrukcijas naudotas gamintojo „Toray“ nepintas aukštos kokybės ištisinis anglies pluoštas. Priklausomai nuo bandymo ir spausdinamos konstrukcijos, eksperimentinėje dalyje buvo naudotas 1K (tūkstančio gijų) T300B-1000 arba 3K (trijų tūkstančių gijų) T300B-3000 ištisinis anglies pluoštas. Šio gamintojo anglies pluoštas yra gaminamas iš poliakrilnitrilo. Kaip armuojanti medžiaga ištisinis anglies pluoštas pasirinktas dėl didelio atsparumo cheminiam poveikiui, puikių mechaninių savybių bei labai plataus panaudojimo aviacijos bei automobilių pramonėje. Toliau pateiktoje 2.1 lentelėje pateikiamos pagrindinės 1K ir 3K ištisinio anglies pluošto charakteristikos.

2.1 lentelė. Pagrindinės ištisinio anglies pluošto savybės [98]

Anglies pluoštas	Gijų skaičius	Stiprumo riba tempiant, MPa	Jungo modulis, GPa	Pailgėjimas, %	DTEX, g/1000 m	Tankis, g/cm ³
T300B-1000	1000	3530	230	1,5	66	1,76
T300B-3000	3000				198	

Prieš spausdinimą anglies pluoštas buvo impregnuotas. Tai daroma dėl dviejų priežasčių: impregnavimo metu surišamos anglies pluošto gijos ir palengvinamas gamybos technologinis procesas. Kita vertus, impregnavimas padidina adheziją tarp matricos ir armuojančios medžiagos bei ženkliai pagerina spausdintų kompozitinių konstrukcijų mechanines savybes, ši hipotezė patvirtinta tyrimų metu.

Atliktų tyrimų metu bandiniai buvo spausdinti naudojant polilaktinės rūgšties (PLA) termoplastiką. Kaip matricos medžiaga PLA pasirinkta dėl paprasto spausdinimo, gana žemos spausdinimo temperatūros, gero sukibimo su spausdinimo platforma, didesnės adhezijos su impregnuotu ištisiniu anglies pluoštu, gerų mechaninių savybių. Taip pat svarbu paminėti, kad polilaktinė rūgštis yra gaminama iš atsinaujinančių šaltinių, tokių kaip kukurūzų krakmolos, ir yra bioskaidi bei kai kurios jos rūšys yra biosuderinamos. Renkantis matricos medžiagą ištisiniu anglies pluoštu armuotų kompozitinių konstrukcijų spausdinimui, svarbu atsižvelgti į du pagrindinius parametrus: termoplastiko lydymosi temperatūrą, kuri dėl naudojamo spausdintuvo ribojimų negali viršyti 250 °C, bei suderinamumą su impregnavimo metu naudojamu tirpalu. Dėl geresnių adhezinių ir suderinamumo savybių matricos medžiaga turi būti tokia pati kaip ir impregnavimui naudotas termoplastikas. Pagrindinės PLA medžiagos savybės pateikiamos 2.2 lentelėje.

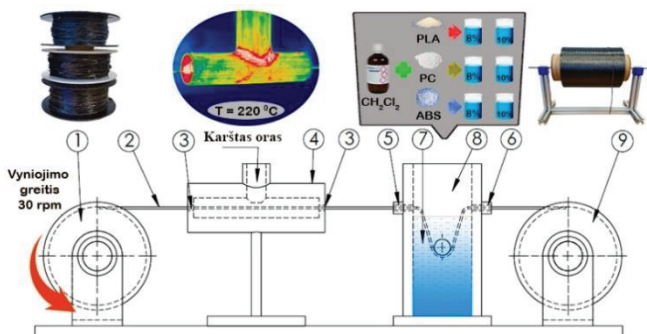
2.2 lentelė. Pagrindinės PLA termoplastiko mechaninės charakteristikos [99]

Lydimosi temperatūra, °C	Jungo modulis, GPa	Stiprumo riba tempiant, MPa	Stiprumo riba lenkiant, MPa	Lenkimo modulis, MPa	Stiklėjimo temperatūra, °C
180–220	2.3	45,6	103	3150	~ 60

2.2. Impregnavimo procesas⁸

Iš anksto neparuoto anglies pluošto, dėl mažo 1K ar 3K gijos standumo, beveik neįmanoma paduoti į spausdinimo galvutę. Jis lengvai susivelia, atskiros gijos linkusios nutrūkti ir kauptis spausdinimo galvutės viduje. Šios pluošto sankaupos užkemša padavimo ar išėjimo kanalus, taip nutraukdamos giją ir sustabdydamos spausdinimo procesą. Kitas svarbus aspektas – prasta adhezija tarp matricos ir armuojančios medžiagos. PLA ar kitas termoplastikas nėra linkęs prikibti prie iš anksto neparuoto ištisinio anglies pluošto. Tai sukelia didelių problemų spausdinant, nes mažas sukibimas tarp šių medžiagų lemia silpną adheziją tarp sluoksnių, spausdinimo gijų bei spausdinimo platformos, o tai turi įtaką spausdintų kompozitinių konstrukcijų mechaninėms savybėms bei jų kokybei. Visas impregnavimo procesas susideda iš dviejų etapų: tirpalo paruošimo ir paties impregnavimo proceso. Nuspręsta ištisinį anglies pluoštą įmirkyti metileno chlorido CH_2Cl_2 ir termoplastiko tirpale. Metileno chloridas pasirinktas dėl spartaus garavimo ir greito įvairių skirtingų termoplastikų, tokių kaip PLA, PETG, PC ir kt., tirpinimo. Impregnavimui buvo išbandyti trys dažniausiai LMF technologijoje naudojami termoplastikai: PLA, ABS, PC. Šie termoplastikai skiriasi ne tik chemine sudėtimi, tačiau ir mechaninėmis bei fizikinėmis savybėmis. Eksperimentiškai buvo nustatyta reikalinga tirpalo koncentracija bei surastas geriausias savybes ištisiniui anglies pluoštui suteikiantis termoplastikas.

Kuriant impregnavimo technologiją buvo sukurtas impregnavimo įrenginys, kurio schema pateikiama 2.1 pav.



2.1 pav. Anglies pluošto impregnavimo schema

Prietaisas buvo pagamintas iš ritės ant kurios yra vyniojamas impregnuotas anglies pluoštas (1), anglies pluošto (2), kaitinimo dalies (4), impregnavimo dalies

⁸ Šio skyriaus medžiaga anksčiau buvo publikuota [100].

(8) ir ritės su standartiniu neįmirkytu anglies pluoštu (9). Kaitinimo dalies įėjimo ir išėjimo angos (4) turi identiško skersmens antgalius (3), o impregnavimo dalis (8) naudoja skirtingo skersmens antgalius – (5) ir (6). Siekiant išlaikyti kuo pastovesnes sąlygas, vyniojimo greitis ir kaitinimo sąlygos išlaikomos pastovios. Vyniojimo greitis ritėje (1) buvo išlaikytas pastovus, t. y. 30 aps/min, nepriklausomai nuo naudotos tirpalo koncentracijos ar ištisinio anglies pluošto. Prietaiso veikimas pagrįstas impregnuoto anglies pluošto traukimu per vonelę, užpildytą impregnavimo tirpalu. Sukant impregnuoto pluošto ritę (1) prieš laikrodžio rodyklę, anglies pluoštas (2) buvo išvyniojamas iš antrosios ritės (9). Visų pirma, per antgalį (6) anglies pluoštas patenka į impregnavimo dalį (8), kurioje jis buvo panardintas į tirpalą (7) iki nejudamai pritvirtinto volelio. Per antgalį (5), pritvirtintą kitoje prietaiso pusėje, pluoštas yra ištraukiamas ir patenka į kaitinimo zoną. Karštas oras yra nuolat tiekiamas į kaitinimo dalį, impregnuotas anglies pluoštas patenka į kaitinimo elementą per antgalius, pagamintus iš politetrafluoretileno (PTFE). Kaitinimo temperatūra matuojama naudojant „Flir T420“ terminio vaizdo kamerą. Siekiant užtikrinti stabilias kaitinimo sąlygas, karštas oras yra tiekiamas į impregnavimo įtaiso kaitinimo dalį (4), kol temperatūra stabilizuojasi. Išmatuota temperatūra kaitinimo prietaiso viduje siekia apie 220 °C.

Kaitinimo dalies antgalių (3) vidinis skersmuo yra 5 mm. Išdžiūvęs impregnuotas anglies pluoštas, ištrauktas iš kaitinimo dalies, susukamas ant ritės (1) pastovių greičiu. Impregnavimo dalyje naudojamas antgalio skersmuo priklauso nuo anglies pluošto tipo. Įėjimo antgalis (6) pagamintas iš PTFE, kurio vidinis skersmuo yra 2 mm. Išėjimo antgalis pagamintas iš bronzos, jo vidinis skersmuo 1K anglies pluoštui – 0,6 mm, o 3K anglies pluoštui – 0,8 mm. Antgalio (5) skersmuo yra svarbus, nes jis sąlygoja, kiek tirpalo pasiliks ant impregnuojamo anglies pluošto. Identiški antgaliai (3) kaitinimo dalyje leidžia išlaikyti anglies pluoštą įtaiso centre ir neleidžia jam prilipti prie prietaiso sienelių.

Impregnavimas termoplastiko ir metileno chlorido tirpale išsprendžia daugelį problemų, kurios iškyla spausdinant su neapdorotu ištisiniu anglies pluoštu. Visų pirma po impregnavimo, anglies pluošto gija tampa standesnė ir vienalytiškesnė, t. y. atskiros 7 µm pluošto gijos yra surišamos į vientisą giją. Tai leidžia pluoštą lengvai paduoti į spausdinimo galvutę spausdinimo proceso metu, toks anglies pluoštas yra daug mažiau linkęs deformuotis, trūkti ar veltis. Impregnuotas anglies pluoštas leidžia turėti labiau prognozuojamą ir patikimesnę 3D spausdinimo procesą. Kitas labai svarbus aspektas didesnė adhezija tarp spausdinimo gijų, tarp konstrukcijos sluoksnių ir spausdinimo platformos. Naudojant impregnuotą anglies pluoštą taip pat sumažinamas oro ertmių kiekis spausdinamoje konstrukcijoje. Oro ertmių kiekis konstrukcijoje priklauso nuo ertmių, atsirandančių spausdinimo proceso metu, ir ertmių, esančių anglies pluošte. Be kokybinių privalumų, lyginant su neimpregnuotu ištisiniu anglies pluoštu, pastebimas daugiau nei ženklus mechaninių savybių pagerėjimas.

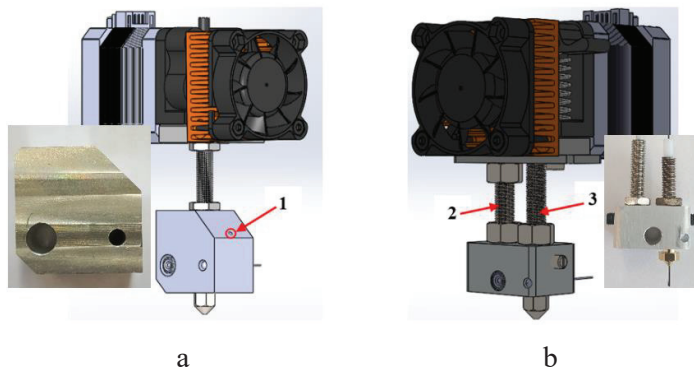
2.3. Spausdinimo galvutė

Du prototipai buvo sukurti standartinės galvutės pagrindu, jie pateikti 2.2 pav. Kaip matyti, šaltoji zona abiem atvejais išliko beveik nepakitusi. Vienintelis

skirtumas, kad patobulintas prototipas (b) šaltojoje zonoje turi kanalą pluošto patekimui į karštąją zoną. Pagrindiniai pokyčiai matomi karštojoje zonoje. Patobulintas prototipas turi du įėjimo vamzdelius: vieną nukreipti matricos medžiagai (2), kitą nukreipti anglies pluoštui (3). Pluošto nukreipimo vamzdelis atlieka kelias funkcijas ir išsprendžia problemas, pastebėtas naudojant ankstyvąjį prototipą (a):

1. vamzdelis užtikrina pastovų ir saugų anglies pluošto patekimą į spausdinimo zoną;
2. padeda išlaikyti temperatūrą kaitinimo elemente;
3. neleidžia plastikui kilti į pluošto padavimo zoną;
4. suteikia galimybę pluoštui patekti tiesiogiai į kaitinimo elementą, išvengiant kampų ar aštrių briaunų.

Spausdinant ankstyvuojų prototipu anglies pluoštas patekdavo į kaitinimo elementą 45° kampu, per angą (1). Buvo pastebėta, kad esant atvirai angai kaitinimo elemente, plastikas yra linkęs tekėti ne į spausdinimo zoną, bet kilti į viršų. Tai sąlygodavo nepakankamą plastiko kiekį konstrukcijose ir komplikotą pluošto padavimą. Komplikuotas anglies pluošto patekimas į kaitinimo elementą, kartu su 45° nukreipimu sukeldavo armuojančios medžiagos trūkius. Šiems faktoriams eliminuoti buvo sukurtas antrasis arba patobulintas prototipas.



2.2 pav. Modifikuota spausdinimo galvutė: a – ankstyvasis prototipas; b – patobulintas prototipas

Spausdinimo technologija skirta spausdinti ištisiniu anglies pluoštu armuotas kompozitines konstrukcijas buvo sukurta eksperimentiniu būdu, tai yra modifikuotu LMF technologijos spausdintuvu su specialiai tam sukurta spausdinimo galvute (ankstyvuojų ir patobulintu prototipais), spausdinant kelių sluoksnių kompozitinius bandinius. Realio laiko keičiant spausdinimo parametrus, tokius kaip sluoksnio aukštį, spausdinimo greitį, plastiko ekstrudavimo procentą, aušinimo intensyvumą, atstumą tarp spausdinimo gijų, spausdinimo antgalio skersmenį ir kaitinimo elemento bei platformos temperatūrą, buvo nustatytos optimalios šių spausdinimo parametrų skaitinės reikšmės. Kiekvienas iš šių parametrų turi įtakos kompozitinės konstrukcijos spausdinimo kokybei ir spausdinimo proceso pakartojamumui. Visus anksčiau išvardintus spausdinimo parametrus galime suskirstyti į dvi grupes:

- 1) pagrindiniai parametrai – kintantys priklausomai nuo naudojamo anglies pluošto (1K ar 3K) bei turintys tiesioginę įtaką anglies pluošto kiekiui ir kompozitinės konstrukcijos mechaninėms bei kokybinėms charakteristikoms;
- 2) pagalbiniai parametrai – nekintantys nuo naudojamo anglies pluošto ir neturintys tokios ryškos įtakos atspausdintos kompozitinės konstrukcijos kokybei bei mechaninėms savybėms.

Rekomenduojami parametrai, kompozitinių konstrukcijų spausdinimui pateikiami 2.3 lentelėje.

2.3 lentelė. Rekomenduojami spausdinimo parametrai

Parametrai	1K	3K
Sluoksnio aukštis, mm	0,3/0,4	0,5/0,6
Atstumas tarp spausdinimo gijų, mm	1/1,2	1,4/1,6
Plastiko kiekis, %	60/80	40/60
Spausdinimo antgalio skersmuo, mm	1,6	
Spausdinimo greitis, mm/s	0,3	
Spausdinimo galvutės temperatūra, °C	220	
Platformos temperatūra, °C	80	
Aušinimas, %	60–90	

Atlikus numatytus bandymus, buvo sukurta nauja inovatyvi adityviosios gamybos technologija ištisiniu anglies pluoštu armuotų kompozitinių konstrukcijų spausdinimui. Eksperimentiškai nustatyti rekomenduojami spausdinimo parametrai, sukurta metodologija ištisinio anglies pluošto paruošimui prieš spausdinimą leido sumažinti oro ertmių kiekį bei pagerinti mechanines savybes. Sukurta ir išbandyta metodologija spausdintų kompozitinių konstrukcijų mechaninių savybių gerinimui jas impregnuojant epoksidine derva.

3. REZULTATAI

3.1. Anglies pluošto impregnavimo proceso analizė⁹

Šio tyrimo tikslas buvo nustatyti, kokią įtaką spausdintų gaminių mechaninėms savybėms turi skirtingos impregnavimui naudojamos medžiagos ir jų koncentracija tirpaluose. Buvo naudotos trys impregnavimo medžiagos (PLA, PC, ABS) ir skirtingos koncentracijos tirpalai (2–10 %). Tas pats įrenginys buvo naudotas impregnuojant visomis koncentracijomis skirtingus anglies pluoštus, kiti impregnavimo parametrai ir sąlygos buvo išlaikomos pastovios. Tempimo bandymas su impregnuotu anglies pluoštu parodė, kad tirpalo koncentracijai padidėjus, pluošto atsparumas trūkimui taip pat padidėja. Koreliacijos analizė atskleidė stiprų ryšį tarp impregnuoto anglies pluošto trūkimo jėgos ir impregnuoto anglies pluošto masės. Koreliacijos koeficientas svyravo nuo 0,82 esant 1K PLA impregnuotam anglies pluoštui iki 0,99 PC impregnuoto anglies pluošto atveju. Siekiant ištirti, ar šie rezultatai galioja 3D spausdintoms kompozitinėms medžiagoms, bandiniai buvo atspausdinti tempimo bandymams naudojant 3

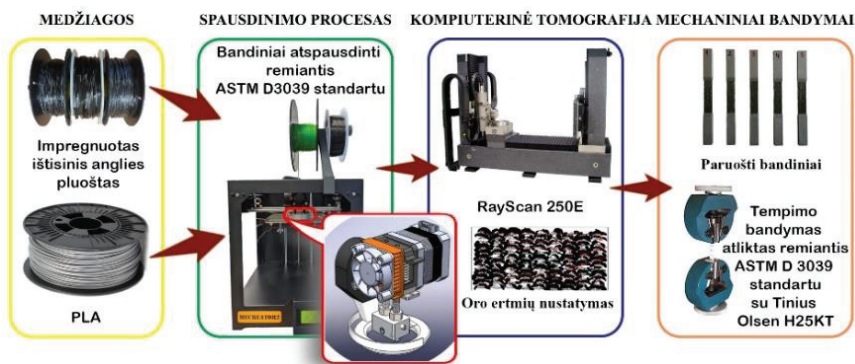
⁹ Šio skyriaus medžiaga anksčiau buvo publikuota [100].

skirtingas impregnavimo medžiagas (PLA, PC, ABS) ir skirtingas anglies pluošto impregnavimo koncentracijas (8–10 %). Gauti rezultatai atskleidė priklausomybę tarp tirpalo koncentracijos ir stiprumo ribos tempiant, t. y. kuo didesnė impregnavimo tirpalo koncentracija, tuo didesnė kompozitinės konstrukcijos stiprumo riba tempiant. Ši tendencija ypač ryški PLA ir PC tirpaluose impregnuotame 3K anglies pluošte, kur stiprumo riba tempiant padidėja nuo 154 MPa iki 165 MPa (7 % padidėjimas) ir nuo 142 MPa iki 152 MPa (6,8 % padidėjimas) atitinkamai nuo naudojamų medžiagų. Tuo tarpu, impregnuojant anglies pluoštą ABS tirpale, rezultatų pokytis buvo labai nežymus, o naudojant 3K anglies pluoštą – bandinių stiprumo riba tempiant net sumažėjo nuo 145 iki 144 MPa (0,7 % sumažėjimas).

Impregnuoto 1K ištisinio anglies pluošto vizualinė analizė parodė, kad impregnuoto ploto procentinė dalis svyruoja nuo 77,2 % iki 88,9 %, tuo tarpu oro ertmių procentas atitinkamai svyruoja nuo 11,1 % iki 22,8 %. Siekiant įvertinti adheziją tarp matricos ir IAP, buvo atliktas anglies pluošto ištraukimo iš matricos medžiagos bandymas. Šis eksperimentas atliktas naudojant ir impregnuotą, ir neimpregnuotą IAP. Rezultatai parodė, kad neparuošto IAP ištraukimo iš matricos jėga vidutiniškai yra 38 N. Impregnavus IAP, sukibimas tarp armuojančios ir matricos medžiagos gali būti padidintas daugiau nei keturis kartus. Po pluošto paruošimo impregnuojant ištempimo jėgos vidutinė reikšmė padidėja iki 138 N arba 114 %.

3.2. Spausdintų kompozitinių konstrukcijų kokybės vertinimas¹⁰

Norint įvertinti 3D spausdintų kompozitinių konstrukcijų savybes, labai svarbu apskaičiuoti anglies pluošto kiekį ir oro ertmių tūrį. Buvo pasirinktos dvi dominuojančios metodikos, siekiant įvertinti jų patikimumą ir veiksmingumą 3D spausdintų konstrukcijų analizei. Pirmuoju metodu oro ertmių kiekis buvo nustatytas pasitelkiant kompiuterinę tomografiją. Šio bandymo schema pateikiama 3.1 pav.

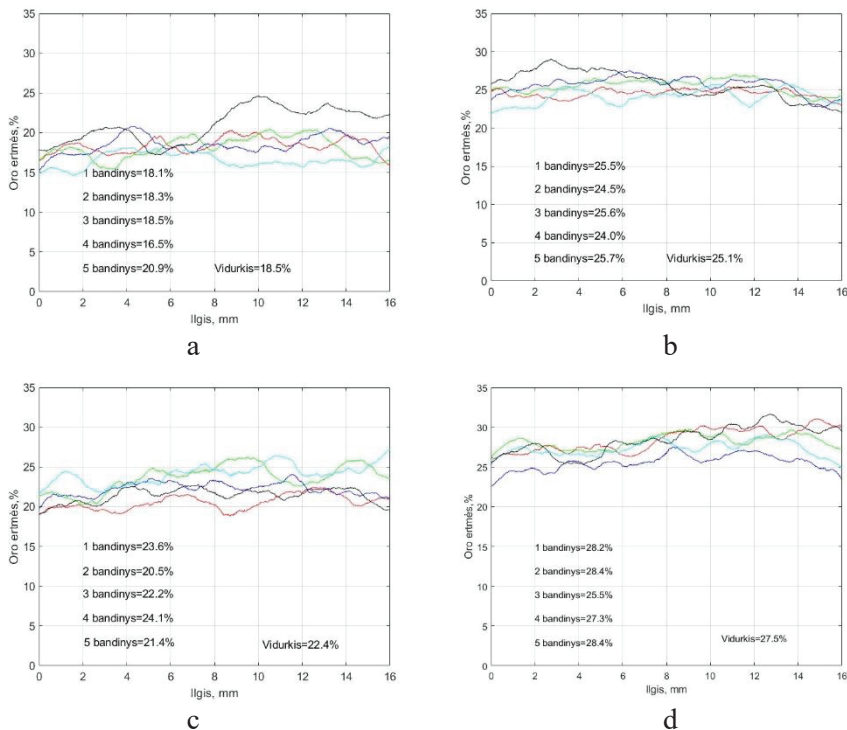


3.1 pav. Oro ertmių nustatymas panaudojant kompiuterinę tomografiją

Žvelgiant į gautus rezultatus bendrai, matoma aiški santykinio oro ertmių tūrio tendencija: tuštumų tūris mažėja, kai sluoksnio aukštis ir atstumas tarp spausdinimo

¹⁰ Šio skyriaus medžiaga anksčiau buvo publikuota [101].

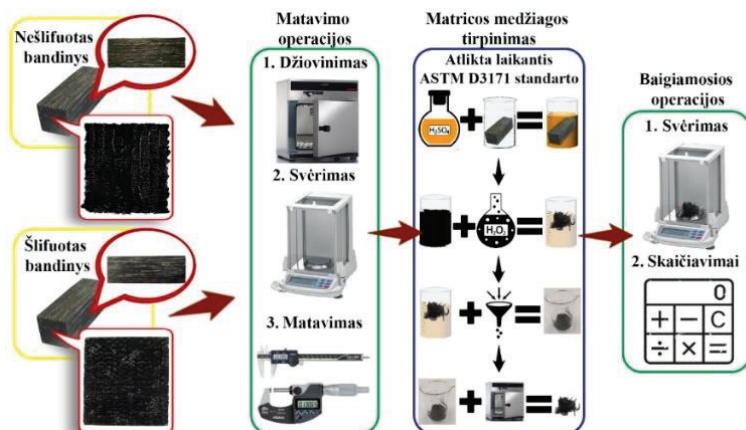
linijų mažėja. Bandiniai šio tyrimo metu buvo suskirstyti į grupes pagal spausdinimo parametrus: 1 grupė – 1 mm atstumas tarp spausdinimo gijų, 0,3 mm sluoksnio aukštis; 2 grupė – 1 mm atstumas tarp spausdinimo gijų, 0,4 mm sluoksnio aukštis; 3 grupė – 1,2 mm atstumas tarp spausdinimo gijų, 0,3 mm sluoksnio aukštis; 4 grupė – 1,2 mm atstumas tarp spausdinimo gijų, 0,4 mm sluoksnio aukštis. Pavyzdžiui, vidutinis santykinis oro ertmių tūris pirmosios grupės bandiniuose buvo 18,5 % (3.2 a pav.), tačiau padidinus atstumą tarp spausdinimo linijų nuo 1 mm iki 1,2 mm (3 grupė) vidutinis oro ertmių tūris padidėjo iki 22,4 % (3.2 c pav.), t. y. 3,9 %. Vertinant rezultatus antroje bandinių grupėje (3.2 b pav.) ir ketvirtoje (3.2 d pav.), matyti, kad padidinus atstumą tarp spausdinimo linijų santykinis ertmių tūris padidėja apie 2,4 %.



3.2 pav. Oro ertmių procentas bandiniuose: a – 1 grupė, b – 2 grupė, c – 3 grupė, d – 4 grupė

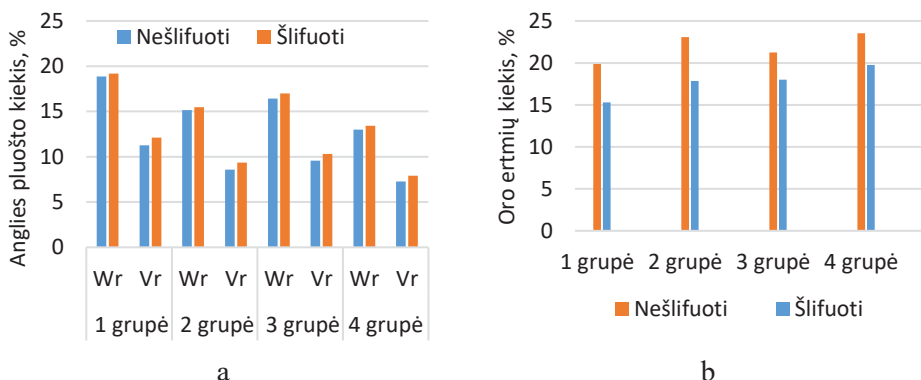
Vertinant spausdinimo parametrų įtaką santykiniam porų tūriui, matyti, kad mažinant sluoksnio aukštį, tačiau išlaikant pastovų atstumą tarp spausdinimo gijų, porų tūris sumažėjo daugiau, t. y. 6,6 %, kai atstumas tarp gijų yra 1 mm (3.2 a pav. ir 3.2 b pav.) ir 5,1 %, kai atstumas yra 1,2 mm (3.2 c pav. ir 3.2 d pav.). Tuo tarpu keičiant atstumą tarp spausdinamų gijų nuo 1 mm iki 1,2 mm, santykinis porų tūris bandiniuose vidutiniškai padidėjo 3,9 % bandiniams su sluoksnio aukščiu 0,3 mm iki 2,4% bandiniams kurių sluoksnio aukštis yra 0,4 mm. Taigi anksčiau iškelta prielaida, kad spausdinimo parametrai, t. y. sluoksnio aukštis ir linijos plotis, turi įtakos oro tuštumų kiekiui bandiniuose yra teisinga.

Antruoju kompozitinės konstrukcijos analizės metodu, kurio bandymo schema pateikiama 3.3 pav., buvo pasirinktas matricos medžiagos tirpinimas.



3.3 pav. Oro ertmių nustatymas naudojant matricos ištirpinimo metodą

Tirpinimo bandymo rezultatai parodė (3.4 a pav.), kad 1,2 mm atstumo tarp linijų ir 0,4 mm sluoksnio aukščio bandiniai yra prastesnės kokybės, t. y. juose esantis anglies kiekis yra mažiausias, o oro porų tūris yra didžiausias. Šiose bandiniuose (4 grupė) vidutiniškai buvo 13 % anglies pluošto pagal masę ir 7,2 % anglies pluošto pagal tūrį. Sumažinus sluoksnio aukštį iki 0,3 mm, anglies kiekis padidėjo iki 16,4 % pagal masę ir 9,5 % pagal tūrį. Didžiausias anglies kiekis nustatytas bandiniuose, kurie buvo atspausdinti naudojant šiuos parametrus: 0,3 mm sluoksnio aukštį ir 1 mm atstumą tarp spausdinimo gijų (1 grupė).



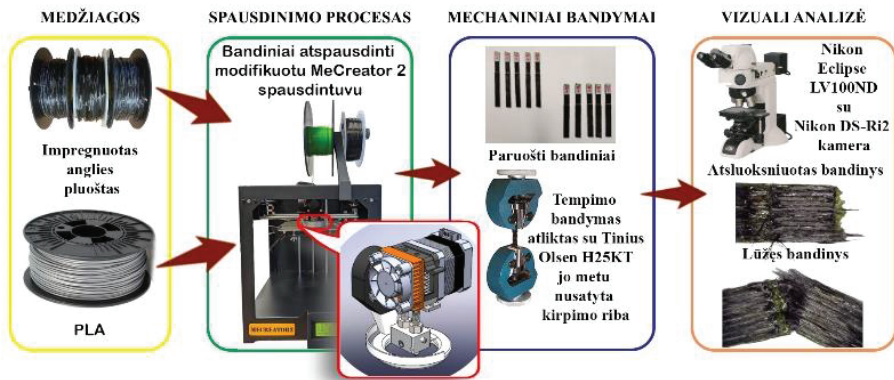
3.4 pav. Kokybiniai rezultatai: a – anglies pluošto kiekis šlifotuose bandiniuose, b – oro ertmių kiekis bandiniuose

Šiuo atveju anglies pluošto kiekis pagal masę buvo 18,8 %, o pagal tūrį – 11,2 %. 3.4 b pav. pavaizduoti oro ertmių tūrio vidurkiai, apskaičiuoti keturioms tiek šlifutoms, tiek nešlifutoms bandinių grupėms. Gauti rezultatai dar kartą patvirtina, kad svarbiausias spausdinimo proceso parametras mažesniai ertmių tūriui pasiekti bandinyje yra sluoksnio aukštis. Bandymo metu buvo nustatyta, kad kai linijos plotis

bandiniuose yra 1 mm, o sluoksnio aukštis – 0,3 mm (1 grupė), porų tūris neapdirbtame bandinyje yra 19 %, o dėl padidėjusio sluoksnio aukščio iki 0,4 mm porų tūris padidėja iki 23 % (2 grupė) neapdirbtuose bandiniuose (3.4 b pav.). Atitinkamai: kai linijos plotis yra 1,2 mm, o sluoksnio aukštis – 0,3 mm (3 grupė), porų tūris neapdirbtuose bandiniuose yra 21,4 %, o padidinus sluoksnio aukštį iki 0,4 mm, porų tūris padidėja iki 23,5 %. Vertinant apdirbtų ir neapdirbtų bandinių rezultatus (3.4 b pav.), pastebėta, kad apdirbtuose bandiniuose oro ertmių tūris yra ženkliai mažesnis. Pavyzdžiui, oro ertmių tūris padidėja nuo 3 % (3 ir 4 grupės) iki 5 % (1 ir 2 grupės). Šią tendenciją galima paaiškinti taip, neapdirbti 3D spausdinti bandiniai turi spausdinimo metu atsirandančių pažeidimų ir paviršiaus mikronelygumų, kurie turi tiesioginės įtakos oro ertmių tūrio skaičiavimui.

3.3. Spausdintų kompozitinių konstrukcijų atsluoksniavimo jėgos ir šlyties stiprio nustatymas¹¹

Atsluoksniavimo jėgos ir šlyties stiprio nustatymo bandymo schema pateikiama 3.5 pav.

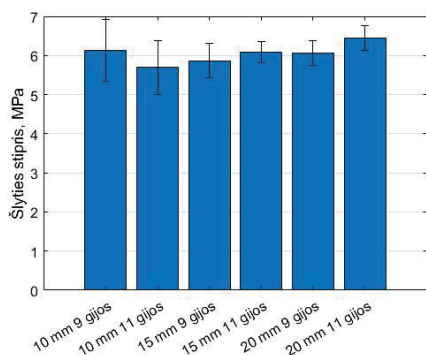


3.5 pav. Atsluoksniavimo jėgos ir šlyties stiprio nustatymo bandymo schema

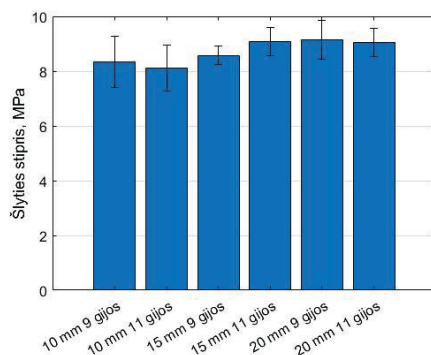
Kaip matyti iš 3.6 pav. pateiktų grafikų, šlyties stipris visiškai nepriklauso nuo bendros zonos pločio. Tačiau šiai mechaninei savybei didelės įtakos turi sluoksnio aukštis bei atstumas tarp gijų.

Pavyzdžiui, bandinių spausdintų sluoksnio aukščiu 0,4 mm ir atstumu tarp linijų 1,2 mm šlyties stipris vidutiniškai siekia 6,1 MPa, tuo tarpu sumažinus atstumą tarp gijų iki 1 mm šlyties stipris padidėja iki 8,7 MPa, tai yra 42,6 % padidėjimas. Jei atitinkamai lygintume atstumo tarp gijų įtaką bandiniams, spausdintiems 0,3 mm sluoksnio aukščiu, pastebėtume, kad šlyties stipris padidėjo nuo 12,5 MPa trečios grupės bandiniams iki 15,1 MPa pirmos grupės bandiniams, o tai yra apie 21 %. Dar didesnės įtakos turi sluoksnio aukščio pokytis spausdinamose konstrukcijose. Sumažinus sluoksnio aukštį 100 μ m šlyties stipris padidėjo vidutiniškai apie du kartus tiek 1 mm, tiek 1,2 mm atstumu tarp gijų spausdintiems bandiniams atitinkamai iki 12,5 MPa ir 15,1 MPa.

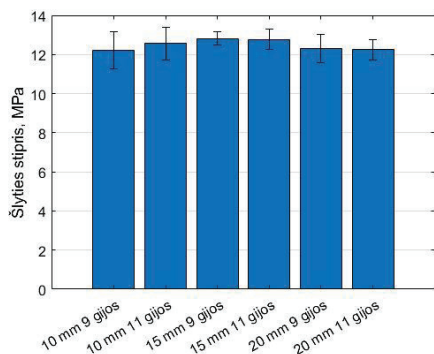
¹¹ Šio skyriaus medžiaga anksčiau buvo publikuota [102].



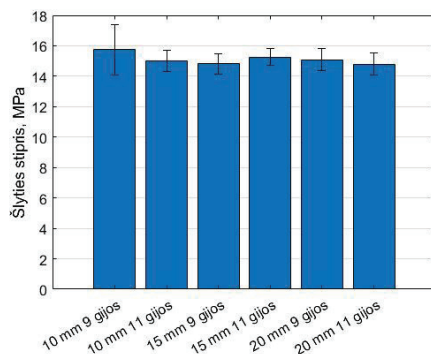
a



b



c

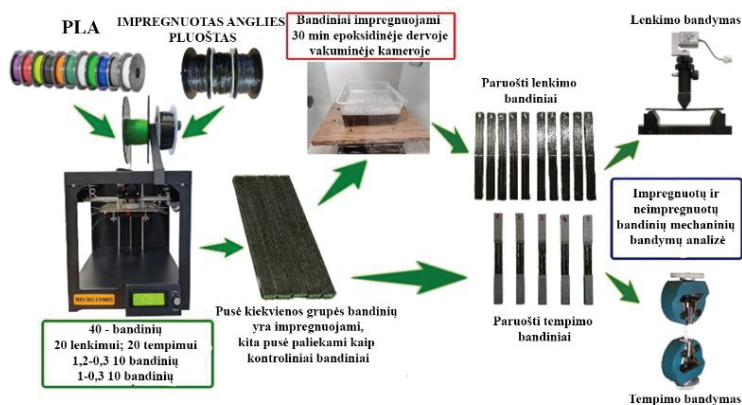


d

3.6 pav. Šlyties stipris: a – 4 grupė, b – 2 grupė, c – 3 grupė, d – 1 grupė

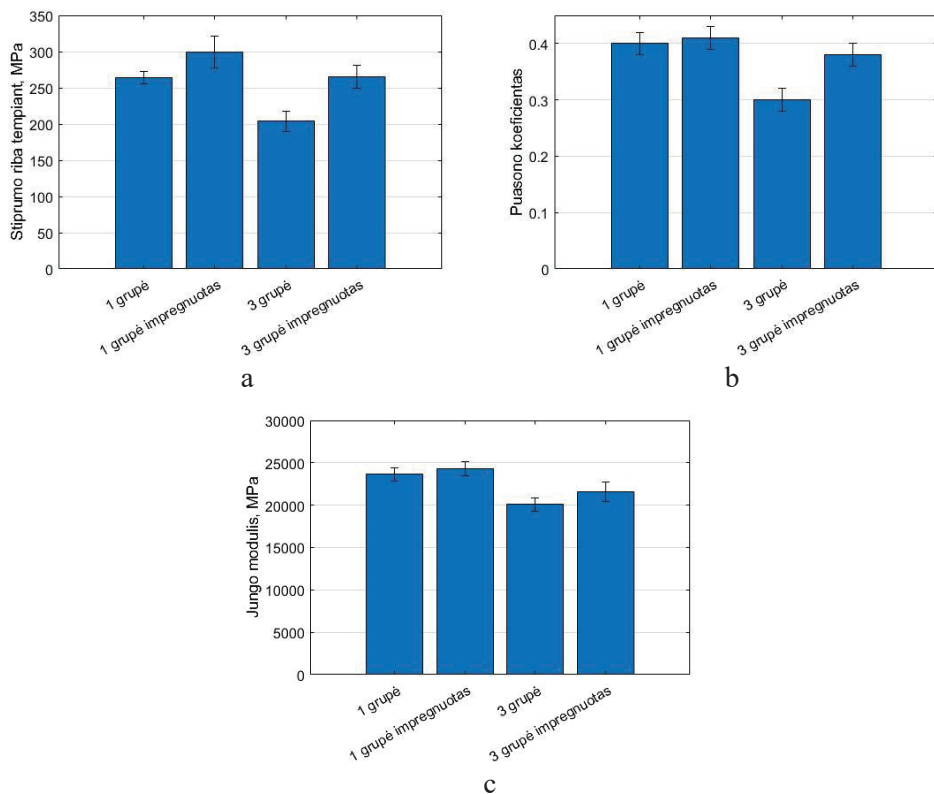
3.4. Mechaninių savybių gerinimas antriniu impregnavimu

Mechaninių savybių gerinimo bandymo schema pateikta 3.7 pav. Bandymo metu atlikti tempimo ir lenkimo bandymai, nustatytos ištisinio anglies pluoštu armuotų konstrukcijų tempimo ir lenkimo stiprumo ribos, Puasono koeficientas, lenkimo ir tempimo moduliai.



3.7 pav. Mechaninių savybių gerinimo impregnuojant bandymo schema

Apibendrinti stiprumo ribos tempiant rezultatai pateikiami 3.8 a pav. Iš šių diagramų matyti, kad impregnavimas epoksidine derva didesnės įtakos turi trečios grupės bandiniams. Vidutinė stiprumo riba tempiant šios grupės impregnuotose bandiniuose siekia 265 MPa, o pirmos grupės bandiniuose ji yra 299 MPa. Skirtumas tarp impregnuotų grupių yra apie 13 %. Palyginus neimpregnuotas grupes tarpusavyje, kai vidutinė stiprumo riba tempiant trečioje grupėje siekia 203 MPa, o pirmoje grupėje – 264 MPa, matyti, kad skirtumas yra apie 30 %. Skirtumas tarp stiprumo ribos tempiant po impregnavimo sumažėja dėl didesnės jo įtakos trečios grupės bandiniams. Puikiausias to įrodymas gaunamas palyginus tos pačios grupės impregnuotus ir neimpregnuotus bandinius. Kaip minėta anksčiau, vidutinė trečios grupės bandinių stiprumo riba tempiant siekia 203 MPa, impregnavus jis padidėja iki 265 MPa. Impregnavus gaunamas 30,5 % padidėjimas. Kai tuo tarpu pirmoje grupėje neimpregnuotų tempimo bandinių stiprumo riba tempiant yra 264 MPa, o impregnuotų – 299 MPa, padidėjimas po impregnavimo siekia apie 13 %. Galime daryti išvadą, kad impregnuojant bandinius su didesniu atstumu tarp spausdintų gijų pasiekiamas net 17,5 % didesnis stiprumo ribos tempiant padidėjimas.



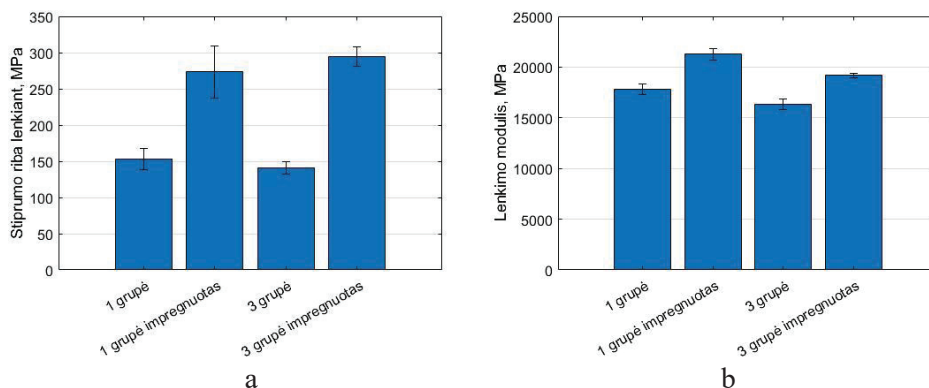
3.8 pav. Mechaninės savybės: a – stiprumo riba tempiant, b – Puasono koeficientas, c – Jungo modulis

Kita medžiagos charakteristika, nustatyta tempimo bandymo metu, yra Puasono koeficientas. Tyrimo metu gauti rezultatai pateikti 3.8 b paveikslėlyje. Spausdintoms

kompozitinėms konstrukcijoms, apskaičiavus koeficientą, jis vidutiniškai svyruoja tarp 0,39 ir 0,3 atitinkamai pirmos ir trečios grupės bandiniuose. Po impregnavimo šis dydis padidėja iki 0,41 ir 0,38 atitinkamai pirmoje ir trečioje bandinių grupėje. Puasono koeficiento padidėjimas po impregnavimo proceso atitinkamų bandinių grupėse yra 5 % pirmoje ir 27 % trečioje bandinių grupėje. Taigi išlieka ta pati tendencija, kad impregnavimas didesnę įtaką turi didesniais atstumais tarp spausdinamų gijų spausdintiems bandiniams. Lyginant impregnuotus ir neimpregnuotus skirtingų grupių bandinius, skirtumas tarp Puasono koeficiento atitinkamai yra 8 % ir 30 %. Kaip matyti, po impregnavimo skirtumas tarp trečios ir pirmos spausdintų bandinių grupės Puasono koeficiento sumažėjo 22 %.

Dar vienas fizikinis dydis, aprašantis spausdintą kompozitinę medžiagą, yra Jungo arba tamprumo modulis. Eksperimento metu gauti rezultatai stulpeline diagrama pateikiami 3.8 c pav. Kaip matyti iš grafiko, neimpregnuotų ištisiniu anglies pluoštu armuotų 3D spausdintų kompozitinių konstrukcijų vidutinis tamprumo modulis yra 23661 MPa pirmoje grupėje ir 20084 MPa trečioje grupėje. Skirtumas tarp šių grupių rezultatų yra 17 %. Po impregnavimo tamprumo modulis padidėja atitinkamoms grupėms iki 24335 MPa ir 21596 MPa. Tamprumo modulio skirtumas sumažėja iki 13 %. Lyginant tų pačių grupių bandinių rezultatus prieš ir po impregnavimo proceso matyti, kad tamprumo modulis padidėja atitinkamai 2,8 % pirmoje ir 7,5 % trečioje bandinių grupėje. Kaip ir anksčiau pateiktuose rezultatuose pastebima ta pati tendencija, kad impregnavimas didesnės įtakos turi trečiajai bandinių grupei, kurioje impregnavimas beveik 5 % yra efektyvesnis lyginant su pirmosios grupės bandiniais.

Apibendrinti stiprumo ribos lenkiant rezultatai pateikiami 3.9 a pav. stulpelinėmis diagramomis. Iš šių diagramų matyti, kad impregnavimas epoksidine derva didesnės įtakos turi trečios grupės bandiniams. Vidutinė stiprumo riba lenkiant trečios grupės impregnuotose bandiniuose siekia 294 MPa, o pirmoje bandinių grupėje ji yra 273 MPa. Skirtumas tarp impregnuotų grupių yra apie 7,7 %, o tempimo bandymo metu jis siekė 13 %. Palyginus neimpregnuotas grupes tarpusavyje, kai vidutinė stiprumo riba lenkiant trečioje bandinių grupėje siekia 140 MPa, o 1 grupėje 153 MPa, matyti kad skirtumas yra apie 9,3 %. Skirtumas tarp grupių po impregnavimo sumažėja dėl didesnės jo įtakos trečios grupės bandiniams. Puikiausias to įrodymas gaunamas palyginus tos pačios grupės impregnuotus ir neimpregnuotus bandinius. Kaip minėta anksčiau, vidutinė bandinių trečioje grupėje stiprumo riba lenkiant siekia 140 MPa, tuo tarpu impregnavus ji padidėja iki 294 MPa. Impregnavus gaunamas 110 % padidėjimas. Kita vertus pirmoje bandinių grupėje neimpregnuotų bandinių stiprumo riba lenkiant yra 153 MPa, o impregnuotų – 273 MPa, t. y. pagerėjimas po impregnavimo siekia apie 78 %. Galime daryti išvadą, kad impregnuojant bandinius su didesniu atstumu tarp spausdintų gijų pasiekiamas 32 % didesnis stiprumo ribos lenkiant padidėjimas. Lyginant impregnavimo įtaką lenkimui ir tempimui matoma aiškiai didesnė nauda lenkimui. Stiprumo riba tempiant po impregnavimo trečios grupės bandiniams padidėjo tik 30,5 %, kai tuo tarpu stiprumo riba lenkiant išaugo net 110 %. Atitinkamai pirmos grupės bandiniuose stiprumo riba tempiant padidėjo 13 %, o lenkiant net 78 %.



3.9 pav. Mechaninės savybės: a – stiprumo riba lenkiant, b – lenkimo modulis

Lenkimo bandymo metu taip pat nustatytas ir 3D spausdintos ištisinio anglies pluoštu armuotos kompozitinės medžiagos lenkimo modulis. Testo metu nustatytas modulis stulpeline diagrama pateikiamas 3.9 b pav. Kaip matyti iš diagramos, neimpregnuotų ištisinio anglies pluoštu armuotų 3D spausdintų kompozitinių konstrukcijų vidutinis lenkimo modulis yra 17808 MPa pirmos grupės bandiniuose ir 16328 MPa trečios grupės bandiniuose. Skirtumas tarp šių grupių lenkimo modulių yra 1480 MPa arba apie 9 %. Po impregnavimo lenkimo modulis padidėja atitinkamoms grupėms iki 21270 MPa ir 19173 MPa. Šiuo atveju lenkimo modulio skirtumas yra 2097 MPa ar 11 %. Lyginant tų pačių grupių bandinių rezultatus prieš ir po impregnavimo proceso matyti, kad lenkimo modulis padidėja atitinkamai 19 % pirmoje ir 17 % trečioje bandinių grupėje. Šiuo atveju skirtingai nei anksčiau didesnė impregnavimo įtaka lenkimo moduliui pastebima pirmai grupei ir skirtumas tarp skirtingais atstumais tarp spausdintų gijų spausdintiems ir impregnuotiems bandiniams yra apie 2 %. Tačiau šie du procentai nepaneigia fakto, kad impregnavimas tiek tempimo, tiek lenkimo stiprumo ribai, didesnės įtakos turi tračiajai bandinių grupei. Šis nukrypimas nuo anksčiau matytos tendencijos gali atsirasti dėl matavimo paklaidų ar nekokybiško bandinių nuvalymo po impregnavimo proceso.

IŠVADOS

Literatūros analizė atskleidžia nepakankamus IAP impregnavimo metodų tyrimus, be gilios ir išsamios impregnavimo tirpalo, koncentracijos, džiovinimo trukmės, temperatūros ir impregnavimo greičio analizės. Aprašyti esami IAP spausdinimo procesai ir įranga nėra plačiai išanalizuoti. Nėra išsamios analizės, kaip spausdinimo parametrai, tokie kaip sluoksnio aukštis, atstumas tarp spausdinimo gijų, spausdinimo greitis, skirtingai impregnuotas IAP, paveikia spausdintų konstrukcijų mechanines savybes, adheziją ar oro ertmių kiekį.

1. Sukurta ir aprašyta 1K ir 3K IAP impregnavimo technologija, impregnuojant pluoštą PLA, ABS, PC termoplastikų ir tirpiklio (metileno chlorido) tirpale. Padidinus impregnavimo tirpalo koncentraciją nuo 2 % iki 10 % trūkimo jėga tempiant padidėja 20 % 1K ir ~105 % 3K anglies pluošte. Ištyrus įvairias

impregnavimo medžiagas, pastebėta, kad anglies pluošto gija geriausias savybes įgyja po impregnavimo 10 wt % PLA ir CH_2Cl_2 tirpale. Po impregnavimo adhezijos jėga tarp matricos ir armuojančios medžiagos padidėja 240 %. Vizualinė analizė parodė, kad po impregnavimo pluošte esančių oro ertmių procentas svyruoja atitinkamai nuo 11 % iki 23 %.

2. Sukurtas adityviosios gamybos procesas, paremtas LMF technologijos pagrindu, ir technologinė įranga, galinti spausdinti kompozitines konstrukcijas, sustiprintas impregnuotu IAP. Sukurtas spausdinimo modulis, turintis du įėjimo ir vieną išėjimo kanalą. Pagamintas modulis gali būti naudojamas kompozitinių konstrukcijų armuotų IAP (1K ir 3K) spausdinimui. Rekomenduojamas sluoksnio aukštis nuo 0,3 iki 0,6 mm, atstumas tarp spausdinimo gijų nuo 1 iki 1,6 mm ir plastiko kiekis nuo 40 iki 60 %, priklausomai nuo pluošto.
3. Spausdintų kompozicinių konstrukcijų defektoskopinė analizė buvo atlikta kompiuterinės tomografijos ir matricos tirpimo metodu, siekiant nustatyti santykinį oro ertmių tūrį. Oro ertmių tūris konstrukcijoje priklauso nuo sluoksnio aukščio ir atstumo tarp spausdinimo gijų. Oro ertmių tūrį galima sumažinti mažinant šiuos spausdinimo parametrus. Abiem metodais nustatytas oro ertmių kiekis yra labai panašus ir svyruoja nuo 19 iki 28 %. Nustatyta, kad oro ertmių tūris labiau priklauso nuo sluoksnio aukščio, nei atstumo tarp spausdinimo gijų.
4. Eksperimentiškai nustatytos pagrindinės spausdintų kompozitinių konstrukcijų, armuotų ištisiniu anglies pluoštu, mechaninės savybės. Stiprumo riba tempiant atitinkamai siekia 264 MPa ir 204 MPa pirmoje ir trečioje bandinių grupėse. Tų pačių grupių bandinių stiprumo riba lenkiant yra 153 MPa ir 140 MPa, o Puasono koeficientas yra 0,39 ir 0,30. Tempimo modulis yra atitinkamai lygus 23,6 GPa ir 20,0 GPa, lenkimo modulis atitinkamai siekia 17,0 GPa ir 16,3 GPa minėtoms bandinių grupėms. Šlyties stipris priklauso tik nuo spausdinimo parametrų, bet nepriklauso nuo šlyties ploto. Ketvirtos grupės šlyties stipris vidutiniškai yra 6,1 MPa, sumažinus atstumą tarp spausdinimo gijų iki 1 mm, šlyties stipris padidėja iki 8,7 MPa. Su 0,3 mm sluoksnio aukščiu spausdintose bandinių grupėse šlyties stipris atitinkamai siekia 12,5 MPa ir 15,1 MPa trečioje ir pirmoje bandinių grupėje.
5. Po antrinio impregnavimo epoksidinėje dervoje pastebėtas ženklus mechaninių savybių pagerėjimas spausdintose kompozitinėse konstrukcijoje, lyginant su neimpregnuotomis. Stiprumo riba tempiant padidėjo 30,5 % pirmoje bandinių grupėje, o lenkimo net 110 % trečioje bandinių grupėje. Pirmos grupės bandiniuose pastebėtas mažesnis stiprumo ribos tempiant ir lenkiant padidėjimas atitinkamai 13 % ir 78 %. Gauti rezultatai parodė, kad impregnavimas epoksidine derva turi didesnę poveikį konstrukcijoms, atspausdintoms didesniu sluoksnio aukščiu ir atstumu tarp spausdinimo gijų. Tai susiję su oro ertmių tūrio priklausomybe nuo šių spausdinimo parametrų, t. y. egzistuoja ryšys tarp oro ertmių ir antrinio impregnavimo efektyvumo. Didesnis oro ertmių tūris leidžia absorbuoti daugiau epoksidinės dervos impregnavimo metu.

REFERENCES

1. PRAKASH, K. Satish; NANCHARAIH, T. and RAO, V. V. Subba. Additive Manufacturing Techniques in Manufacturing -An Overview. *Materials Today: Proceedings*. 2018, **5**(2, Part 1), 3873-3882. ISSN 2214-7853.
2. COMPTON, Brett Gibson, et al. Direct-write 3D printing of NdFeB bonded magnets. *Null*. 2018, **33**(1), 109-113. ISSN 1042-6914.
3. PALMERO, Ester M., et al. Development of permanent magnet MnAlC/polymer composites and flexible filament for bonding and 3D-printing technologies. *Null*. 2018, **19**(1), 465-473. ISSN 1468-6996.
4. TAMAYO, José A., et al. Additive manufacturing of Ti6Al4V alloy via electron beam melting for the development of implants for the biomedical industry. *Heliyon*. 2021, **7**(5), e06892. ISSN 2405-8440.
5. DOÑATE-BUENDÍA, Carlos, et al. On the selection and design of powder materials for laser additive manufacturing. *Materials & Design*. 2021, , 109653.
6. CHOLLETI, Eshwar Reddy. A Review on 3D printing of piezoelectric materials. *IOP Conference Series: Materials Science and Engineering*. 2018, **455**, 012046. ISSN 1757-899X.
7. CHEN, Zhangwei, et al. 3D printing of ceramics: A review. *Journal of the European Ceramic Society*. 2019, **39**(4), 661-687. ISSN 0955-2219.
8. MAQSOOD, Nabeel; and RIMAŠAUSKAS, Marius. Characterization of carbon fiber reinforced PLA composites manufactured by fused deposition modeling. *Composites Part C: Open Access*. 2021, **4**, 100112. ISSN 2666-6820.
9. KHOO, Zhong, et al. 3D printing of smart materials: A review on recent progresses in 4D printing. *Virtual and Physical Prototyping*. 2015, **10**, 103-122.
10. GANBOLD, Boldbayar, et al. Human Stem Cell Responses and Surface Characteristics of 3D Printing Co-Cr Dental Material. *Materials*. 2019, **12**, 3419.
11. DILBEROGLU, Ugur M., et al. The Role of Additive Manufacturing in the Era of Industry 4.0. *Procedia Manufacturing*. 2017, **11**, 545-554. ISSN 2351-9789.
12. MATSUZAKI, Ryosuke, et al. Three-dimensional printing of continuous-fiber composites by in-nozzle impregnation. *Scientific Reports*. 2016, **6**, 23058.
13. ANAKHU, Peter, et al. Fused Deposition Modeling Printed Patterns for Sand Casting in a Nigerian Foundry: A Review. *International Journal of Applied Engineering Research*. 2018, **13**.
14. EZEH, O. H.; and SUSMEL, L. On the notch fatigue strength of additively manufactured polylactide (PLA). *International Journal of Fatigue*. 2020, **136**, 105583. ISSN 0142-1123.
15. ANDÓ, Mátyás; BIROSZ, Márton and JEGANMOHAN, Sudhanraj. Surface bonding of additive manufactured parts from multi-colored PLA materials. *Measurement*. 2021, **169**, 108583. ISSN 0263-2241.
16. RIDDICK, Jaret C., et al. Fractographic analysis of tensile failure of acrylonitrile-butadiene-styrene fabricated by fused deposition modeling. *Additive Manufacturing*. 2016, **11**, 49-59. ISSN 2214-8604.

17. GARCÍA-DOMÍNGUEZ, A.; CLAVER, J. and SEBASTIÁN, M. A. Methodology for the optimization of work pieces for additive manufacturing by 3D printing. *Procedia Manufacturing*. 2017, **13**, 910-915. ISSN 2351-9789.
18. YADAV, Dinesh, et al. Optimization of FDM 3D printing process parameters for multi-material using artificial neural network. *Materials Today: Proceedings*. 2020, **21**, 1583-1591. ISSN 2214-7853.
19. DOMINGO-ESPIN, Miquel, et al. Mechanical property characterization and simulation of fused deposition modeling Polycarbonate parts. *Materials & Design*. 2015, **83**, 670-677. ISSN 0264-1275.
20. TIAN, Xiaoyong, et al. Interface and performance of 3D printed continuous carbon fiber reinforced PLA composites. *Composites Part A: Applied Science and Manufacturing*. 2016, **88**, 198-205. ISSN 1359-835X.
21. DE LEON, Al C., et al. High performance polymer nanocomposites for additive manufacturing applications. *Reactive and Functional Polymers*. 2016, **103**, 141-155. ISSN 1381-5148.
22. HERGENROTHER, Paul M. The Use, Design, Synthesis, and Properties of High Performance/High Temperature Polymers: An Overview. *High Performance Polymers*. 2003, **15**(1), 3-45. ISSN 0954-0083.
23. GNANASEKARAN, K., et al. 3D printing of CNT- and graphene-based conductive polymer nanocomposites by fused deposition modeling. *Applied Materials Today*. 2017, **9**, 21-28. ISSN 2352-9407.
24. KIM, Hoejin, et al. Integrated 3D printing and corona poling process of PVDF piezoelectric films for pressure sensor application. *Smart Materials and Structures*. 2017, **26**(8), 085027. ISSN 0964-1726.
25. VALINO, Arnaldo D., et al. Advances in 3D printing of thermoplastic polymer composites and nanocomposites. *Progress in Polymer Science*. 2019, **98**, 101162. ISSN 0079-6700.
26. MASOOD, S. H.; and SONG, W. Q. Development of new metal/polymer materials for rapid tooling using Fused deposition modelling. *Materials & Design*. 2004, **25**(7), 587-594. ISSN 0261-3069.
27. SA'UDE, Nasuha; IBRAHIM, Mustaffa and IBRAHIM, Mohd Halim Irwan. Mechanical Properties of Highly Filled Iron-ABS Composites in Injection Molding for FDM Wire Filament. *Materials Science Forum*. 2014, **773-774**, 448-453. ISSN 1662-9752.
28. NIKZAD, M.; MASOOD, S. H. and SBARSKI, I. Thermo-mechanical properties of a highly filled polymeric composites for Fused Deposition Modeling. *Materials & Design*. 2011, **32**(6), 3448-3456. ISSN 0261-3069.
29. TORRADO, Angel R., et al. Characterizing the effect of additives to ABS on the mechanical property anisotropy of specimens fabricated by material extrusion 3D printing. *Additive Manufacturing*. 2015, **6**, 16-29. ISSN 2214-8604.
30. KALITA, Samar Jyoti, et al. Development of controlled porosity polymer-ceramic composite scaffolds via fused deposition modeling. *Materials Science and Engineering: C*. 2003, **23**(5), 611-620. ISSN 0928-4931.

31. SENATOV, F. S., et al. Mechanical properties and shape memory effect of 3D-printed PLA-based porous scaffolds. *Journal of the Mechanical Behavior of Biomedical Materials*. 2016, **57**, 139-148. ISSN 1751-6161.
32. JIA, Yunchao, et al. High through-plane thermal conductivity of polymer based product with vertical alignment of graphite flakes achieved via 3D printing. *Composites Science and Technology*. 2017, **145**, 55-61. ISSN 0266-3538.
33. LE, Bao, et al. A Review on Nanocomposites. Part 1: Mechanical Properties. *Journal of Manufacturing Science and Engineering*. 2020, **142**, 1-57.
34. CHEN, Qiyi, et al. 3D Printing Biocompatible Polyurethane/Poly(lactic acid)/Graphene Oxide Nanocomposites: Anisotropic Properties. *ACS Applied Materials & Interfaces*. 2017, **9**(4), 4015-4023. ISSN 1944-8244.
35. NAJERA, Sandra; MICHEL, Monica and KIM, Namsoo. 3D Printed PLA/PCL/TiO₂ Composite for Bone Replacement and Grafting. *MRS Advances*. 2018, **3**, 1-6.
36. SINGH, Mohit, et al. On 3D-printed ZnO-reinforced PLA matrix composite: Tensile, thermal, morphological and shape memory characteristics. *Journal of Thermoplastic Composite Materials*. 2020, , 0892705720935961. ISSN 0892-7057.
37. EZEH, O. H.; and SUSMEL, L. Fatigue strength of additively manufactured polylactide (PLA): effect of raster angle and non-zero mean stresses. *International Journal of Fatigue*. 2019, **126**, 319-326. ISSN 0142-1123.
38. DUL, Sithiprumnea; FAMBRI, Luca and PEGORETTI, Alessandro. Fused deposition modelling with ABS–graphene nanocomposites. *Composites Part A: Applied Science and Manufacturing*. 2016, **85**, 181-191. ISSN 1359-835X.
39. WANG, Xin, et al. 3D printing of polymer matrix composites: A review and prospective. *Composites Part B: Engineering*. 2017, **110**, 442-458. ISSN 1359-8368.
40. LE DUIGOU, Antoine, et al. A review of 3D and 4D printing of natural fibre biocomposites. *Materials & Design*. 2020, **194**, 108911. ISSN 0264-1275.
41. CARNEIRO, O. S.; SILVA, A. F. and GOMES, R. Fused deposition modeling with polypropylene. *Materials & Design*. 2015, **83**, 768-776. ISSN 0264-1275.
42. ZHONG, Weihong, et al. Short fiber reinforced composites for fused deposition modeling. *Materials Science and Engineering: A*. 2001, **301**(2), 125-130. ISSN 0921-5093.
43. SODEIFIAN, Gholamhossein; GHASEMINEJAD, Saghar and YOUSEFI, Ali Akbar. Preparation of polypropylene/short glass fiber composite as Fused Deposition Modeling (FDM) filament. *Results in Physics*. 2019, **12**, 205-222. ISSN 2211-3797.
44. HOLMES, Mark. Global carbon fibre market remains on upward trend. *Reinforced Plastics*. 2014, **58**(6), 38-45. ISSN 0034-3617.
45. SANEI, Seyed H.; and POPESCU, Diana. *3D-Printed Carbon Fiber Reinforced Polymer Composites: A Systematic Review*. , 2020. ISBN 2504-477X.
46. TEKINALP, Halil L., et al. Highly oriented carbon fiber–polymer composites via additive manufacturing. *Composites Science and Technology*. 2014, **105**, 144-150. ISSN 0266-3538.

47. NING, Fuda, et al. Additive manufacturing of carbon fiber reinforced thermoplastic composites using fused deposition modeling. *Composites Part B: Engineering*. 2015, **80**, 369-378. ISSN 1359-8368.
48. MAGRI, Anouar El, et al. Mechanical properties of CF-reinforced PLA parts manufactured by fused deposition modeling. *Journal of Thermoplastic Composite Materials*. 2021, **34**(5), 581-595. ISSN 0892-7057.
49. LEE, B. H.; ABDULLAH, J. and KHAN, Z. A. Optimization of rapid prototyping parameters for production of flexible ABS object. *Journal of Materials Processing Technology*. 2005, **169**(1), 54-61. ISSN 0924-0136.
50. KIM, Jaeyoon; and KANG, Bruce S. *Enhancing Structural Performance of Short Fiber Reinforced Objects through Customized Tool-Path*. , 2020. ISBN 2076-3417.
51. HERNANDEZ-CONTRERAS, Adriana, et al. Extended CT Void Analysis in FDM Additive Manufacturing Components. *Materials (Basel, Switzerland)*. 2020, **13**(17), 3831. ISSN 1996-1944.
52. ZHANG, Wei, et al. Interfacial bonding strength of short carbon fiber/acrylonitrile-butadiene-styrene composites fabricated by fused deposition modeling. *Composites Part B: Engineering*. 2018, **137**, 51-59. ISSN 1359-8368.
53. HU, Qingxi, et al. Manufacturing and 3D printing of continuous carbon fiber prepreg filament. *Journal of Materials Science*. 2018, **53**(3), 1887-1898. ISSN 1573-4803.
54. YANG, Chuncheng, et al. 3D printing for continuous fiber reinforced thermoplastic composites: mechanism and performance. *Rapid Prototyping Journal*. 2017, **23**(1), 209-215. ISSN 1355-2546.
55. LI, Nanya; LI, Yingguang and LIU, Shuting. Rapid prototyping of continuous carbon fiber reinforced polylactic acid composites by 3D printing. *Journal of Materials Processing Technology*. 2016, **238**, 218-225. ISSN 0924-0136.
56. BETTINI, Paolo, et al. Fused Deposition Technique for Continuous Fiber Reinforced Thermoplastic. *Journal of Materials Engineering and Performance*. 2017, **26**(2), 843-848. ISSN 1544-1024.
57. XIU, Hao, et al. Simultaneously reinforcing and toughening of polylactide/carbon fiber composites via adding small amount of soft poly(ether)urethane. *Composites Science and Technology*. 2016, **127**, 54-61. ISSN 0266-3538.
58. KARSLI, Nevin Gamze; and AYTAC, Ayse. Tensile and thermomechanical properties of short carbon fiber reinforced polyamide 6 composites. *Composites Part B: Engineering*. 2013, **51**, 270-275. ISSN 1359-8368.
59. QUAN, Zhenzhen, et al. Microstructural design and additive manufacturing and characterization of 3D orthogonal short carbon fiber/acrylonitrile-butadiene-styrene preform and composite. *Composites Science and Technology*. 2016, **126**, 139-148. ISSN 0266-3538.
60. LI, Zhen Hua, et al. Effect of Fiber Length on Mechanical Properties of Short Carbon Fiber Reinforced PTFE Composites. *Advanced Materials Research*. 2011, **311-313**, 193-196. ISSN 1662-8985.

61. ASHORI, Alireza; MENBARI, Saman and BAHRAMI, Reza. Mechanical and thermo-mechanical properties of short carbon fiber reinforced polypropylene composites using exfoliated graphene nanoplatelets coating. *Journal of Industrial and Engineering Chemistry*. 2016, **38**, 37-42. ISSN 1226-086X.
62. GUO, Nannan; and LEU, Ming C. Additive manufacturing: technology, applications and research needs. *Frontiers of Mechanical Engineering*. 2013, **8**(3), 215-243. ISSN 2095-0241.
63. SKORSKI, Matthew R., et al. The chemical, mechanical, and physical properties of 3D printed materials composed of TiO₂-ABS nanocomposites. *Null*. 2016, **17**(1), 89-97. ISSN 1468-6996.
64. JACKIEWICZ, Jacek. Manufacturing of instructional aids for students at low cost by means of 3D printing. *Null*. 2017, **32**(10), 1116-1130. ISSN 1042-6914.
65. KABIR, S. M. Fijul; MATHUR, Kavita and SEYAM, Abdel-Fattah M. A critical review on 3D printed continuous fiber-reinforced composites: History, mechanism, materials and properties. *Composite Structures*. 2020, **232**, 111476. ISSN 0263-8223.
66. GAROFALO, James; and WALCZYK, Daniel. In situ impregnation of continuous thermoplastic composite prepreg for additive manufacturing and automated fiber placement. *Composites Part A: Applied Science and Manufacturing*. 2021, **147**, 106446. ISSN 1359-835X.
67. *3D Printing with Continuous Fiber: A Landscape*. Available from: <<https://www.compositesworld.com/articles/3d-printing-with-continuous-fiber-a-landscape>>. Information retrieved 2021.08.15
68. MEI, Hui, et al. Influence of mixed isotropic fiber angles and hot press on the mechanical properties of 3D printed composites. *Additive Manufacturing*. 2019, **27**, 150-158. ISSN 2214-8604.
69. EKOI, Emmanuel J.; DICKSON, Andrew N. and DOWLING, Denis P. Investigating the fatigue and mechanical behaviour of 3D printed woven and nonwoven continuous carbon fibre reinforced polymer (CFRP) composites. *Composites Part B: Engineering*. 2021, **212**, 108704. ISSN 1359-8368.
70. ZHANG, Jun, et al. *Performance of 3D-Printed Continuous-Carbon-Fiber-Reinforced Plastics with Pressure*. , 2020. ISBN 1996-1944.
71. ZHANG, Haiguang, et al. Three-Dimensional Printing of Continuous Flax Fiber-Reinforced Thermoplastic Composites by Five-Axis Machine. *Materials*. 2020, **13**, 1678.
72. MOHAMMADIZADEH, M., et al. 3D printed fiber reinforced polymer composites - Structural analysis. *Composites Part B: Engineering*. 2019, **175**, 107112. ISSN 1359-8368.
73. XU, Weiheng, et al. 3D printing for polymer/particle-based processing: A review. *Composites Part B: Engineering*. 2021, **223**, 109102. ISSN 1359-8368.
74. HANDWERKER, Michael; WELLNITZ, J. örgan and MARZBANI, Hormoz. Review of mechanical properties of and optimisation methods for continuous fibre-reinforced thermoplastic parts manufactured by fused deposition modelling. *Progress in Additive Manufacturing*. 2021, . ISSN 2363-9520.

75. HEIDARI-RARANI, M.; RAFIEE-AFARANI, M. and ZAHEDI, A. M. Mechanical characterization of FDM 3D printing of continuous carbon fiber reinforced PLA composites. *Composites Part B: Engineering*. 2019, **175**, 107147. ISSN 1359-8368.
76. UEDA, Masahito, et al. 3D compaction printing of a continuous carbon fiber reinforced thermoplastic. *Composites Part A: Applied Science and Manufacturing*. 2020, **137**, 105985. ISSN 1359-835X.
77. PAPPAS, John M., et al. A parametric study and characterization of additively manufactured continuous carbon fiber reinforced composites for high-speed 3D printing. *The International Journal of Advanced Manufacturing Technology*. 2021, **113**(7), 2137-2151. ISSN 1433-3015.
78. YUAN, Xiaomin, et al. Optimization of interfacial properties of carbon fiber/epoxy composites via a modified polyacrylate emulsion sizing. *Applied Surface Science*. 2017, **401**, 414-423. ISSN 0169-4332.
79. YUAN, Hao-jie, et al. Preparation and characterization of a polyimide coating on the surface of carbon fibers. *New Carbon Materials*. 2015, **30**(2), 115-121. ISSN 1872-5805.
80. CHEN, Junlin; WANG, Kai and ZHAO, Yan. Enhanced interfacial interactions of carbon fiber reinforced PEEK composites by regulating PEI and graphene oxide complex sizing at the interface. *Composites Science and Technology*. 2018, **154**, 175-186. ISSN 0266-3538.
81. LIU, Guang; XIONG, Yi and ZHOU, Limin. Additive manufacturing of continuous fiber reinforced polymer composites: Design opportunities and novel applications. *Composites Communications*. 2021, **27**, 100907.
82. SAFARI, Faraz; KAMI, Abdolvahed and ABEDINI, Vahid. *3D Printing of Continuous Fiber Reinforced Composites: A Review of the Processing, Pre-and Post-Processing Effects on Mechanical Properties*. , 2021.
83. IRAGI, M., et al. Ply and interlaminar behaviours of 3D printed continuous carbon fibre-reinforced thermoplastic laminates; effects of processing conditions and microstructure. *Additive Manufacturing*. 2019, **30**, 100884. ISSN 2214-8604.
84. LIU, Tengfei, et al. Interfacial performance and fracture patterns of 3D printed continuous carbon fiber with sizing reinforced PA6 composites. *Composites Part A: Applied Science and Manufacturing*. 2018, **114**, 368-376. ISSN 1359-835X.
85. HEIDARI-RARANI, M.; RAFIEE-AFARANI, M. and ZAHEDI, A. M. Mechanical characterization of FDM 3D printing of continuous carbon fiber reinforced PLA composites. *Composites Part B: Engineering*. 2019, **175**, 107147. ISSN 1359-8368.
86. YE, Wenli, et al. Separated 3D printing of continuous carbon fiber reinforced thermoplastic polyimide. *Composites Part A: Applied Science and Manufacturing*. 2019, **121**, 457-464. ISSN 1359-835X.
87. HAO, Wenfeng, et al. Preparation and characterization of 3D printed continuous carbon fiber reinforced thermosetting composites. *Polymer Testing*. 2018, **65**, 29-34. ISSN 0142-9418

88. DICKSON, Andrew N., et al. Fabrication of continuous carbon, glass and Kevlar fibre reinforced polymer composites using additive manufacturing. *Additive Manufacturing*. 2017, **16**, 146-152. ISSN 2214-8604.
89. AL ABADI, Haider, et al. Elastic properties of 3D printed fibre-reinforced structures. *Composite Structures*. 2018, **193**, 8-18. ISSN 0263-8223.
90. ISOBE, T., et al. Comparison of strength of 3D printing objects using short fiber and continuous long fiber. *IOP Conference Series: Materials Science and Engineering*. 2018, **406**, 012042. ISSN 1757-899X.
91. OZTAN, Cagri, et al. Microstructure and mechanical properties of three dimensional-printed continuous fiber composites. *Journal of Composite Materials*. 2019, **53**(2), 271-280. ISSN 0021-9983.
92. DOU, Hao, et al. Effect of Process Parameters on Tensile Mechanical Properties of 3D Printing Continuous Carbon Fiber-Reinforced PLA Composites. *Materials (Basel, Switzerland)*. 2020, **13**(17), 3850. ISSN 1996-1944.
93. TIAN, Xiaoyong, et al. Recycling and remanufacturing of 3D printed continuous carbon fiber reinforced PLA composites. *Journal of Cleaner Production*. 2017, **142**, 1609-1618. ISSN 0959-6526.
94. LIAO, Guangxin, et al. Properties of oriented carbon fiber/polyamide 12 composite parts fabricated by fused deposition modeling. *Materials & Design*. 2018, **139**, 283-292. ISSN 0264-1275.
95. CHACÓN, J. M., et al. Additive manufacturing of continuous fibre reinforced thermoplastic composites using fused deposition modelling: Effect of process parameters on mechanical properties. *Composites Science and Technology*. 2019, **181**, 107688. ISSN 0266-3538.
96. LI, Nanya, et al. Path-designed 3D printing for topological optimized continuous carbon fibre reinforced composite structures. *Composites Part B: Engineering*. 2020, **182**, 107612. ISSN 1359-8368.
97. LIU, Tengfei, et al. High-pressure interfacial impregnation by micro-screw in-situ extrusion for 3D printed continuous carbon fiber reinforced nylon composites. *Composites Part A: Applied Science and Manufacturing*. 2020, **130**, 105770. ISSN 1359-835X.
98. *TORAYCA™ Yarn Data Sheet*. Available from:<https://www.cf-composites.toray/resources/data_sheets/pdf/ds_torayca_yarn.pdf>. Information retrieved 2021.08.30
99. *PRUSA PLA Data Sheet*. Available from:<https://prusament.com/media/2018/07/PLA_datasheet.pdf>. Information retrieved 2021.09.02
100. RIMAŠAUSKAS, Marius; KUNCIUS, Tomas and RIMAŠAUSKIENĖ, Rūta. Processing of carbon fiber for 3D printed continuous composite structures. *Null*. 2019, **34**(13), 1528-1536. ISSN 1042-6914.
101. RIMAŠAUSKAS, M., et al. Investigation of influence of printing parameters on the quality of 3D printed composite structures. *Composite Structures*. 2022, **281**.
102. KUNCIUS, Tomas; RIMAŠAUSKAS, Marius and RIMAŠAUSKIENĖ, Rūta. *Interlayer Adhesion Analysis of 3D-Printed Continuous Carbon Fibre-Reinforced Composites*. , 2021. ISBN 2073-4360.

CIRRCULUM VITAE

Name/Surname: Tomas Kuncius

Nationality: Lithuanian

Date of Birth: June 29, 1992

Email: tomas.kuncius@ktu.lt



Education:

1999–2011 Secondary Education

Kaunas Simono Daukanto High School, Taikos pr. 68, LT 51300 Kaunas, Lithuania

2011–2015 Production Engineering and Technologies (Bachelor)

Kaunas University of Technology, K. Donelaičio g. 73, LT 44249 Kaunas, Lithuania

2015–2017 Industrial Engineering and Management master studies (Master)

Kaunas University of Technology, K. Donelaičio g. 73, LT 44249 Kaunas, Lithuania

2017 – 2022 Mechanical Engineering (PhD)

Kaunas University of Technology, K. Donelaičio g. 73, LT 44249 Kaunas, Lithuania

Work experience:

Quality Engineer

UAB Littec, Inovacijų 6, Biruliškių k., LT 54469 Kaunas District Municipality Lithuania

Production Worker

UAB Mondelez Lietuva Production, Taikos pr. 88, LT 51182 Kaunas, Lithuania

Design Engineer

UAB Baltic Orthoservice, Taikos pr. 131, LT 51124 Kaunas, Lithuania

Young researcher, Lecturer

Kaunas University of Technology, K. Donelaičio g. 73, LT 44249 Kaunas, Lithuania

Research interests:

Additive Manufacturing, 3D Printing, Composite Materials, Mechanical Properties, FDM, SLA, SLS, Innovative Manufacturing Technologies and Materials.

APPROBATION OF THE RESEARCH RESULTS

The results of this dissertation have been published in 4 scientific papers: 3 in journals with the impact factor indexed in the *Web of Science* database, and 1 without it. The research results have also been presented at 7 international scientific conferences:

List of Scientific Publications Related to the Dissertation

ARTICLES IN PEER-REVIEWED SCIENTIFIC PUBLICATIONS

Indexed in the Web of Science with Impact Factor

International Publishers

1. **Kuncius, Tomas**; Rimašauskas, Marius; Rimašauskienė, Rūta. Interlayer adhesion analysis of 3D-printed continuous carbon fibre-reinforced composites // *Polymers*. Basel : MDPI. ISSN 2073-4360. 2021, vol. 13, iss. 10, art. no. 1653, p. 1–14. DOI: 10.3390/polym13101653. [Science Citation Index Expanded (Web of Science); Scopus; DOAJ] [IF: 4.329; AIF: 4.680; IF/AIF: 0.925; Q1 (2020, InCites JCR SCIE)] [CiteScore: 4.70; SNIP: 1.200; SJR: 0.770; Q1 (2020, Scopus Sources)] [FOR: T 008] [Input: 0.334]
2. Rimašauskas, Marius; **Kuncius, Tomas**; Rimašauskienė, Rūta. Processing of carbon fiber for 3D printed continuous composite structures // *Materials and Manufacturing Processes*. Philadelphia, PA : Taylor & Francis. ISSN 1042-6914. eISSN 1532-2475. 2019, vol. 34, iss. 13, p. 1528–1536. DOI:10.1080/10426914.2019.1655152. [Science Citation Index Expanded (Web of Science); Scopus] [IF: 3.046; AIF: 4.371; IF/AIF: 0.696; Q2 (2019, InCites JCR SCIE)] [CiteScore: 6.80; SNIP: 1.685; SJR: 1.077; Q1 (2019, Scopus Sources)] [FOR: T 008] [Input: 0.333]
3. Rimašauskas, Marius; Jasiūnienė, Elena; **Kuncius, Tomas**; Rimašauskienė, Rūta; Cicėnas, Vaidotas. Investigation of influence of printing parameters on the quality of 3D printed composite structures // *Composite structures*. Oxford : Elsevier. ISSN 0263-8223. eISSN 1879-1085. 2022, vol. 281, art. No. 115061, p. 147–161. DOI: 10.1016/j.compstruct.2021.115061. [Science Citation Index Expanded (Web of Science); Scopus] [IF: 5.407; AIF: 4.807; IF/AIF: 1.124; Q1 (2020, InCites JCR SCIE)] [CiteScore: 9.60; SNIP: 2.040; SJR: 1.630; Q1 (2020, Scopus Sources)] [S.fl.d.: T 010, T 009, T 001] [Contribution: 0.200]

Indexed in the Web of Science or Scopus without ImpactFactor or SNIP

International Publishers

1. **Kuncius, Tomas**; Rimašauskas, Marius. Research of impregnated carbon fiber tow quality for 3D composites printing // *Macromolecular symposia: Progress on polymers and composites products and manufacturing technologies — POLCOM 2020, Part I: selected contributions from the virtual 4th international conference POLCOM 2020 — Progress on polymers and composites products and manufacturing technologies collaboration between the University of Campania “Luigi Vanvitelli” in Italy and Politehnica University of Bucharest in Romania, 26–28 November 2020 / G. Lamanna,*

C.G. Opran (eds.). Weinheim : Wiley-VCH. ISSN1022-1360. eISSN 1521-3900. 2021, vol. 395, spec. iss.1, art. No. 2000259, p. 1–4. DOI: 10.1002/masy.202000259. [Conference Proceedings Citation Index - Science (Web of Science); Scopus; Academic Search Complete] [CiteScore: 1.20; SNIP: 0.322; SJR: 0.257; Q3 (2020, Scopus Sources)] [FOR: T008] [Input: 0.500]

Articles in conference proceedings

International Publishers

1. Rimašauskas, Marius; **Kuncius, Tomas**. Tensile testing of 3D printed continuous carbon fibrereinforced PLA composites // Proceedings of 7th international conference on additive technologies, iCAT 2018, Maribor, Slovenia, 10. - 11. October 2018 / Editors: Igor Drstvenšek, Dietmar Drummer, Nataša Ihan Hren and Nicolae Balci. Ljubljana : Interesansa - zavod, 2018. ISBN 9789612887896. p. 98–101. [FOR: T 008] [Input: 0.500]

National Publishers

1. **Kuncius, Tomas**; Rimašauskas, Marius. Review and perspectives of additive layer manufacturing technologies for composites structures production // Mechanika 2018: proceedings of the 23rd international scientific conference, 18 May 2018, Kaunas University of Technology, Lithuania / Kaunas University of Technology, Lithuanian Academy of Science, IFTOMM National Committee of Lithuania, Baltic Association of Mechanical Engineering. Kaunas : Kaunas University of Technology. ISSN 1822-2951. 2018, p. 101–108. [FOR: T 008] [Input: 0.500]

Other Conference Abstracts and non-peer Reviewed Conference Papers

1. **Kuncius, Tomas**; Maqsood, Nabeel. Additive manufacturing of continuous carbon fibers reinforced polymer composites for structural applications // Technorama 2020: from vision to innovation. Kaunas : KTU. 2020, p. 69–71. [FOR: T 008]
2. **Kuncius, Tomas**; Rimašauskas, Marius. Manufacturing of continuous carbon fiber reinforced thermoplastic composites using FDM technology : poster // Advanced materials and technologies: book of abstracts of 21st international conference - school, 19-23 August 2019, Palanga, Lithuania. Kaunas : Kaunas University of Technology. ISSN 1822-7759. 2019, P88, p. 123. [FOR: T 008]
3. Rimašauskiene, Ruta; Rimašauskas, Marius; **Kuncius, Tomas**; Jasiuniene, Elena; Cicenai, Vaidotas; Griškevičius, Paulius. Experimental analysis of carbon fibre impregnation influence on 3D printed composites mechanical properties // Journal of material sciences & engineering: 3rd international conference on 3D printing technology and innovations, March 25-26, 2019, Rome, Italy. [S.l.] : OMICS International. ISSN 2169-0022. 2019, vol. 8, p. 60-61. DOI: 10.4172/2169-0022-C2-129. [FOR: T 009]

List of Participation in Conferences Related to the Dissertation

1. 23rd international scientific conference: Mechanika 2018 (Kaunas, Lithuania)
2. 7th international conference on additive technologies, iCAT 2018 (Maribor, Slovenia)
3. 3rd international conference on 3D printing technology and innovations 2019 (Rome, Italy),

4. 24th International Conference-School on advanced materials and technologies 2019 (Palanga, Lithuania),
5. 4th International Conference POLCOM Progress on Polymers and Composites Products and Manufacturing Technologies 2020 (Bucharest, Romania)
6. ICC24 – 24th International conference on composite structures 2021 (Oporto, Portugal)
7. 7th International Conference on Mechanics of Composites - MECHCOMP7 2021, (Oporto, Portugal).

ACKNOWLEDGEMENTS

The completion of this dissertation could not have been possible without the substantial help, assistance and guidance from my supervisor Assoc. Prof. Marius Rimašauskas. I would like to express deep appreciation for his time, patience, understanding, knowledge and experience given during all PhD years.

I am thankful for all the advices and enlightenment for colleagues of Department of Production Engineering and head of it Assoc. Prof. Rūta Rimašauskienė.

My sincere thanks go to reviewers of dissertation Assoc. Prof. Regita Bendikienė and senior researcher dr. Rolanas Daukševičius for very helpful and constructive remarks, advices, suggestion given to make dissertation more complete.

I want to say big thank you for Akvilė Mirauskaitė for help and contribution for one of the research completion, her time, fellowship, effort and high standards that helped me during this journey.

I am also grateful for Kaunas University of Technology, Faculty of Mechanical Engineering and Design, Department of Production Engineering, Institute of Mechatronics, Institute of Ultrasound for provided all necessary equipment, needed to complete the researches and thesis.

I would like to say massive thanks for my family and all people who be with me during this amazing and interesting journey and gave me the helping hand when it was needed.

UDK 658.5(043.3)

SL 344. 2022-03-30, 16,75 leidyb. apsk. l. Tiražas 14 egz. Užsakymas 70.

Išleido Kauno technologijos universitetas, K. Donelaičio g. 73, 44249 Kaunas
Spausdino leidyklos „Technologija“ spaustuvė, Studentų g. 54, 51424 Kaunas

